Coordinated Operation of Battery Energy Storage Systems and Load Ratio Control Transformer for Photovoltaic-supplied Microgrids

February, 2015

Waseda University

Graduate School of Advanced Science and Engineering

Department of Electrical Engineering and Bioscience, Research on Advanced Electrical Energy Systems

LE, Khoa Dinh

Contents

CHAPTER 1: INTRODUCTION

1.1. Research background

In response to the depletion of fossil fuels such as natural gas and oil, researchers have been encouraged to develop renewable energy sources (RESs) as alternative sources [1–3]. It is difficult to integrate various types of RES into distribution networks because of unidirectional power flow characteristics and limits on network capacity. These barriers have served as motivation for researcher into integration of RESs into distribution networks. Microgrids (MGs), have been proposed as a type of distributed power system that can handle various loads and distributed energy resources (DERs), such as renewable energy sources, energy storage systems, and distributed generators (DGs). An MG can be operated as an isolated grid or an islandable grid as a solution for integrating numerous DERs into a distribution system. The size of grid that constitutes an MG has not been strictly defined, but two types of MGs are defined according to connections:

- a locally controlled system as an isolated MG, and
- a locally controlled system as an isolated grid and with a function to connect to a larger utility grid.

An MG offers many advantages to customers and utilities. These include minimization of total energy consumption, improved energy efficiency, improved reliability of supply, reduced environmental impact, voltage control, power loss reduction, and security of power supply. MGs have been proposed as an innovative distribution network structure [4–12], and they allow full benefit to be obtained from the integration of large numbers of small-scale DERs into distributed power systems.

MGs use many types of RESs, such as photovoltaic (PV) systems, wind turbines, and fuel cells. To achieve high penetration of RESs in MGs, we must address some challenges. The main challenges are overvoltage, voltage imbalances, reverse power flow, line overloading, and transformer overloading [13–22]. Consequently, operators of traditional networks will enforce limitations on RESs in the distribution network, and new strategies will be required to address these limitations.

There are many different methods that have been suggested by researchers to achieve these challenges. Some are listed here.

1. Wire enhancement, such as increasing the size of conductor to reduce the impedance of line. This method needs additional investment. [22–25].
2. Change of the secondary transformer tap of the distribution grid in the MG. Since the RES output power is unpredictable, this approach may cause the transformer tap to change often [25–26].
3. Installation of auto-transformers or voltage regulators [5], [27].
4. Curtailment of output power from RESs. This method can be used with either centralized or decentralized control. However, it is incompatible with the main purpose of using the maximum amount of renewable energy in the MG [28–31]
5. A system for allowing the DGs to absorb reactive power [33–38].
6. Utilization of batteries [39–57] on the demand side to deal with power quality issues. Batteries are used to increase the storage capacity for power from RESs in MGs during periods of high generation.

In this thesis, the author focuses on overvoltage caused by RESs. Since the output of RESs is unpredictable, they reduce an MG's stability. One of the main reasons for limiting the capacity of active power from RESs, such as PV cells that can be connected to a medium voltage (MV) distribution system, is overvoltage. During high PV generation and low load periods, the PV output is sent as a reverse power flow that causes the voltage in the MV feeder to increase. One solution that addresses this issue is using a battery energy storage system (BESS). In previous studies [39–45], BESSs were designed to lower the peak demand and to store surplus energy from renewable and conventional energy sources and were also designed for load leveling. BESSs have additionally been used to increase the reliability of power systems. Vandoorn et al. [5] introduced a method to predict the ability of a BESS to increase the penetration of intermittent integrated RESs into weak electricity grids. Baran et al. [36] proposed utilization of distribution static compensators (DSTATCOMs) with BESSs for smoothing the intermittent power output from large wind farms; however, the method of operating the BESS by monitoring the state of charge of the BESS between STATCOM

mode and voltage source inverter (VSI) mode was not introduced in that study. In this thesis, the author proposes a central BESS that can operate as a VSI or as a DSTATCOM, which allows both active and reactive power control. The thesis also describes the effectiveness of coordinated BESSs in MGs whose electricity is supplied by utility power and RESs. In the proposed system, a central BESS is installed at the MG's interconnection point with the utility grid, and local BESSs are installed on the load buses.

Optimal power flow (OPF) has been used to solve the optimization problem for planning, reconfiguration, and operation of distribution systems [37–45]. Solutions to OPF problems give the optimal settings for the active power output and voltage of the generator, tap position of the transformer, and paraemeters of the static compensator along with values for other control parameters to minimize distribution loss while ensuring the voltage, reactive power output of the generator, power flows in the distribution system, and other state variables are within operational and safety constraints [94–98]. Because installing BESSs is one key solution to many issues in MGs, the optimal mode of operation, location, and sizes of BESSs were also studied in previous research. Chen et.al. [55] introduced a method for determining the optimal size of BESSs in MGs based on a cost–benefit analysis. References [99–101] discuss a method to determine the optimal placements and sizes of BESSs by optimizing losses in the system through a particle swarm optimization (PSO) technique. In this thesis, optimization algorithms are proposed to control BESSs and determine the placement and sizes of BESSs by using self-organizing hierarchical particle swarm optimizer (HPSO) with time-varying acceleration coefficients (TVAC). In 1995, Kennedy and Eberhart proposed PSO, which is a search optimization algorithm that uses a population of self-adaptive agents. Since 1995, there has been a great amount of research on this subject, using empirical simulations to develop an original version of PSO [58–79]. For use in population-based optimization methods during the optimization process, Shi et.al. [70] proposed a modified PSO constructed by adding an inertial weight parameter to the original PSO to stabilize the local and global search. Typically, it is necessary to consider a highly diverse set of solutions to use the full range of the search space in

population-based search optimization techniques during the early part of the optimization search. By using an intertial weight parameter that varies linearly over generations, Shi et al. [79] introduced an important method for the PSO method performance enhancement and in [79], the modified PSO is known as a PSO with time-varying inertia weight factor (TVIW). Ratnaweera et al. [93] suggested PSO-TVAC, which uses TVAC to increase the social component and reduce the cognitive component by varying the acceleration coefficients over time. In [93], the HPSO algorithm is introduced for supplying the required motivation to find the globally optimal solution without using previous velocity. The combination of HPSO and TVAC, together called the HPSO-TVAC method, has been introduced as a consistent and robust optimization approach.

1.2. Contribution and structure of the thesis

In this thesis, the author proposes a novel central BESS that is installed at the interconnection point between an MG and a utility grid and can operate as either a or a DSTATCOM, allowing control of the voltage in an MG by using a reactive power controller instead of a DSTATCOM in the MG. Under normal operating conditions, the central BESS is operated as a VSI for controlling active power to charge and discharge battery banks and reactive power to control the voltage in the MG. However, the battery capacity of the central BESS is limited. When the batteries are fully discharged or fully charged, the central BESS cannot control the reactive power to regulate load bus voltage. The DSTATCOM mode ensures that the proposed method does not depend on battery capacity. Nevertheless, the rated power of the inverter in the central BESS is also limited, and so when the reactive power reaches the limit of the inverter, the load bus voltage cannot be controlled. Therefore, coordinated control between a central BESS and a load-ratio control transformer (LRT) is needed to keep the load bus voltages in an acceptable voltage range. For this reason, the author proposes a novel coordinated control for a central BESS, local BESSs, and an LRT for stabilizing the load bus voltages. In addition, a control method that uses the optimal active power flow of local BESSs to minimize the distribution loss and a coordinated control with a central BESS and LRT to stabilize the voltages of PV-supplied MG is proposed for the first time. Optimal power flow has been widely used to solve the optimization problem for planning,

reconfiguration, and operation of distribution systems. Solutions to OPF problems give the optimal settings for active power output and voltage of the generator, tap position of the transformer, and parameters of the static compensator as well as values for other control variables to minimize distribution loss while ensuring the load bus voltage, reactive power output of the generator, power flows in the distribution system, and other state variables are within operational and safety limits.

In a PV-supplied MG, the local bus voltages may exceed the voltage-range due to fluctuation in the output power of the PV system according to circumstances. Therefore, BESSs needs to be installed in the MG as a solution for voltage problems. However, there are difficulties with this, including determination of optimal locations on the system and the sizes of the BESSs. In this thesis, the author proposes a new optimization method for determining the placement and sizes of BESSs to stabilize the voltages, using HPSO-TVAC to do so.

To check the validity of the proposed operations for BESSs, numerical simulation of a PV-supplied MG model with BESSs and an LRT are carried out and experiments are performed on a real-time distribution network simulator to measure the load bus voltage.

This thesis consists of six chapters, organized as follows:

Chapter 1 [Introduction] This chapter presents detailed background information and describes works related to the study, including an overview of MGs and voltage control methods of MGs. The idea of a coordinated BESS and LRT control for photovoltaic-supplied MG, based on previous research, is proposed.

Chapter 2 [Battery Energy Storage System with VSI mode and DSTATCOM mode] Recently, more powerful and responsive power converters have been developed that build on the development of power electronics such as inverters that allow a complex control algorithm for accepting DERs through a combination of BESSs and inverters. In this chapter, a novel structure is proposed; this structure has a central BESS that can control in both VSI mode and DSTATCOM mode by changing the position of a mode switch. In VSI mode, the central BESS can control both active power, to charge and discharge the battery banks of the central BESS, and reactive power, to stabilize the

voltage. When the batteries of the central BESS are fully discharged or fully charged and other appropriate conditions are met, the central BESS switches to DSTATCOM mode to control reactive power flow by using active power flow from the MG. Therefore, the DSTATCOM mode ensures that the method of controlling the load bus voltages in the central BESS is not affected by battery capacity.

Chapter 3 [Coordinated control with a central BESS, local BESSs, and an LRT to stabilize the voltage of PV-supplied MG] In an MG with high-penetration PV and a local BESS connected to each PV system, the local bus voltages may exceed the voltage range as a result of environmental conditions that affect the output power of the PV system and the capacity of the local BESS. In this chapter, a novel coordinated central BESS, local BESSs, and an LRT control for stabilizing the load bus voltages is newly proposed. The author suggests installation of a central BESS that can operate as both a VSI and a DSTATCOM at the point of interconnection with the grid. The central BESS controls the reactive power to regulate the load bus voltages of the MG. Since the power rating of inverter of central BESS is limited, the load bus voltage cannot be controlled when the reactive power reaches the limit. Therefore, coordinated control with the central BESS and LRT is needed to keep the load bus voltages in the acceptable voltage range. The central BESS consumes active power to charge its batteries when the active power demand is smaller than the PVs' generation rate and the local BESSs are fully charged. Conversely, the central BESS discharges energy to the MG when the active power demand exceeds the PVs' generation rate and the local BESSs are fully discharged. Each local BESS is controlled to minimize the active power flow to the feeder where the local BESS is connected. A PV-supplied MG model with BESSs and an LRT was simulated by MATLAB/Simulink. The experiments were carried out on the real-time distribution network simulator. The simulation results and experimental results illustrate the success of the proposed control algorithm for MGs with loop and radial structures.

Chapter 4 [OPF for local BESSs by HPSO-TVAC to minimize distribution loss and coordinating between central BESS and LRT to stabilize the voltage of PV-supplied MG] In an MG with high-penetration PV and local BESSs installed at local buses, control of energy storage must be addressed. This chapter proposes an online OPF

method based on HPSO-TVAC to control the active power flow of local BESSs in a way that minimizes distribution loss while stabilizing the MG local bus voltages with the central BESS and LRT. Simulation results and experimental results illustrate the usefulness of the proposed control method. These results show that an MG with a loop structure has less energy loss than one with a radial structure; however, when using the proposed OPF method the disparity is reduced.

Chapter 5 [Optimizing placement and sizes of BESSs to stabilize voltage in PV-supplied MG] The proposed control algorithms described above are used to control the central BESS and existing local BESSs in a PV-supplied MG. In this chapter, the author proposes a two-step algorithm to optimize the placement and sizes of BESSs in a grid-connected PV-supplied MG. As the first step, an algorithm based on HPSO-TVAC is used to find the best locations for installing BESSs so that the number of BESSs is the lowest that can satisfy the voltage constraints. From among the candidates for the lowest number of BESSs, the minimum total absolute value of active power flows of BESSs is chosen as the optimal solution. As the second step, the sizes of the BESSs are determined on the basis of optimal locations and prediction data about demand and the output of PVs. Finally, the author proposes a control algorithm for the BESSs, which are chosen by using the optimal placement algorithm. This control algorithm keeps the local bus voltages in the acceptable voltage range. The local BESSs control the active power to regulate the local bus voltages. An example of a radially structureed PV-supplied MG model is used to validate the proposed optimization method. The algorithm for controlling the BESSs is verified by analyzing simulation results and experimental results.

Chapter 6 [Conclusions, limitations, and future works] The author summarizes the proposals and concludes the thesis. Future works related to MG controllers are discussed.

CHAPTER 2: BATTERY ENERGY STORAGE SYSTEMS WITH VSI MODE AND DSTATCOM MODE

2.1. Introduction

Energy storage systems (ESSs) mediate between variable energy sources and variable loads. Without an ESS, energy sources must generate energy equal to instantaneous energy consumption to avoid shortfalls or excesses. An ESS allows storing the generated energy, thereby allowing generated energy to be used at another time. Electrical ESSs are one type of ESS. Other types of ESSs rely on oil in storage tanks, chemical energy storage, thermal energy storage, mechanical energy storage, or thermal mass.

The application of an electrical ESS to distribution in a power network can create a significant range of benefits. Specifically, electrical ESSs can be expected to contribute in the following areas.

- They allow electric energy time-shifting which is the purchase of inexpensive electrical energy when electricity prices are low, charging the electrical ESS with the purchased energy, and then, when the price is high, the energy that is stored in the ESS is used or sold. Furthermore, storage can provide similar time-shifting by storing excess energy production from RESs, such as wind or photovoltaics. Both are useful functions of an electrical ESS.
- Electrical ESSs are especially suitable for use in grid regulation. Following scheduled interchange flows, regulation controls interchange flows with other control areas. This control is used to regulate the grid frequency and to smooth temporary differences caused by oscillations in generation and load.
- Utility grid operators are required to regulate voltage so that it remains within a specified voltage range. Typically, it is necessary to manage reactance, which is caused by equipment that uses, transmits, or generates electricity and connects to the grid. To manage reactance, either voltage support resources are used to regulate reactive effects or specified power plants are used to generate reactive power to compensate for reactance. ESSs could replace these power plants in the system to compensate for reactive power.

- ESSs are highly useful for smoothing (damping) the variability of power from wind and PV systems. They are commonly used for this purpose.
- Electrical ESSs can be used for frequency response. Generally, this function of an ESS is similar to the regulatory function. However, when there is a sudden change in a generation unit or a distribution line, the ESS must rapidly react to system requirements, adapting in a period of seconds to less than a minute.
- ESSs can be used to defer equipment upgrades. For this purpose, ESSs are used to delay or avoid investments such as replacement of an aging or overstressed distribution transformer at a substation or resizing of distribution lines with larger wire sufficient to maintain distribution capacity and satisfy all load requirements.
- ESSs can provide voltage support on the distribution lines. Normally, the operator changes the tap position at the distribution substation and switches capacitors in line with load changes to regulate voltage to within specified limits. In this case, ESSs with minimal active power are effectively used to damp these voltage fluctuations.

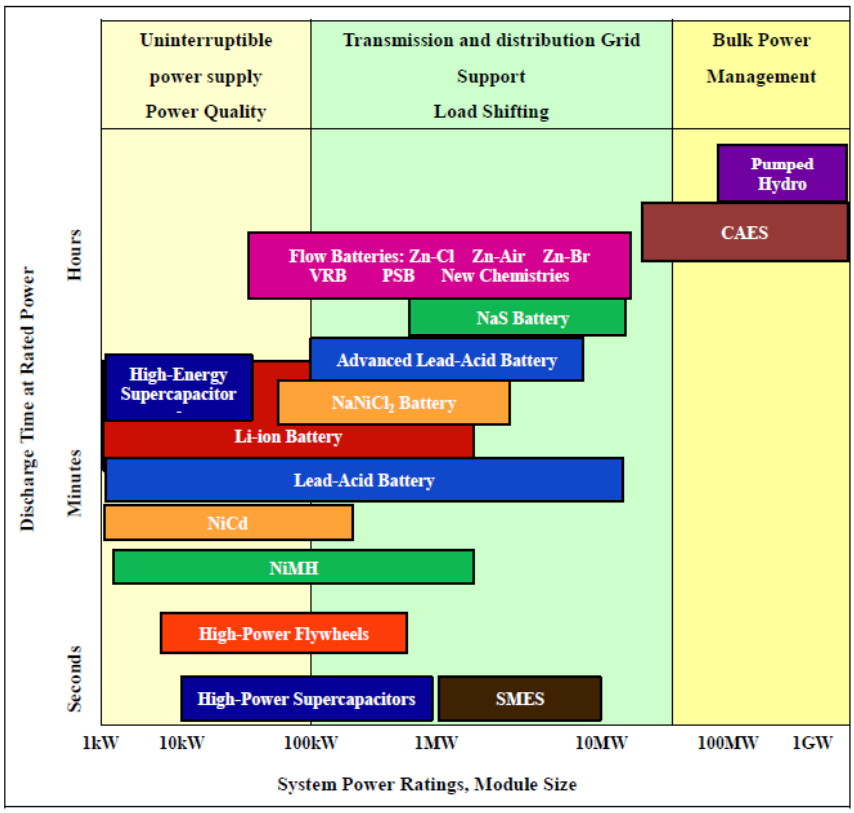

Fig. 2.1. Positioning of Energy Storage Technologies, Reproduced from [57].

The relations between storage technologies are illustrated in Fig. 2.1, which shows that compressed air energy storage and pumped hydro have correspondingly large capacities, which can reach 1 GW, and are capable of discharge across tens of hours. When lower power and shorter discharge times are acceptable, various electrochemical batteries and flywheels can be used, as seen in the figure. In recent years, Lithium-ion (Li-ion) batteries have become a fast growing platform for stationary storage applications. Li-ion batteries are the leading technology platform for plug-in hybrid electric vehicles and electric vehicles. These vehicles use large cells and battery packs with capacities up to 50 kWh. The popularity of Li-ion batteries in defense, aerospace, and automotive applications is increasing owing to their high energy density. Figure 2.1 shows that Li-ion battery banks can have a capacity higher than 1 MW and a discharge time at the rated power of more than 30 min. In this research, Li-ion batteries are assumed as the ESS.

In recent times, more powerful and responsive power converters have been built as a result of the development of power electronics, such as inverters that allow complex control algorithm for DERs through a combination of BESSs and an inverter. In this chapter, a structure with a central BESS that can operate in both VSI mode and DSTATCOM mode by changing the position of a mode switch is newly proposed. In VSI mode, the central BESS controls both active power, charging and discharging battery banks in the central BESS, and reactive power. In DSTATCOM mode, the central BESS controls reactive power flow by using the active power flow from the MG.

2.2. State of charge of BESS

The charge and discharge equations for Li-ion batteries are as follows [55]:

$$\begin{aligned} \text{Discharge}: C_{t+1} &= \ _{t} - \Delta \cdot P_t^{E,d} / \eta_{d} \\ \text{Charge}: C_{t+1} &= \ _{t} + \Delta \cdot \ _{t} \cdot \eta_{c} \end{aligned}, \tag{2.1}$$

where C_t is the energy stored in the battery at each time t,

$P_t^{E,d}$ is the power discharged by the battery bank during the period t,

$P_t^{E,c}$ is the power that is charged from the MG to the batteries during the period t,

Δt is the duration of each interval,

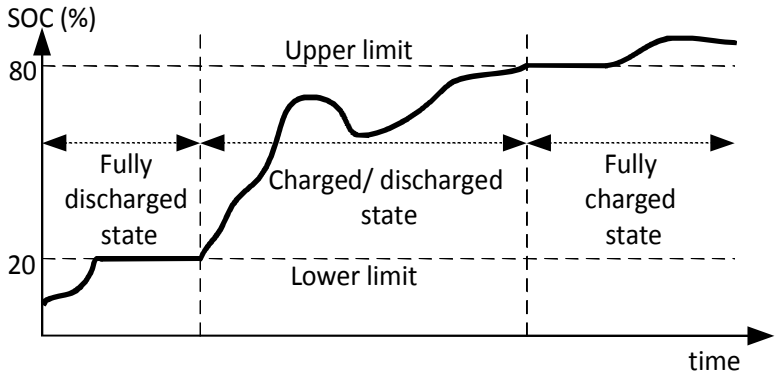

Fig. 2.2. Battery SOC.

η_d and η_c are the discharge and charge efficiencies, respectively. In this research, η_d and η_c are both taken as 100%.

The state of charge (SOC) of a BESS is the percentage of maximum energy that is stored in the batteries at the examined moment. To prolong battery life and to prevent damage, a minimum allowable SOC is set. To ensure efficient operation, the SOC should be maintained between the lower limit and upper limit (together, the SOC range). In this thesis, the SOC range is taken as from 20% to 80%.

Depending on the SOC of the BESS and the battery capacity constraints, there are three possible battery states, as follows (Fig. 2.2).

- Charge/discharge (state 1): 20% < SOC < 80%. In this state, the battery can be discharged to generate energy or charged to absorb energy.
- Fully charged (state 2): $SOC \geq 80\%$. In this state, the battery cannot be charged further.
- Fully discharged (state 3): $SOC \leq 20\%$. In this state, the battery cannot be discharged further.

2.3. Structure of BESS with VSI mode and DSTATCOM mode

The following parameters are used in this section.

i_a , i_b , i_c are the three-phase currents.

i_d is the d-axis (direct) current.

i_{d_ref} is the reference direct current.

i_q is the q-axis (quad) current.

i_{q_ref} is the reference quad current.

θ= *wt* is the angle between the fixed coordinate system αβ and the rotating coordinate system dq at each time *t*.

v_d is the direct voltage (d-axis).

v_{d_ref} is the reference direct voltage (d-axis).

v_q is the quad voltage (q-axis).

v_{q_ref} is the reference quad voltage (q-axis).

Q_{BESS}, P_{BESS} are the reactive power and active power of the BESS.

P_{BESS_ref} is the active power of the BESS ordered by the controller.

Q_{BESS_ref} is the reactive power of the BESS ordered by the controller.

V_{DC} is the direct current voltage of the C_{BESS}.

V_{DC_ref} is the reference voltage ordered by the controller.

Figure 2.3 shows the BESS structure used in this study. The BESS can be operated in both VSI and DSTATCOM modes. The BESS can control both reactive and active power. However, the difference between the two modes is the purpose of the active power control. Figure 2.4 shows the control schema of the BESS inverter.

The phase-locked loop (PLL) block synchronizes the fundamental component of the MG voltages. This block calculates the angle θ between the fixed coordinate system αβ and the rotating coordinate system dq at each time *t*.

The abc_to_dq block computes the quad component and direct component of the currents by using the dq0 transform of Eq. 2.2. A rotating coordinate system (dq0) is transformed from a three-phase time-domain signal to a stationary-phase coordinate system (abc) by apply this space vector transform to the synchronous reference, as determined by θ and provided by the PLL.

$$\begin{bmatrix} \\ \\ \end{bmatrix} = \frac{2}{3}\begin{bmatrix} \\ \\ \end{bmatrix}\begin{bmatrix} \\ \\ \end{bmatrix} \qquad (2.2)$$

The i_d and i_q currents are controlled by the current regulation loop, which includes two proportional integral (PI) controllers. The outputs of the controllers are the reference

voltages v_d and v_q that will be generated by the pulse-width modulation inverter acccording to Eqs. (2.3) and (2.4).

$$v_{d\_ref} = K_p(i_d - i_{d\_ref}) + K_i \int (i_d - i_{d\_ref}) \tag{2.3}$$

$$v_{q\_ref} = K_p(i_q - i_{q\_ref}) + K_i \int (i_q - i_{q\_ref}) \tag{2.4}$$

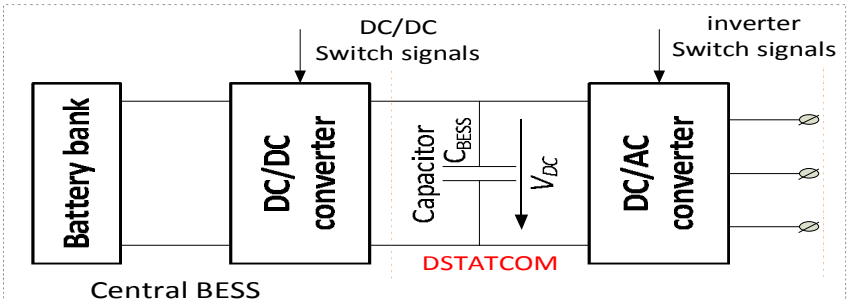

Fig. 2.3. Proposed BESS structure.

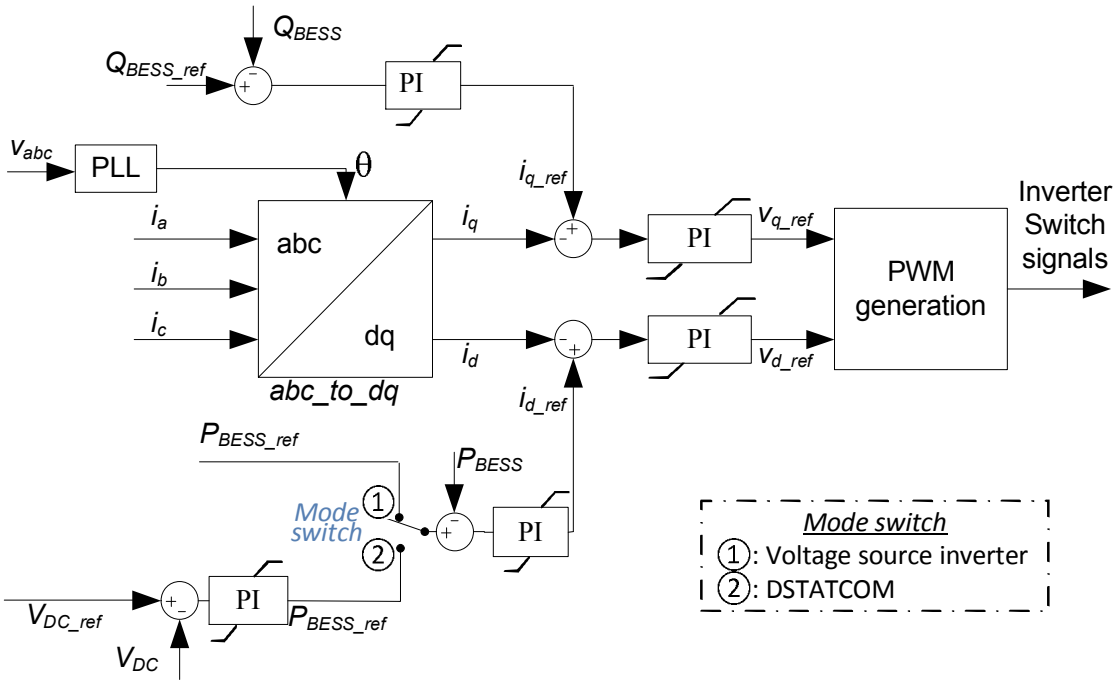

Fig. 2.4. Reactive power and active power control diagram of the BESS inverter.

The reference value of the quad current i_{q_ref} is inferred from the reference reactive power of BESS Q_{BESS_ref}. The reference value of direct current i_{d_ref} is calculated by the DC voltage regulator (in DSTATCOM mode) or by the reference active power of BESS P_{BESS_ref} (in VSI mode). In DSTATCOM, a voltage regulator keeps the capacitor voltage constant.

- VSI mode

In the charge/discharge state, the BESS turns the mode switch to position 1 (Fig. 2.4). In this mode, the BESS controls the active power and reactive power according to Eqs. (2.5) and (2.6). The BESS controls the active power for the charge and discharge processes. The BESS controls the reactive power to compensate for reactive power in the distributed system and can be used for any reactive power control application.

$$i_{q\_ref} = K_p(Q_{BESS\_ref} - Q_{BESS}) + K_i\int(Q_{BESS\_ref} - Q_{BESS}) \quad (2.5)$$

$$i_{d\_ref} = K_p(P_{BESS\_ref} - P_{BESS}) + K_i\int(P_{BESS\_ref} - P_{BESS}) \quad (2.6)$$

- DSTATCOM mode

In the fully discharged and fully charged states, the BESS turns the mode switch to position 2 (Fig. 2.4). In this mode, the BESS controls the DC/DC converter to disconnect the battery banks from the inverter. The active power of the BESS controls the voltage of the DC capacitor C_{BESS} by using a PI controller, as modeled in Eq. (2.9). The BESS controls the reactive power to compensate for the reactive power in distributed systems and can be used for any reactive power control application.

$$i_{q\_ref} = K_p(Q_{BESS\_ref} - Q_{BESS}) + K_i\int(Q_{BESS\_ref} - Q_{BESS}) \quad (2.7)$$

$$i_{d\_ref} = K_p(P_{BESS\_ref} - P_{BESS}) + K_i\int(P_{BESS\_ref} - P_{BESS}) \quad (2.8)$$

Here,

$$P_{BESS\_ref} = K_p(V_{DC\_ref} - V_{DC}) + K_i\int(V_{DC\_ref} - V_{DC}) \quad (2.9)$$

2.4. Modeling and simulation results.

2.4.1. Modeling BESS with VSI mode and DSTATCOM mode.

The BESS model is simulated by MATLAB/Simulink (Fig. 2.5).

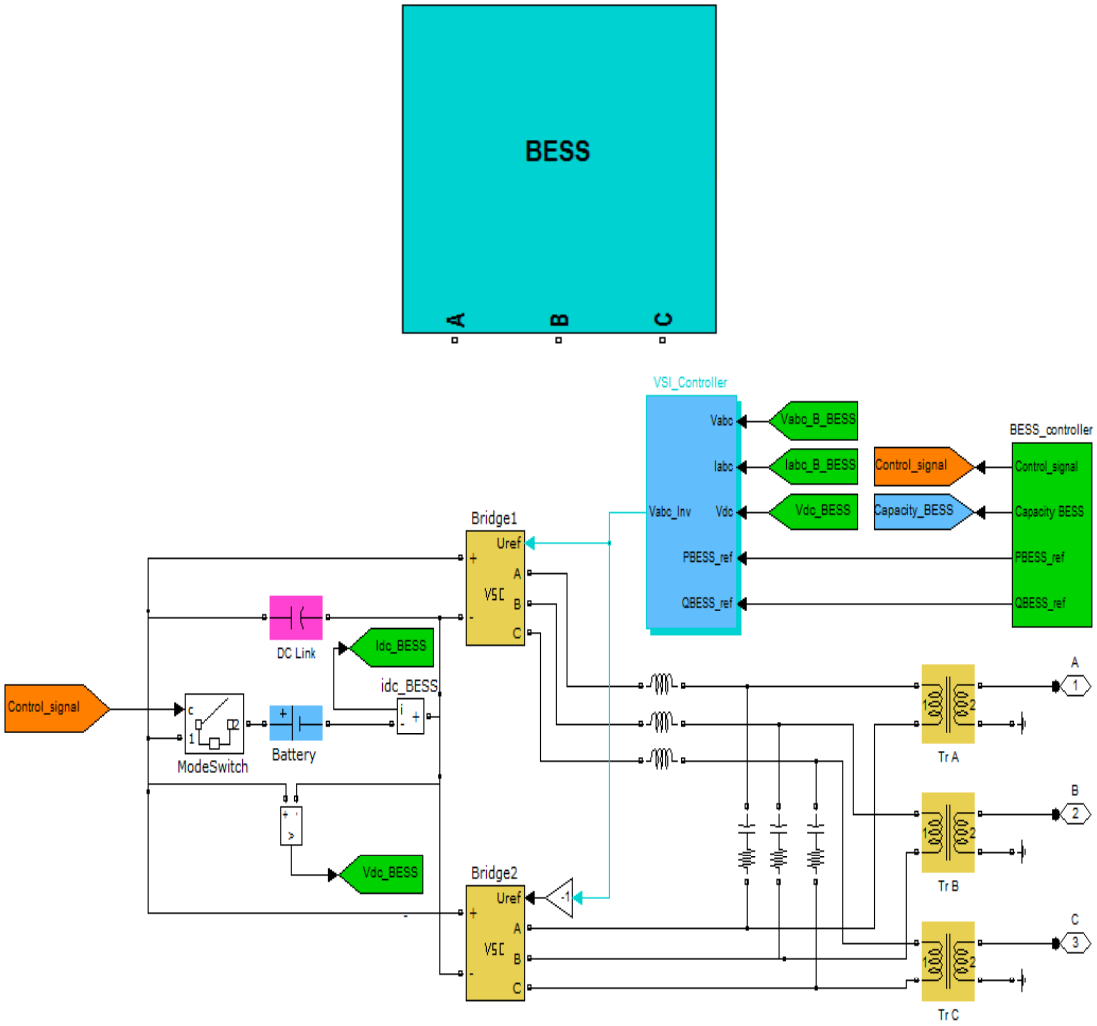

Fig. 2.5. Matlab/Simulink model of central BESS.

2.4.2. Simulation results.

The simulation is carried out with the simulation parameters as shown in Table 2.1. Figure 2.6 shows that the BESS was controlling the reactive power and active power at the same time. The reactive power and active power of the BESS were adapted to reach the reference value.

Table 2.1. Simulation parameters

Three-phase source	Base voltage	6600 V
	Base power	1 MVA
	Frequency	50 Hz

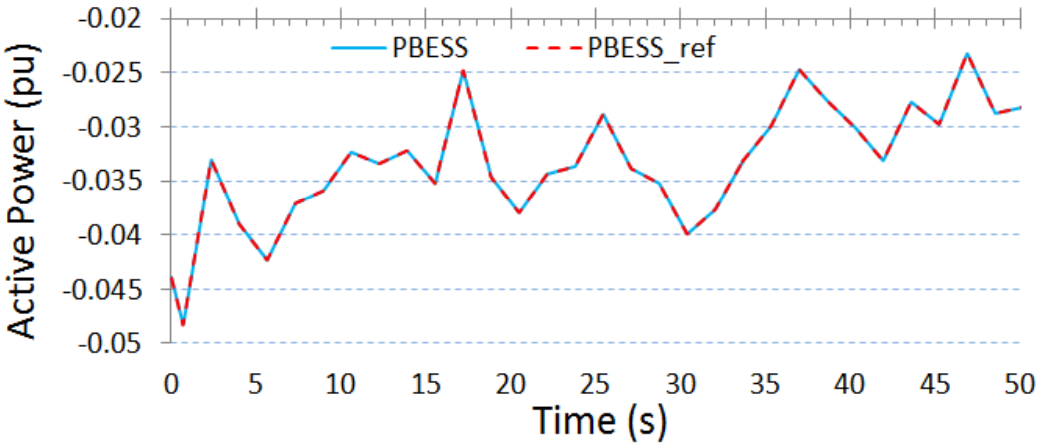

(a) Active power waveform of BESS.

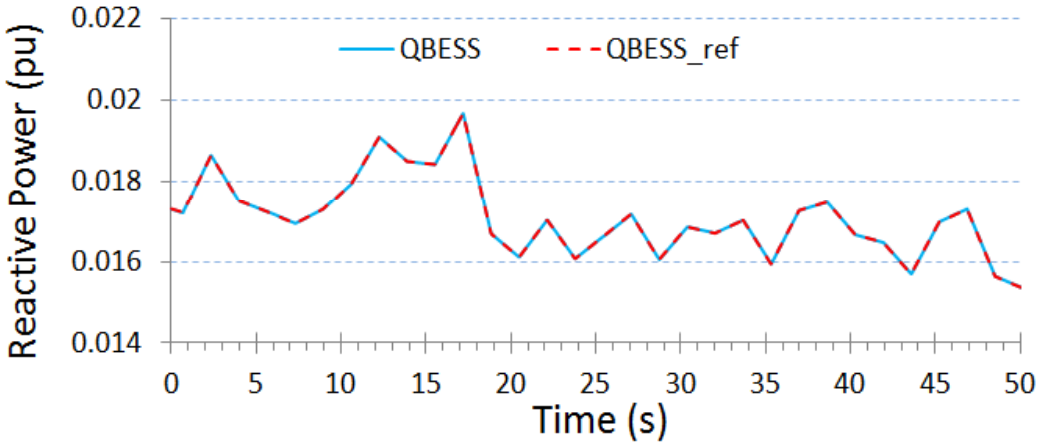

(b) Reactive power waveform of BESS.

Fig. 2.6. Active power and reactive power of BESS.

CHAPTER 3: COORDINATED CONTROL WITH A CENTRAL BESS, LOCAL BESSs, AND AN LRT TO STABILIZE THE VOLTAGE OF PV-SUPPLIED MG

3.1. Introduction

In an MG with high-penetration PV and a local BESS connected to each PV system, the load bus voltages may exceed the allowed voltage range as a result of environmental conditions affecting output power from the PV system and the capacity of the local BESS. In this chapter, a novel coordinated system comprising a central BESS, local BESSs, and an LRT control for stabilizing the load bus voltages is proposed. The author suggests installing a central BESS that can operate as either a VSI or a DSTATCOM at the grid interconnection point. In this proposed system, the central BESS controls the reactive power to regulate the load bus voltages of the MG. However, the power rating of the inverter in the central BESS is limited, and when the reactive power reaches the limit, the load bus voltage cannot be controlled by this method. Therefore, coordinated control between the central BESS and an LRT is needed to keep the load bus voltages in the acceptable voltage range. The central BESS consumes active power to charge its batteries when the output from PVs are smaller than demanded and the local BESSs are fully charged. Conversely, when the demand exceeds the output from PVs and the local BESSs are fully discharged, the central BESS discharges its batteries to generate active power to the MG. The target of the control algorithm for the local BESSs is to minimize the active power flow in the feeder where the local BESSs are connected. MATLAB/Simulink is used to simulate the PV-supplied MG model with BESSs and an LRT. Additionally, experiments are carried out on a real-time distribution network simulator. MGs with radial and loop structures are studied to validate the effectiveness of the proposed method. The simulation results and experimental results illustrate the success of the proposed control algorithm.

3.2. Proposed concept of coordinated control of central BESS, local BESSs, and LRT by an algorithm to stabilize the voltage of a PV-supplied MG

3.2.1. Network effects

This chapter studies an MG model with six buses (Fig. 3.1). The MG has five residential load groups and five PV systems. A central BESS connects to bus 1. Five

local BESSs are arranged on buses 2 through 6. Each residential load group handles active and reactive power for 100 houses, which are simulated from actual residential load data from 500 houses in Ota City, Japan. As alternative concepts for the next-generation power distribution system summarized in [1], loop and radial structures in an MG are considered in the present study to investigate the efficiency of the proposed technique. The convention for signs in the power–power vector directions is shown in Fig. 3.1.

In Japan, no voltage-range standard is imposed for 6.6-kV networks; however, a standard is in place for 200-V networks. Based on this standard [102] and on a low-voltage transformer ratio, the voltage-range scale of the 6.6-kV network is set at 0.982 to 1.018 per unit (pu). This range is used to regulate the load bus voltage. Thus, in this chapter, the voltages of load buses 2 to 6 are controlled. We assume that each load bus has equipment for monitoring the bus voltage and sends the obtained data to a central computer via a communication network.

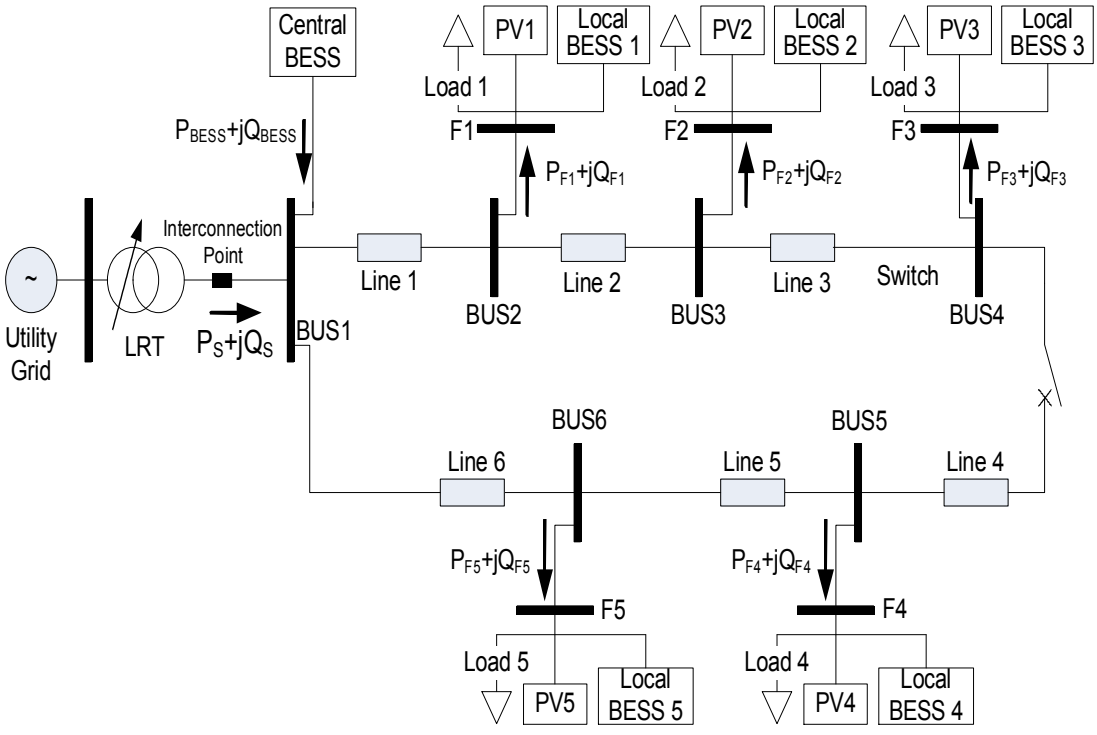

Fig. 3.1. MG model.

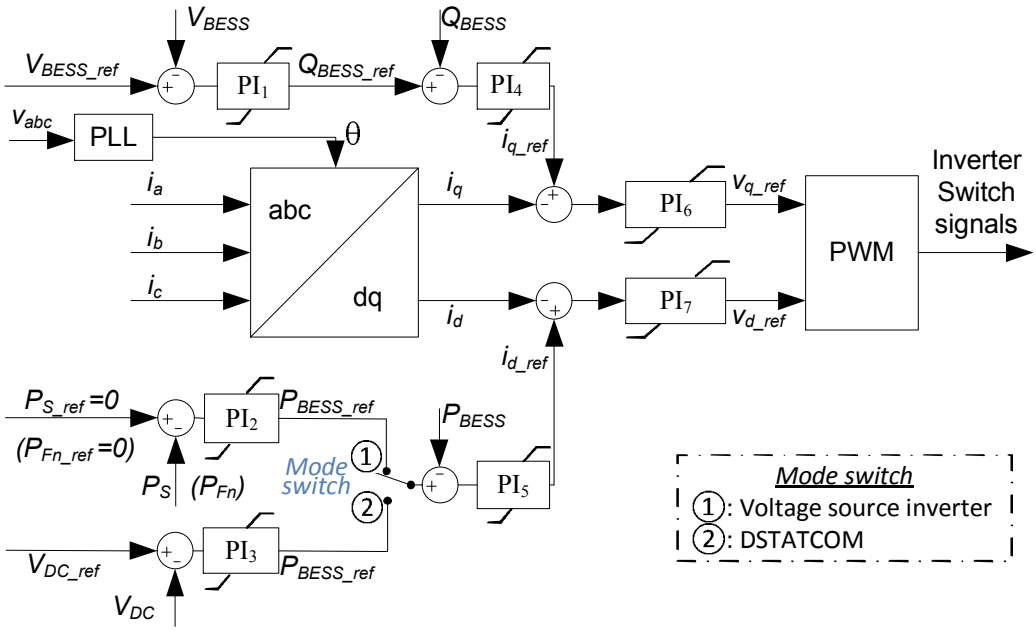

Fig. 3.2. Voltage, reactive power, and active power control diagram of the central BESS inverter.

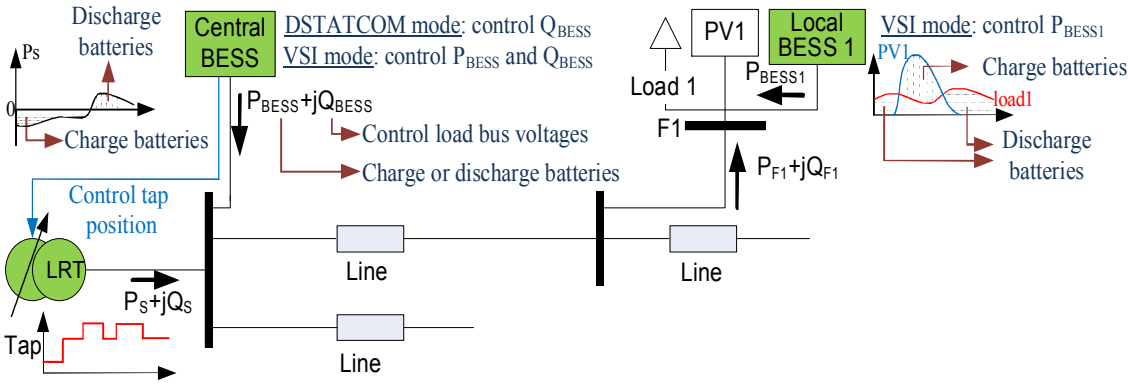

Fig. 3.3. Schematic diagram of proposed control algorithm.

3.2.2. Central BESS, local BESS and LRT control algorithms

In an MG with high-penetration PV and integrated local BESSs, the load bus voltages may exceed the specified voltage range as a result of environmental conditions that affect the output power from the PV systems and the capacities of local BESSs. Typically, an LRT is used to regulate the voltage at the interconnection point. However, because the voltage per step of the tap is large, the LRT cannot regulate the load bus

voltage to within the desired voltage range in some cases. In addition, the operating time of an LRT is large owing to the mechanical operation; moreover, the life cycle of an LRT depends on the number of tap position changes.

The author proposes installing a central BESS at the interconnection point with the MG. In the system, the central BESS controls the reactive power to regulate the load bus voltage of the MG. The advantage of using reactive power control is quick response, owing to the speed of a power converter built from semiconductor devices and a powerful microcontroller. The central BESS uses the active power to charge its batteries when the demand is lower than the amount generated by the PVs. Conversely, the central BESS discharges its batteries to generate active power to the MG when the demand exceeds the amount generated by the PVs. However, the battery capacity of the central BESS is limited. Therefore, when the batteries are fully discharged or charged, the central BESS cannot control the reactive power in this way to regulate the load bus voltage. The authors propose a structure with a central BESS that operates as both a VSI and a DSTATCOM. The DSTATCOM mode addresses the limits on battery capacity. When the battery of the central BESS installed at an interconnection point is fully discharged or charged, the central BESS switches to DSTATCOM mode to control reactive power flow by using active power flow from the MG. The DSTATCOM mode is not affected by battery capacity. However, the rated power of the central BESS is also limited. Thus, when the reactive power reaches the limit, the central BESS cannot regulate the load bus voltages. In this case, the tap position of the LRT is controlled to regulate the load bus voltage. The authors propose a coordinated control system for the central BESS and an LRT to stabilize the load bus voltages. A simple charge-and-discharge algorithm is proposed for local BESSs to control power flow at the load feeder. Figure 3.3 shows the schematic of the proposed control algorithm. The proposed coordinated control with a central BESS, an LRT, and local BESSs is described here.

(1) Central BESS control algorithm

The central BESS discharges its batteries to generate reactive and active power into the MG and receives active power from the MG to charge its batteries. When the BESS

battery banks are in the charge/discharge state, a PI controller minimizes the active power flow between the MG and the utility grid by using the active power of the BESS, with the aim of zeroing this according to Eq. (3.7). Moreover, another PI controller stabilizes the load bus voltages to within the range from V_{lower_limit} to V_{upper_limit} (see Eqs. (3.2) and (3.4)) by using the reactive power of the central BESS. However, the battery capacity is limited, and so the batteries may become fully discharged or fully charged. Consequently, when the battery banks of central BESS are fully charged or fully discharged, the active power flow between the MG and the utility grid and the reactive power flow of the central BESS cannot be controlled in the same way. In these instances, the central BESS is controlled in DSTATCOM mode. The central BESS controls the reactive power to maintain the required voltage level. In this case, a PI controller is used to control the voltage of the DC-link capacitor (V_{DC} in Fig. 2.3) according to Eq. (3. 6). Because PV sources are connected to every load bus, the load bus voltages depend on the active power from PV sources. Therefore, the central BESS must monitor all the load bus voltages for voltage control. The objectives of the proposed control method are (a) to minimize the active power flow between the MG and the utility grid and (b) to stabilize the load bus voltage by using the central BESS as a centralized controller. The centralized control algorithm is described here.

(i) Voltage control algorithm for the central BESS:

Step 1: Measure all load bus voltages and calculate V_{min} and V_{max} as follows.

$$V_{\min} = min(V_{BUSi}) \text{ , } V_{\max} = max(V_{BUSi}) \tag{3.1}$$

Step 2: Calculate the reference voltage of the central BESS.

$$V_{BESS\_ref} = \begin{cases} V_{BESS} + \Delta & \text{if } V_{\min} \le V_{lower\_limit} \\ V_{BESS} - \Delta & \text{if } V_{\max} \ge V_{upper\_limit} \\ V_{BESS} \end{cases} \tag{3.2}$$

Here, V_{BESS} is the voltage of the central BESS, V_{upper_limit} is the upper voltage limit, V_{lower_limit} is the lower voltage limit, and V_{BUSi} is the voltage magnitude of load bus i (i = 2, 3, …, 6).

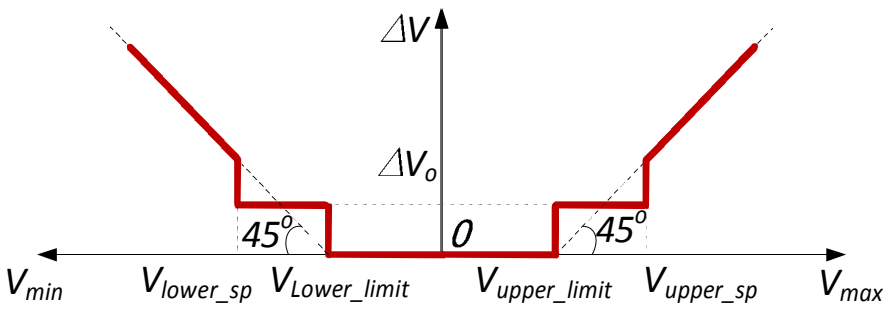

Fig. 3.4. Voltage adjustment curve.

Figure 3.4 shows the adjusted voltage (ΔV) curves. The value of ΔV is determined by the value of V_{max} or V_{min} and the load bus voltages. V_{lower_sp} and V_{upper_sp} are two voltage points that are set to calculate ΔV, as follows:

$$\Delta = \begin{cases} V_{\min} - \text{[illegible]} \le V_{lower\_sp} \\ \text{[illegible]} \ge V_{upper\_sp} \\ \Delta V_o \end{cases}. \quad (3.3)$$

When a voltage violation occurs at a load bus, if this voltage is outside the range [V_{lower_sp}, V_{upper_sp}], the central BESS quickly controls the reactive power to adjust this load bus voltage to lie in the range [V_{lower_limit}, V_{upper_limit}], using a large voltage step change to effect this. If this voltage is within the range [V_{lower_sp}, V_{upper_sp}], the central BESS adjusts the load voltage by using a small voltage step change ΔV_0 to regulate the load bus voltage within the limits.

Step 3: Control the reactive power of the central BESS.

$$Q_{BESS\_ref} = \text{[illegible]} \quad (3.4)$$

Here, Q_{BESS_ref} is a reference value used to control the central BESS's reactive power; this value is limited to the range from $Q_{BESS\_\min}$ to $Q_{BESS\_\max}$.

$$Q_{BESS\_ref} = \begin{cases} Q_{BESS\_\max} & \text{if } Q_{BESS\_ref} \ge Q_{BESS\_\max} \\ \text{[illegible]} & \text{if } \text{[illegible]} \le Q_{BESS\_\min} \\ Q_{BESS\_ref} \end{cases} \quad (3.5)$$

(ii) Active power control algorithm of the central BESS:

Step 1: Measure the active power P_S and calculate the SOC of the central BESS (SOC_{BESS}).

Step 2: If (($SOC_{BESS} \ge 80\%$) and ($P_S \le 0$)) or

((*SOC*$_{BESS}$ ≤ 20%) and (*P*$_S$ ≥ 0))

$$P_{BESS\_ref} = K_{p2}(V_{DC\_ref} - V_{DC}) + K_{i2}\int (V_{DC\_ref} - V_{DC}) \tag{3.6}$$

Else

$$P_{BESS\_ref} = K_{p3}(0 - P_S) + K_{i3}\int (0 - P_S) \tag{3.7}$$

End

Here, P_s is the active power flow between the MG and the utility grid; P_{BESS_ref} is the reference value of the central BESS active power, limited to the range from P_{BESS_min} to P_{BESS_max} in Eq. (3.8); and V_{DC} is the DC-link inverter voltage.

$$P_{BESS\_ref} = \begin{cases} P_{BESS\_\max} & if\ P_{BESS\_ref} \geq P_{BESS\_\max} \\ P_{BESS\_\min} & if\ P_{BESS\_ref} \leq P_{BESS\_\min} \\ P_{BESS\_ref} & \end{cases} \tag{3.8}$$

(2) Decentralized local BESS$_i$ control algorithm

Power flow causes the load bus voltage to fluctuate. Thus, the goal of the local BESS control algorithm is to reduce the power flow in the MG by reducing the power flow in the load bus to which the local BESS$_i$ is connected. The local BESS uses only controlled active power. The reactive power of the local BESS is always zero. When the battery bank of local BESS$_i$ is in the charge/discharge state, the BESS controls the active power to minimize the active power flow in feeder *j* by using a PI controller. The goal of the local BESS control algorithm can therefore be stated as minimizing the active power flow in the feeder to which BESS$_i$ is connected. The proposed algorithm is described here.

Step 1: Measure active power P_{Fj} at load bus *i*, where local BESS$_i$ is connected, and calculate SOC_{BESSi} for the local BESS$_i$.

Step 2: If ((SOC$_{BESSi}$ ≥ 80%) and (P_{Fi} ≤ 0))

or if ((SOC_{BESSi} ≤ 20%) and (P_{Fi} ≥ 0)),

P_{BESSi_ref} = 0

Else,

$$P_{BESSi\_ref} = K_{p4}(0 - P_{Fj}) + K_{i4}\int (0 - P_{Fj}) \tag{3.9}$$

End

Here, P_{BESSi_ref} is the reference value used to control the active power in the local BESS$_i$, and this value is limited to the range from P_{BESSi_min} to P_{BESSi_max}, as in Eq. (3.10).

$$P_{BESSi\_ref} = \begin{cases} P_{BESSi\_\max} & if\ P_{BESSi\_ref} \geq P_{BESSi\_\max} \\ P_{BESSi\_\min} & if\ P_{BESSi\_ref} \leq P_{BESSi\_\min} \\ P_{BESSi\_ref} & \end{cases} \quad (3.10)$$

(3) Centralized algorithm to control LRT tap position

The LRT coordinates with the central BESS to stabilize the load bus voltages. The central BESS has higher priority for its actions than the LRT does. However, the apparent power rating of the BESS is limited; thus, the LRT tap position must be controlled to ensure that the load bus voltage is stable within the acceptable limit when the BESS reactive power approaches the limit. The control algorithm is described as follows.

Step 1: Wait for LRT to be ready to control

Step 2: If ($S_{BESS} > S_{limit}$) or (abs(Q_{BESS}) > Q_{limit})

If $Q_{BESS} > 0$,

Increase tap position

Else

Decrease tap position

End

End

Here, S_{BESS} and Q_{BESS} are the apparent and reactive power of the central BESS, respectively, and S_{limit} and Q_{limit} are the respective conditional values of the LRT tap control. We note that these parameters are different from S_{BESS_max} and Q_{BESS_max}. In some cases, the reactive power flow between the MG and the utility grid must be controlled according to the power factor standard; hence, Q_{limit} is used to allow reactive power flow between the MG and the utility grid. S_{limit} is used to ensure that the inverter always operates at no more than the rated power. Figure 3.5 shows the BESS's capability during first-quadrant operation. The green curve indicates the maximum apparent power curve with Q_{limit}; the red curve shows the apparent power curve limit. Under normal conditions, the central BESS operates inside the red curve. However, under transient conditions, the central BESS's apparent power can reach up to the green curve. The tap position is changed in single steps. The time required for a one-step change is 3 s.

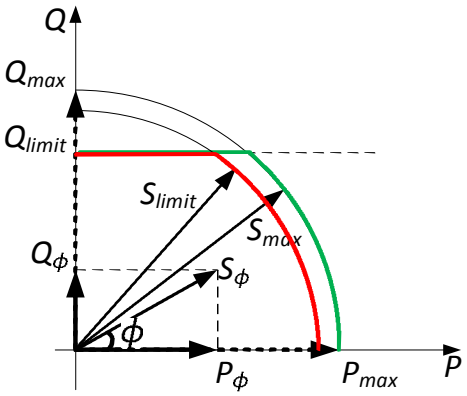

Fig. 3.5. BESS capability.

3.3. Modeling and simulation results

The simulation parameters are listed in Table 3.1. The components of the MG are modeled by using the MATLAB/Simulink software (Fig. 3.6). The simulation time is 48 h. Figure 3.7 shows the PV power and the resident load power flow of the five groups. The PV data represent a sunny day and a cloudy day. The range of values for the active and reactive power was [–1, 1] pu. The LRT has 17 tap positions. When the LRT tap position is zero, the LRT secondary voltage is the base voltage. The impedance of copper wire with 60 mm^2 cross section is used in the simulation model.

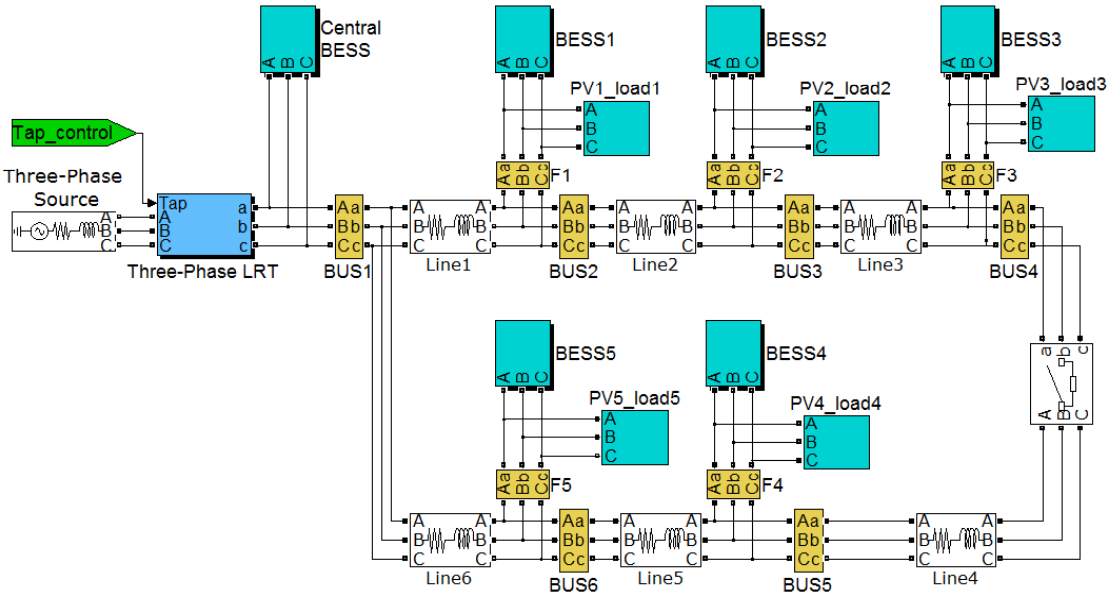

Fig. 3.6. MATLAB /Simulink of the MG model.

Table 3.1. Simulation and experimental parameters

		Simulation	Experiment
Central BESS	Capacity	2 MWh	7.5 kWh
	Power rating	1.5 MVA	10 kVA
Local BESSs: BESS1, BESS2, BESSS3, BESS4, BESS5	Capacity	1 MWh	7.5 kWh
	Power rating	0.3 MVA	2 kVA
Three-phase source	Base voltage	6600 V	200 V
	Base power	1 MVA	10 kVA
	Frequency	50 Hz	50 Hz
Line 1	Impedance	2 + j2.04 Ω	0.291 + j0.158 Ω
	Length	6.4 km	1 km
Line 2	Impedance	2 + j2.04 Ω	0.290 + j0.162 Ω
	Length	6.4 km	1 km
Line 3	Impedance	2 + j2.04 Ω	0.285 + j0.161 Ω
	Length	6.4 km	1 km
Line 4	Impedance	2 + j2.04 Ω	0.301 + j0.156 Ω
	Length	6.4 km	1 km
Line 5	Impedance	2 + j2.04 Ω	0.296 + j0.169 Ω
	Length	6.4 km	1 km
Line 6	Impedance	2 + j2.04 Ω	0.280 + j0.160 Ω
	Length	6.4 km	1 km
LRT	Tap	17 positions [-8, +8]	9 positions [0, 8]
	Voltage step $\triangle U$ per tap	0.0045 pu	0.02 pu
Controller sample time		0.02s	0.2 s
Centralized BESS controller parameters	$[V_{lower\_limit}, V_{upper\_limit}]$	[0.982, 1.018] pu	[0.982, 1.018] pu
	$[V_{lower\_sp}, V_{upper\_sp},]$	[0.9815, 1.0185] pu	[0.98, 1.02] pu
	S_{limit}	1 pu	0.72 pu
	Q_{limit}	0.8 pu	0.56 pu
	ΔV_0	0.0001 pu	0.0001 pu

3.3.1. MG without BESS and LRT

This section explains the simulation results of an MG without a BESS, which is not suitable for the proposed approach. Figures 3.8 and 3.9 show that the MG load bus voltages oscillate outside the allowed voltage range. It is notable that the deviation in the MG with a loop structure is smaller than that in the MG with a radial structure.

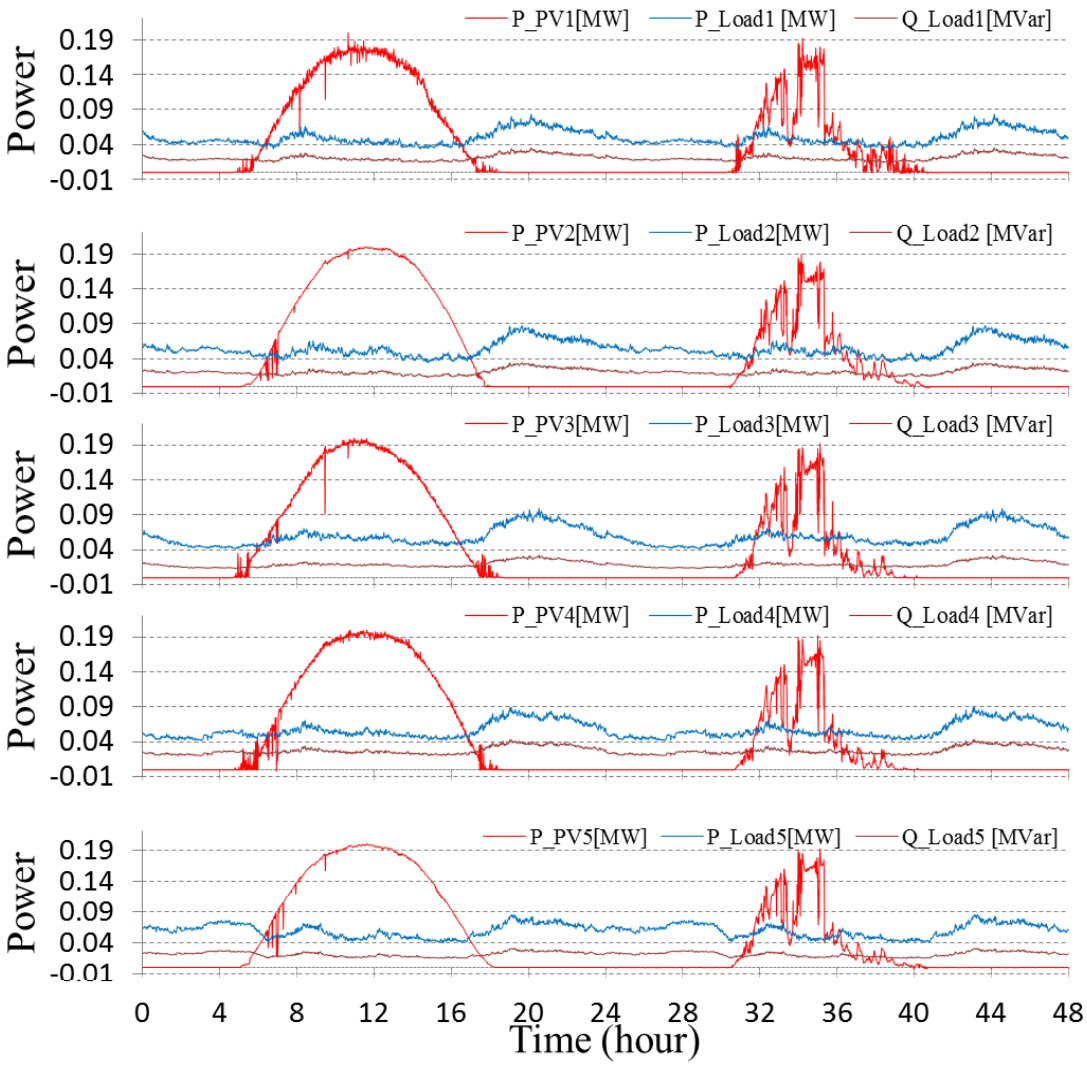

Fig. 3.7. Daily active power output of the PV and daily residential load profile over 48 h.

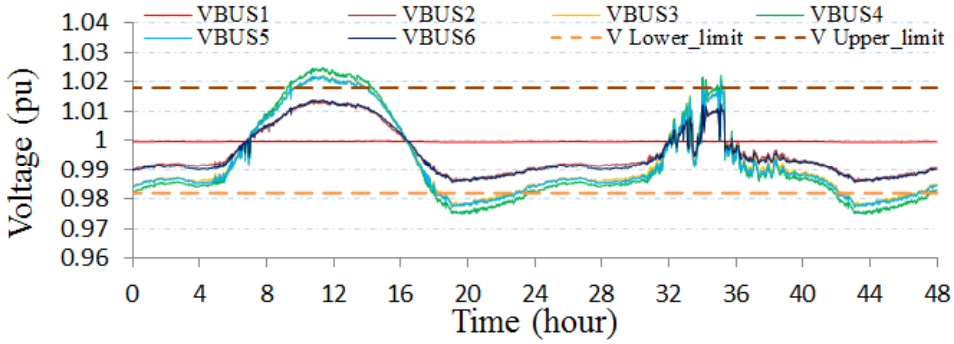

Fig. 3.8. Load bus voltage profile of an MG with a loop structure without LRT and BESS control.

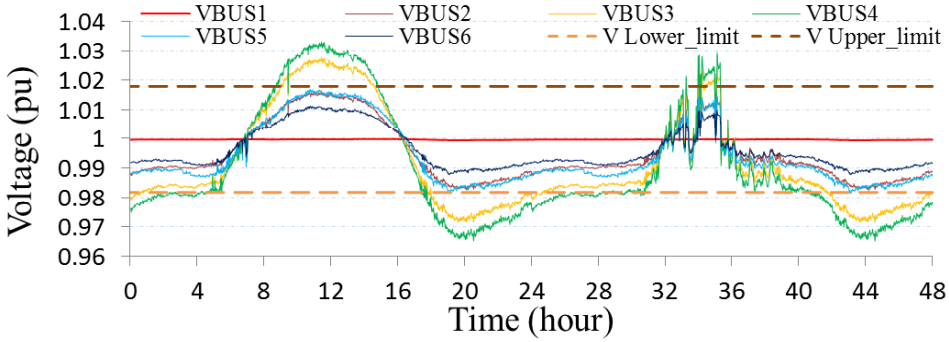

Fig. 3.9. Load bus voltage profile of an MG with a radial structure without LRT and BESS control.

3.3.1. MG with BESSs and LRT

This section describes the simulation with a central BESS, local BESSs, and an LRT controlled by the proposed method. Figure 3.10 shows the simulation results for an MG with a loop structure. Figure 3.11 shows the results for an MG with a radial structure. Figures 3.10(c) and 3.11(c) show the SOCs of the central and local BESSs over 48 h. The proposed method is effective in keeping the SOC of the central BESS and local BESSs to within 20%–80% (i.e., in the charge/discharge state).

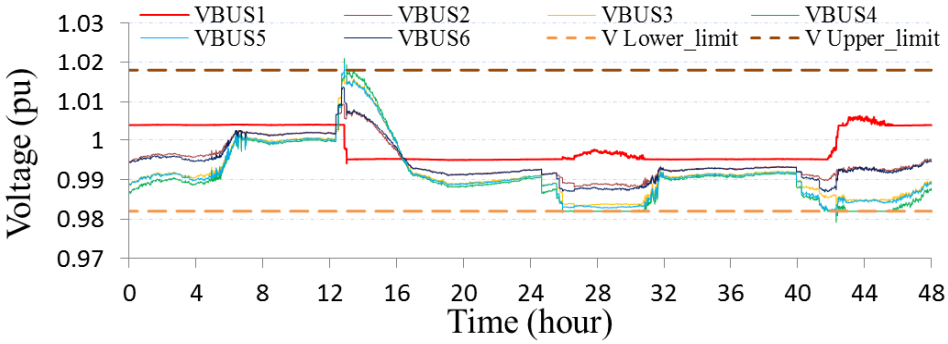

(a) Voltage profile at load buses

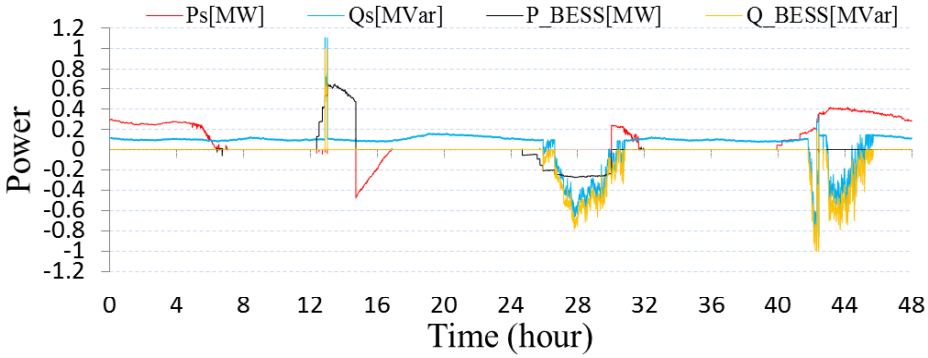

(b) Power flow at the interconnection point and central BESS

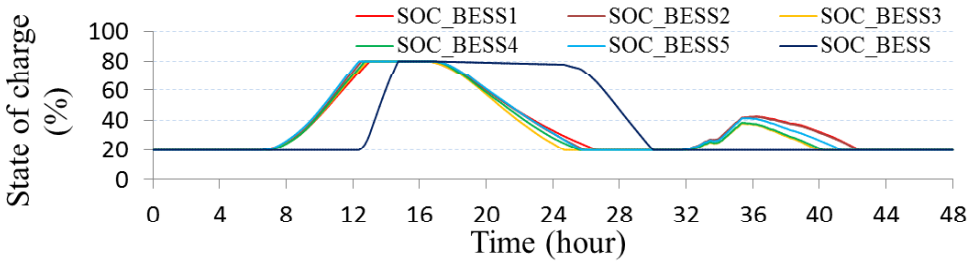

(c) BESSs energy storage

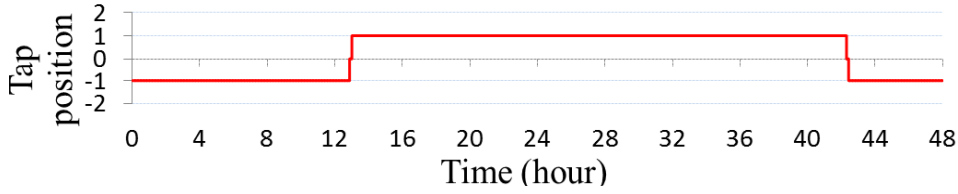

(d) LRT tap position

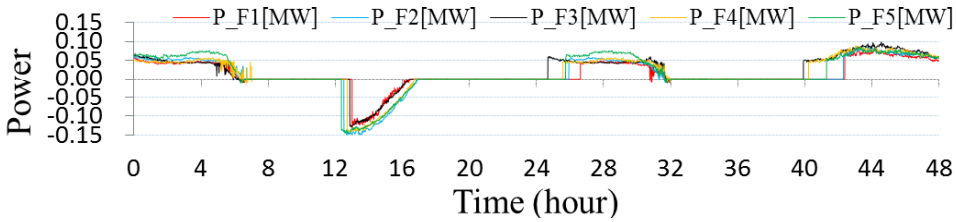

(e) Active power flow at the MG load feeders

Fig. 3.10. MG with a loop structure and the proposed control structure.

Figures 3.10(a) and 3.11(a) show that the load bus voltages V_{BUS2} to V_{BUS6} stayed

between 0.982 and 1.018 pu for the full 48 h. When each local $BESS_i$ was fully charged or discharged, it could not control the power flow at the local feeder F*i*. The load bus voltages exceeded the allow range as a result of output from the PV system and the load power flow; however, the central BESS instantly corrected the load bus voltages to within the permitted range by using the BESS reactive power and LRT tap position. Figure 3.10 shows that when the local BESSs were fully charged, from hour 12, the load bus voltages were rapidly elevated. Immediately, the central BESS controlled the reactive power to decrease the load bus voltages; however, the reactive power reached the limit, and at that time the central BESS controlled the tap position of the LRT to keep the load bus voltages to within the allowed voltage range. At the moment of changing the tap position, the load bus voltages exceeded the allowed voltage range until the tap position of the LRT finished changing to an appropriate position. The time for which the constraints were violated was the operating time of LRT, chosen as 3 s here. At hour 26, the load bus voltages were lower than the lower limit as a result of increased load and the fully discharged state of local BESSs. The central BESS controlled the reactive power to keep the load bus voltages in the allowed voltage range and generated active power to supply the MG by discharging its batteries. At hour 30, the central BESS was fully discharged; the BESS was then switched to DSTATCOM mode to control reactive power, which kept the load bus voltages within the permitted voltage range. The use of the DSTATCOM mode ensures that the central BESS can always control the reactive power to regulate the load bus voltages. This mode helps to free the proposed method from dependence on the capacity of the batteries in the central BESS. For the cloudy-day case, because the local BESS controlled the power flow at the local feeder, the PV output did not influence the load bus voltages. The voltage drop of the radial structure was larger than that in the loop structure, as shown in Figs. 3.8 and 3.9. Therefore, compared with the reactive power in an MG with a radial structure, the reactive power of the central BESS in the MG with a loop structure was small. When the value of the reactive power exceeded the limit, the LRT tap position changed, which occurred between hours 12 and 16 and between hours 40 and 44, as shown in Figs. 3.10 and 3.11. In addition, the number of tap position changes (NoTC) is smaller

in the MG with a loop structure than in that with a radial structure, as shown in Figs. 3.10(d) and 3.11(d).

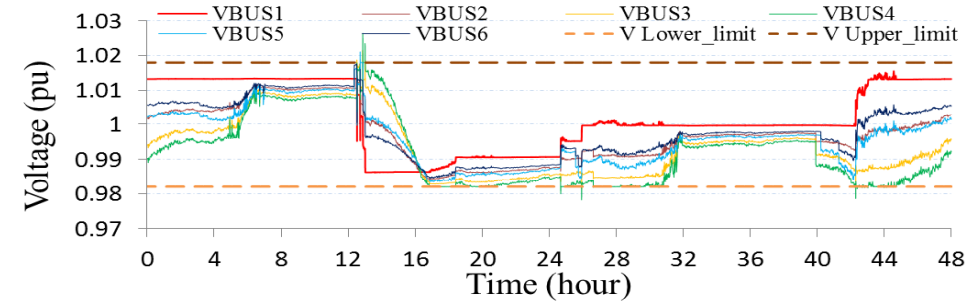

(a) Voltage profile at the load buses

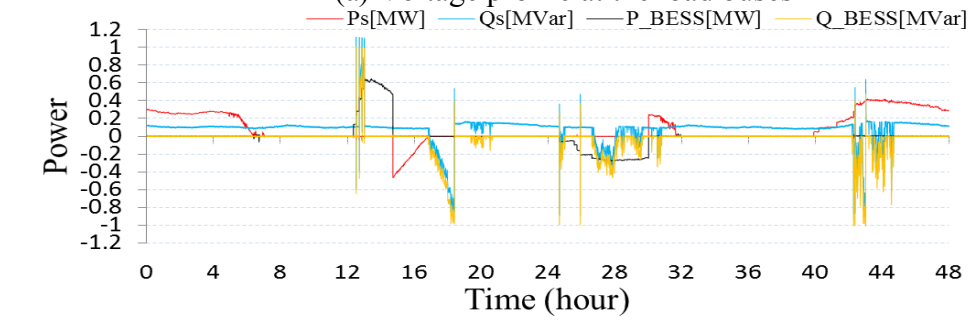

(b) Power flow at the interconnection point and central BESS

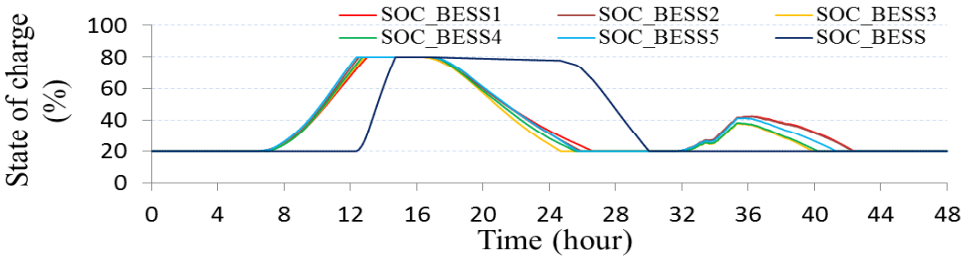

(c) BESSs' energy storage

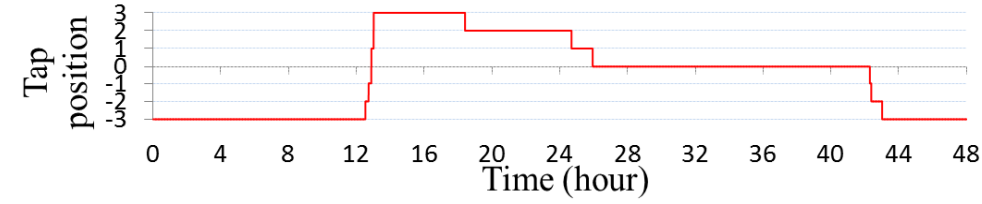

(d) LRT tap position

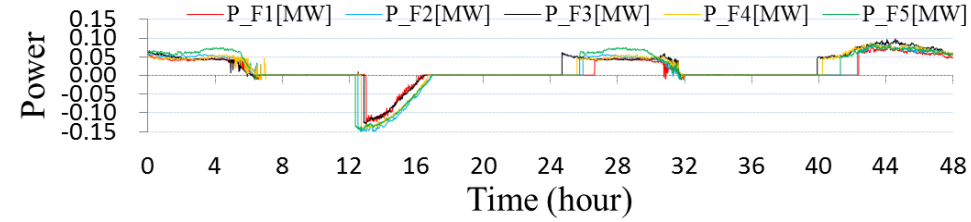

(e) Active power flow at the MG load feeders

Fig. 3.11. MG with a radial structure with the proposed control structure.

Table 3.2. NoTC of simulation.

NoTC		LRT only	LRT and local BESSs	Proposed method
Simulation	Loop structure	14	7	4
	Radial structure	29	13	12

Figures 3.10(e) and 3.11(e) show that when the local BESS battery banks are in the charge/discharge state, the active power at the feeders where the local BESSs are connected is minimized. Thus, the load bus voltage drops are reduced, as shown in Figs. 3.8 and 3.10(a) and Figs. 3.9 and 3.11(a). This can be seen particularly between hours 20 and 24.

Figures 3.9(b) and 3.11(b) show that the active power flow between the MG and the utility grid is minimized by the active power of the BESS when the central BESS is in the charge/discharge state from hour 12.5 to hour 30.

Table 3.2 shows the NoTC in three simulation cases. In the first case, no BESS is installed in the MG model, and the LRT is controlled to stabilize the load bus voltages. In the second case, five local BESSs are installed at five local load buses. In the third case, central and local BESSs are installed. In the MG with a loop structure, the third case has the smallest NoTC. Using the central BESS voltage control, the NoTC is reduced by 71.4% relative to the first case and by 42.8% relative to the second case. In the MG with a radial structure, these differences are 58.6% and 7.7%, respectively.

3.4. Experimental results

3.4.1. Real-time distribution network simulator: ANSWER

The real-time distribution network simulator at Waseda University in Japan is a scaled-down version of an actual 6.6-kV distribution system to a 200-V distribution system (Fig. 3.12). The bus voltage and equipment current are respectively 1/33rd and 1/25th of the bus voltage and current of an actual 6.6-kV system. The equipment includes program control equipment, a digital measuring instrument, equipment for transmitting voltage, an automatic voltage regulator, an LRT, a step voltage regulator (SVR), 18 single-phase constant-impedance loads, 15 distribution lines with switches,

and 15 inverter apparatuses modeled as PV sources, load, BESS, DSTATCOM, and DG. The states of the sectionalizing switches (open or closed), SVR (tap position), load profile, and inverter output can be controlled over time by a personal computer using dSPACE 1105.

Table 3.1 lists the experimental parameters. In this experiment, the inverter is used to simulate the PV sources, load, and BESS. The range of values for the active and reactive power in the central BESS is [–0.72, 0.72] pu. When the LRT tap is in position four, the LRT secondary voltage is the base voltage.

3.4.2. Experimental results

Figure 3.13 shows the PV1 output and residential load 1 curves used in this experiment. These data have the same shape as the simulation data, which have been appropriately scaled to the experimental conditions. The remaining PV and load data are also scaled at the same ratio.

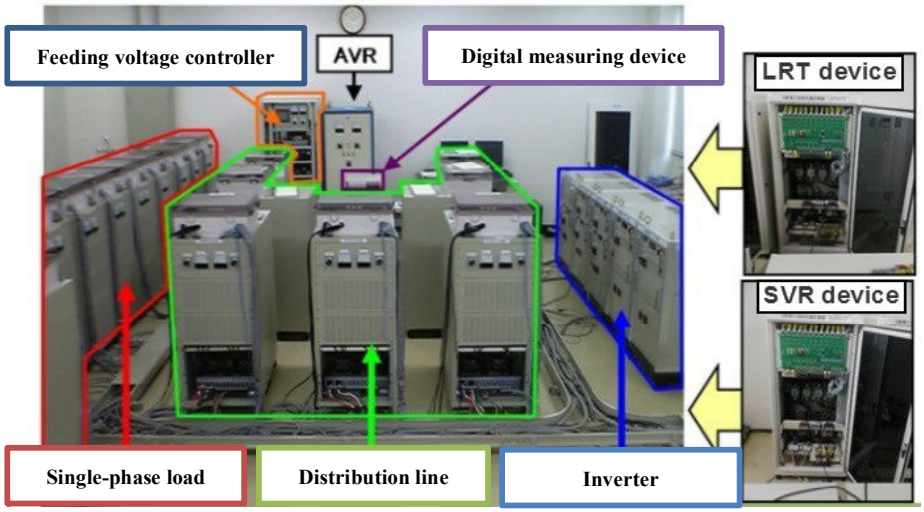

Fig. 3.12. Real-time distribution network simulator (ANSWER: Active Network System with Energy Resources)

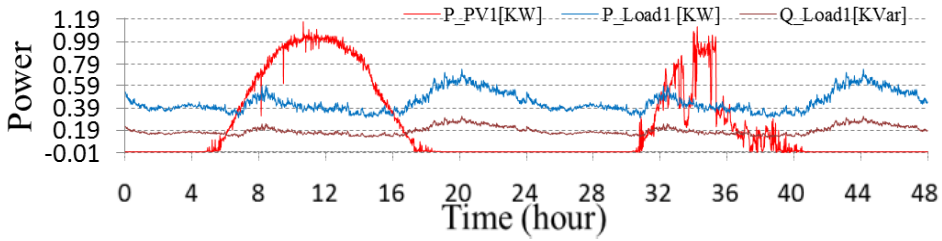

Fig. 3.13. Experimental waveforms of daily active power output of the PV and daily residential load profile over 48 h.

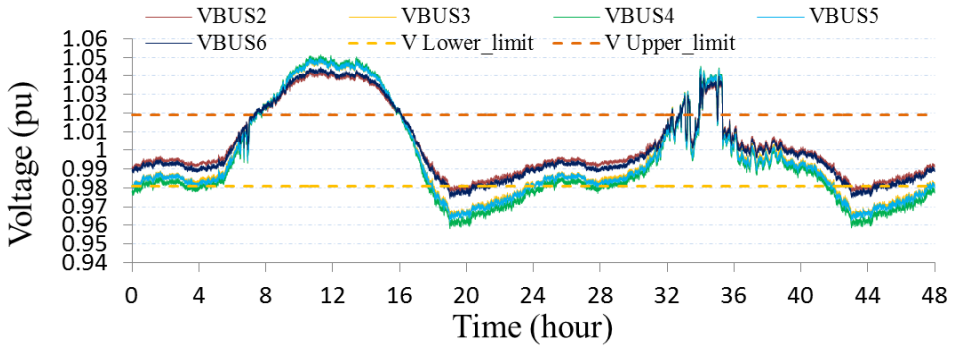

Fig. 3.14. Experimental waveforms of load bus voltages of an MG with a loop structure, without LRT and BESS control.

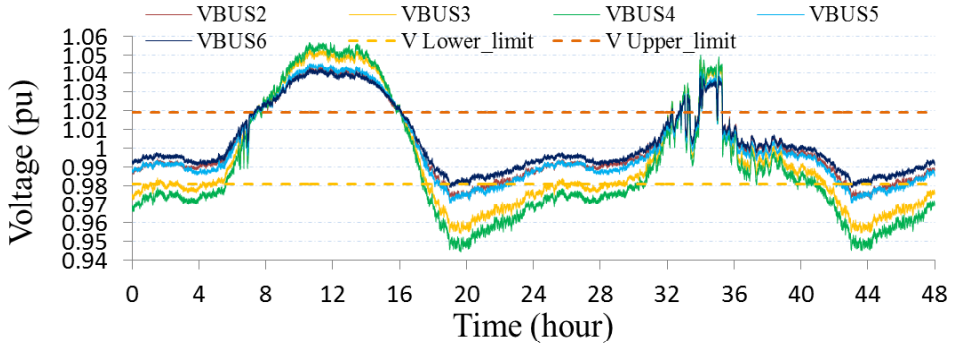

Fig. 3.15. Experimental waveforms of load bus voltages of an MG with a radial structure, without LRT and BESS control.

Figures 3.14 and 3.15 show that the MG load bus voltages fluctuate beyond the voltage-range when no BESSs are connected to the MG. However, when a central BESS, local BESSs, and an LRT controlled by the proposed method, the load bus voltages V_{BUS2} to V_{BUS6} remained within the prescribed limits, as shown in Figs. 3.16(a) and 3.17(a). At the hour 14.3, the local BESSs were fully charged, and the surplus power from the PV raised the load bus voltages over the allowed voltage; immediately, the central BESS controlled the reactive power to regulate the voltage. The SOCs of the central and local BESSs were kept within 20%–80%, as shown in Figs. 3.16(c) and 3.17(c). Figures 3.16(b) and 3.17(b) show the power flow at the interconnection point and the central BESS. When the battery of the central BESS was fully discharged or fully charged, the BESS switched to DSTATCOM mode to control the voltage by using reactive power. However, when the reactive power reached the limit, the central BESS

changed the LRT tap position to regulate the load bus voltages, as shown in Figs. 3.16 and 3.17 from hour 40 to hour 44.

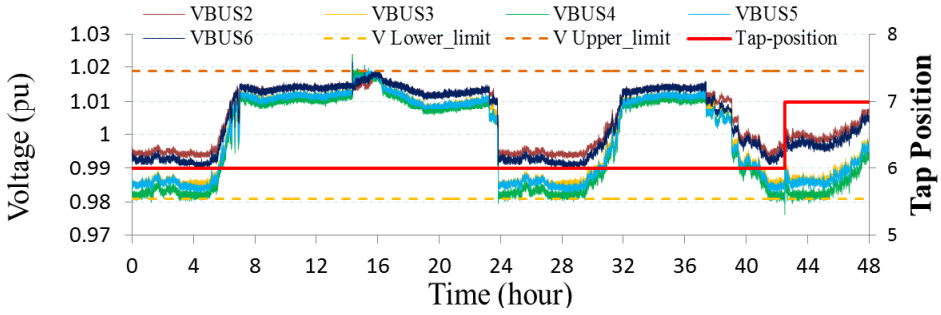

(a) Voltage profile at the load buses and tap position

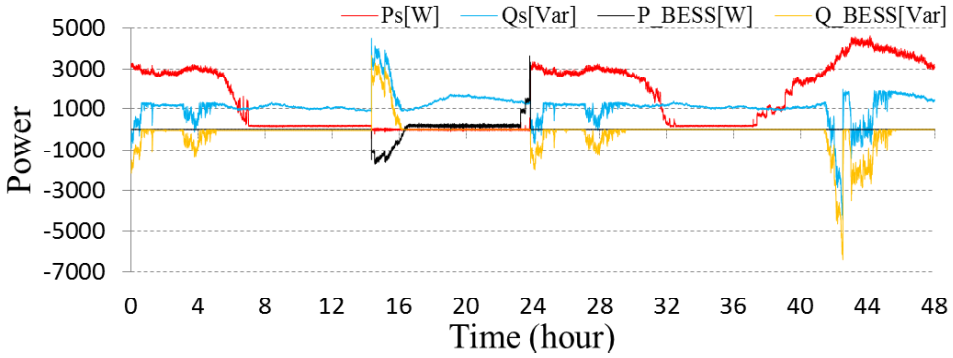

(b) Power flow at the interconnection point and central BESS

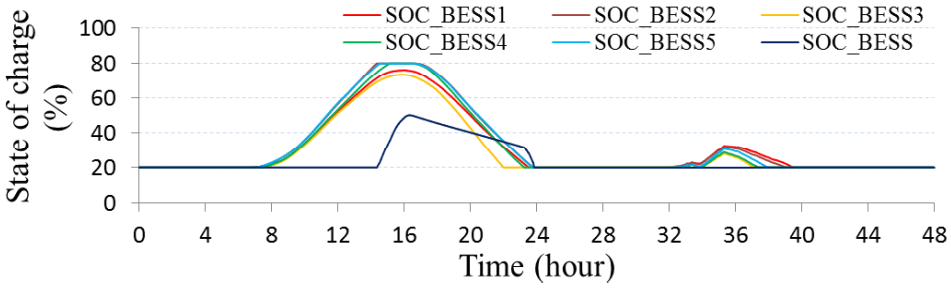

(c) BESS energy storage

Fig. 3.16. Experimental waveforms of MG with a loop structure, with the proposed control structure.

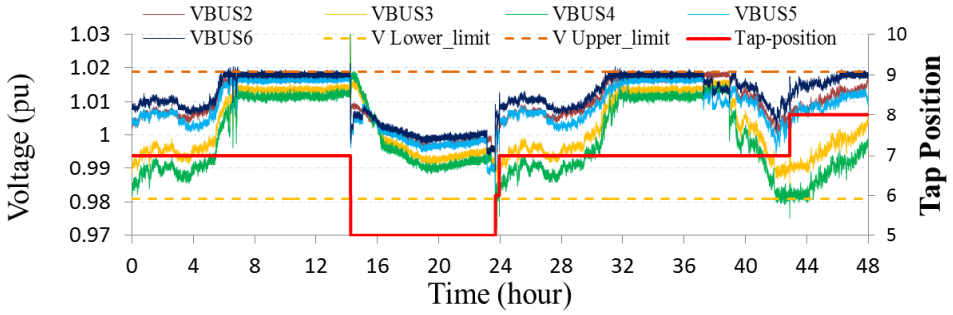

(a) Voltage profile at the load buses and tap position

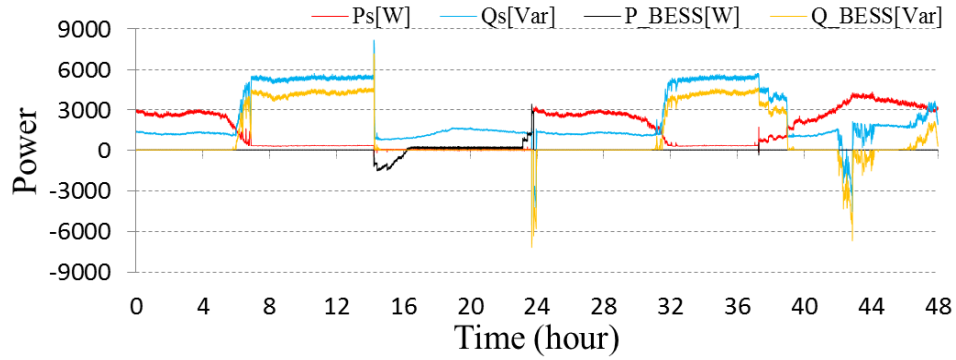

(b) Power flow at the interconnection point and central BESS

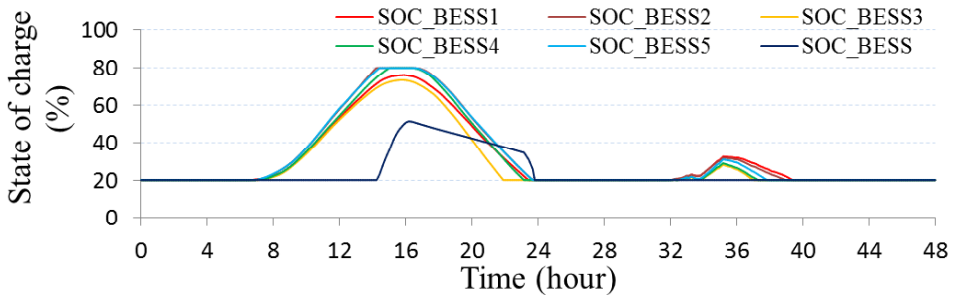

(c) BESS energy storage

Fig. 3.17. Experimental waveforms of MG with a radial structure, with the proposed control structure.

3.5. Comparison with conventional methods

In this section, the proposed method is compared with conventional methods. In the conventional method, the LRT tap position is controlled to keep the load bus voltage in the allowable voltage range but not BESSs are installed.

(1) A central BESS with and without DSTATCOM mode. Figures 3.18 and 3.19 are magnifications of hour 42 for an MG with a radial structure, as captured during the

experiment on ANSWER. From hour 42, the battery banks of the central BESS were fully discharged, as shown in Fig. 3.17(c). Figure 3.18 shows that when in DSTATCOM mode the central BESS still controlled the reactive power to regulate the minimum load bus voltage to within the lower limit. Figure 3.19 shows that without the DSTATCOM mode, the central BESS controlled the LRT tap position to regulate the load bus voltage; nevertheless, the controller could not find an appropriate tap position to keep the load bus in the allowed voltage range, leading the tap position to change continuously. Figure 3.18(a) shows the rapidity of the central BESS controller compared with the operating time of the LRT, shown in Fig. 3.19.

Figures 3.10, 3.11, 3.16, and 3.17 show the advantages of allowing multi-mode operation in the central BESS. From hour 30, the batteries of the central BESS are fully discharged, as shown in Figs. 3.10(c) and 3.11(c); the central BESS changes to DSTATCOM mode and controls the reactive power flow and DC-link voltage. The use of DSTATCOM mode ensures that the central BESS can always control the reactive power to regulate the load bus voltages. This mode helps the proposed method to not depend on the capacity of batteries in the central BESS.

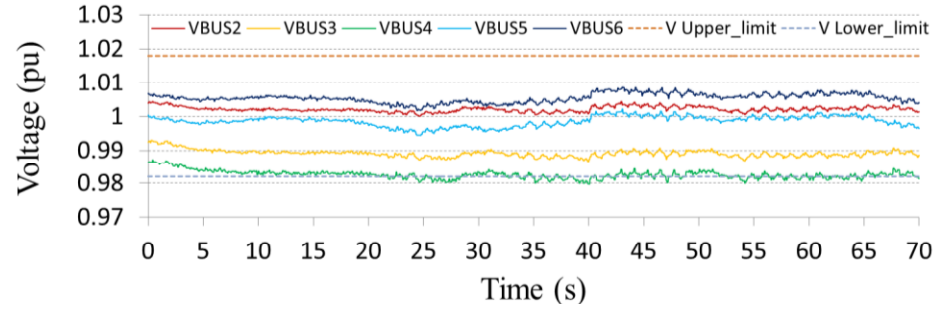

(a) Voltage profile at the load buses

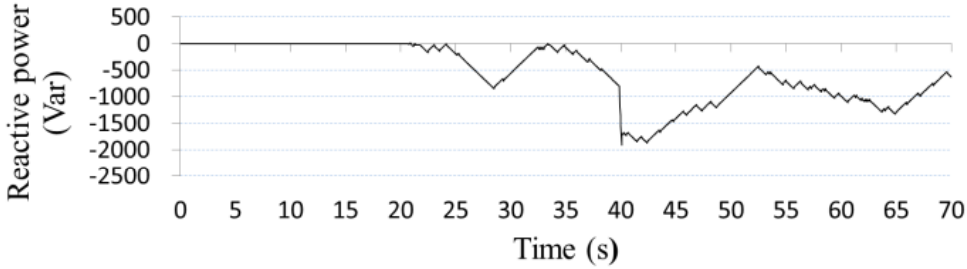

(b)Reactive power of central BESS

Fig. 3.18. Experimental waveforms of MG with a radial structure, with the proposed control method, from hour 42.

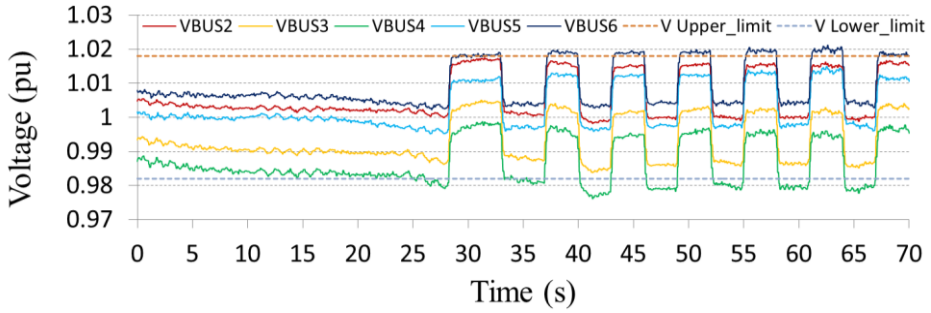

(a) Voltage profile at the load buses

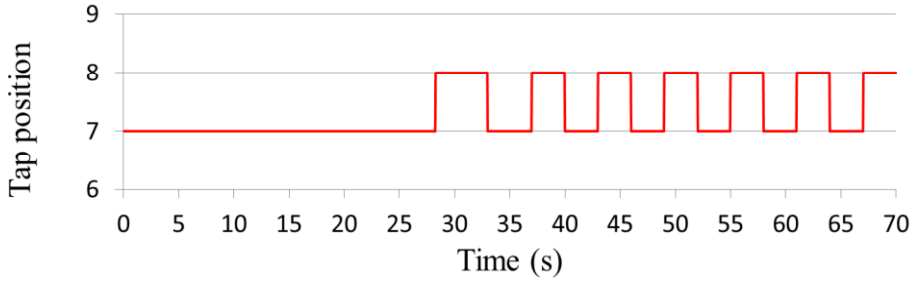

(b) LRT tap position

Fig. 3.19. Experimental waveforms in MG with a radial structure with local BESSs, LRT, and central BESS without DSTATCOM mode, from hour 42.

(2) An MG without a central BESS. In the PV-supplied MG with neither local BESSs nor a central BESS, load bus voltage changes owing to the power flow of PV. As a consequence, the LRT had to change tap position many times to control load bus voltages to within the permitted voltage range, as shown in Fig. 3.20. When local BESSs were installed in the load bus feeder, the number of tap position changes was decreased, as shown in Fig. 3.21. Additionally, the voltage drop in the MG was decreased. When a central BESS was installed in the MG, the central BESS controlled reactive power to regulate the load bus voltage, which further reduced the number of tap position changes, as shown in Fig. 3.16(a). Furthermore, Figs. 3.18 and 3.19 also show that when a central BESS with the proposed control method is not connected to the MG with radial structure, the LRT cannot regulate the load bus voltages to within the desired voltage range; however, the central BESS with a DSTATCOM mode coordinated with the LRT was able to keep the load bus voltages within the specified voltage range.

Table 3.3 shows that when the MG has a radial structure, the load bus voltage cannot be controlled to within the range if the central BESS is not connected to the MG. Because the voltage step per tap position is large, the controller cannot choose an

appropriate LRT tap position to stabilize the load bus voltage to within the correct range. When the MG has a loop structure with a central BESS voltage control, the NoTC is reduced by 95% from the first case and by 90% from the second case.

Table 3.4 shows that the NoTC depends on the reactive power limit Q_{limit}. When the reactive power limit was increased for the central BESS, the NoTC decreased. However, Q_{limit} affects the interconnection point's power factor. Therefore, the Q_{limit} value needs to be determined from the standard for the interconnection point power factor.

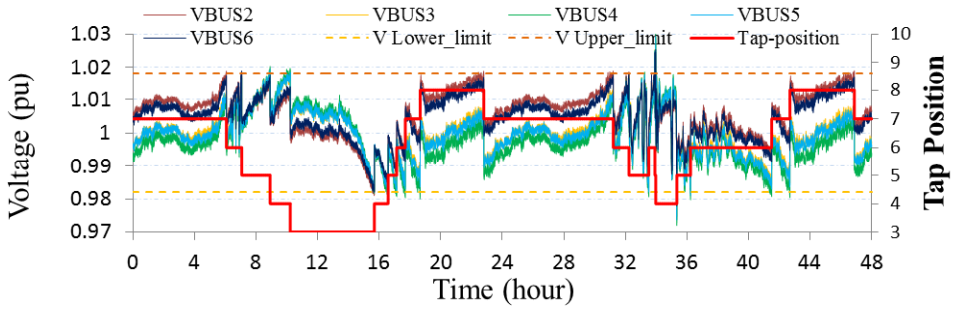

Fig. 3.20. Experimental waveforms of load bus voltages and tap position of an MG with a loop structure, with LRT.

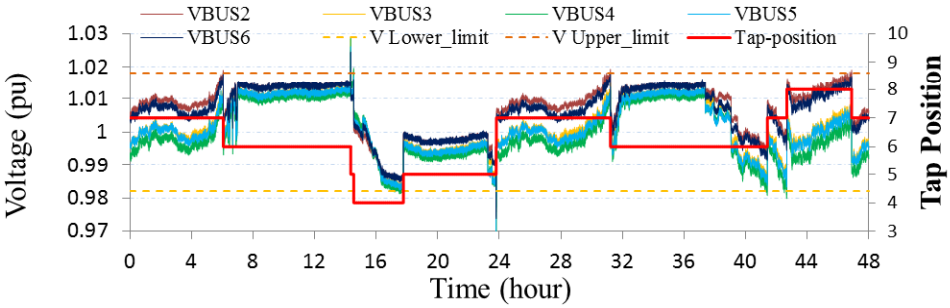

Fig. 3.21. Experimental waveforms of load bus voltages and tap position of an MG with a loop structure, with LRT and local BESSs.

Table 3.3. NoTC from experiment.

NoTC		LRT	LRT and local BESS	Proposed method
Experiment	Loop structure	20	10	1
	Radial structure	-	-	4

Table 3.4. Dependence of NoTC on the reactive power limit.

Reactive power limit Q_{limit} (pu)		0.16	0.32	0.56
Experiment	Loop structure	8	5	1
	Radial structure	12	5	4

The simulation results and experimental results illustrate the idea of coordination between the central BESS and the local BESSs. This coordination is intended to control load bus voltages. Each local BESS controls the active power generated from its assigned PV source to reduce the power flow in the MG; the central BESS controls the reactive power and the tap position of the LRT to regulate the load bus voltage to within the allowed voltage range, as shown in Figs. 3.10, 3.11, 3.16, and 3.17.

3.6. Conclusion

The author has proposed a coordinated BESS and LRT control algorithm to stabilize the voltage of a PV-supplied MG. The simulation and experimental results show the effectiveness of the proposed control structure in regulating the load bus voltages. The drop in load bus voltage is reduced by using local BESSs, and the load bus voltages of a PV-supplied MG are controlled to within the prescribed limit by the coordination between the central BESS and the LRT. The combination of the two operating modes (VSI and DSTACOM) helps the central BESS to control the load bus voltages, even when the battery system is disconnected from the central BESS, and reduces the NoTC.

CHAPTER 4: OPF FOR LOCAL BESSs BY HPSO-TVAC TO MINIMIZE DISTRIBUTION LOSS AND COORDINATING BETWEEN CENTRAL BESS AND LRT TO STABILIZE THE VOLTAGE OF PV-SUPPLIED MG

4.1. Introduction

In an MG with high-penetration PV and local BESSs installed at some local buses, the control of energy storage and release for each local BESS is a complex issue. This chapter proposes an online OPF method based on HPSO-TVAC to control the active power flow of the local BESSs so as to minimize the distribution loss while stabilizing the MG local bus voltages by a centralized control with a central BESS and an LRT. Simulation results and experimental results illustrate the effectiveness of the proposed method. Comparing the proposed method with a conventional method, the simulation and experimental results show that an MG with a loop structure has lower energy loss than a radial structure; however, using the proposed method reduces this disparity.

4.1.1. Network effects

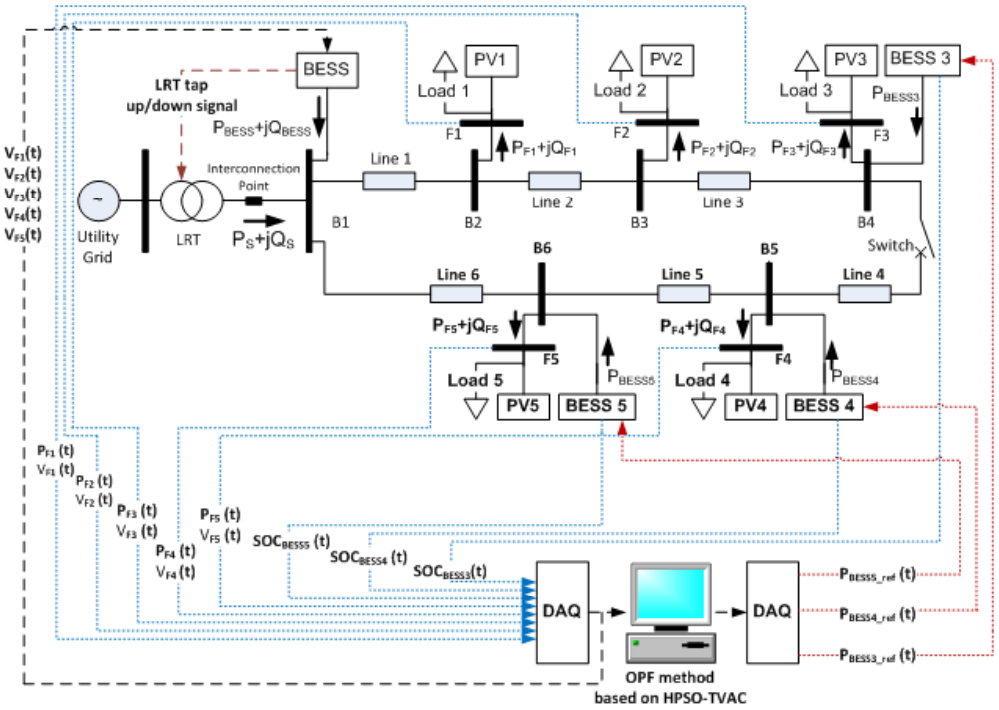

Fig. 4.1. MG model.

This chapter studies an MG model with six buses. The MG has five residential load groups and five PV systems. A central BESS connects to bus 1 (Fig. 4.1). Three local BESSs are arranged on buses 4, 5, and 6. Each residential load group includes 100 houses, with usage based on actual residential load data from Ota City, Japan, and shown in Fig. 4.5. The sign convention for power-by-power vector directions is shown in figure 4.1. The MG can operate with a loop or radial structure, selected by changing a switch that is at the end of line 4.

The voltage range for the 6.6 KV network is 0.982 to 1.018 pu. This range is used to control the local voltage bus that contains the load. Thus, in this chapter, local buses 2 to 6 will have controlled voltage. Every local bus is assumed to have equipment suitable for monitoring the bus voltage and load power flow from PVs connected to the bus, and sends the obtained values to a central controller through a communication network. Communication is assumed to be fast enough for the central controller to receive data every second.

In this chapter, two controllers control the MG as shown in Fig. 4.2. Controller 1 is a central BESS controller that coordinates with the LRT to stabilize the local bus voltage. Controller 2 is used to optimize the power flow in the local BESS so as to minimize distribution power loss. These two controllers operate independently and in parallel, both with 1 s cycles. When solving power flow in controller 2, it is assumed that the MG line impedances are known in advance and remain constant during operation.

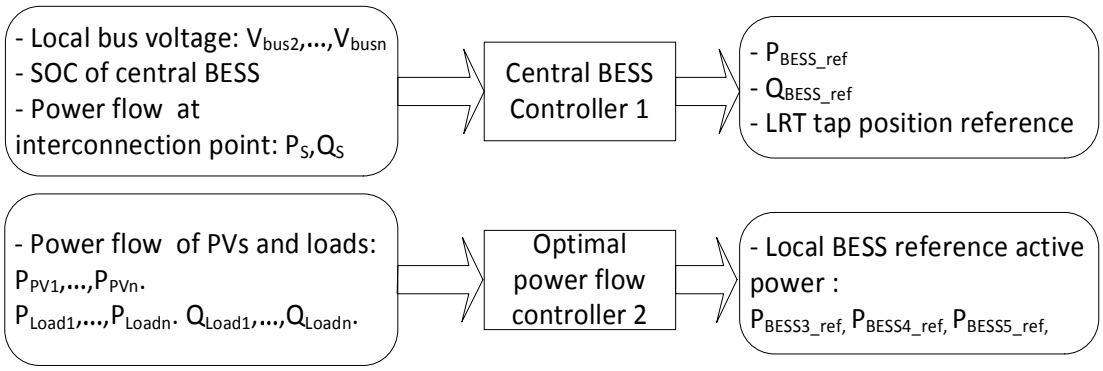

Fig. 4.2. Controllers in proposed method.

4.1.2. BESS structure

Figure 3.2 from Chapter 3 shows the structure and control diagram of the BESS inverter used in this chapter. The BESS can be operated in both VSI mode and DSTATCOM mode. The BESS can be controlled in terms of both active and reactive power. Reactive power is used to control the voltage of the bus to which it connects. However, the difference between the two modes is the purpose of active power control.

4.2. Centralized control with central BESS and LRT

4.2.1. Central BESS control algorithm

In the proposed control method, a central BESS is used as a centralized controller to stabilize local bus voltage and minimize the active power flow between the MG and the utility grid. When the central BESS battery bank is fully discharged or fully charged, the central BESS cannot control the active power flow between the MG and the utility grid. In such cases, the central BESS is operated in DSTATCOM mode. The central BESS then controls the reactive power so as to maintain the voltage within constraints. The centralized control algorithm is defined as follows.

(1) Voltage control algorithm of Central BESS

Step 1: Measure all local bus voltages V_{bus2} to V_{bus6}, calculating $V_{\min}$ and $V_{\max}$ as:

$$V_{\min}=\min(V_{busi}),\ V_{\max}=\max(V_{busi})\ (i=2,..,6). \tag{4.1}$$

Step 2: If $V_{\min} \le V_{lower\_limit}$,

$V_{BESS\_ref}=V_{BESS}+\Delta V$;

Else if $V_{\max} \ge V_{upper\_limit}$,

$V_{BESS\_ref}=V_{BESS}-\Delta V$;

Else $V_{BESS\_ref}=V_{BESS;}$

End

3: $Q_{BESS\_ref} = K_p(V_{BESS\_ref} - V_{BESS}) + K_i\int(V_{BESS\_ref} - V_{BESS})$ (4.2)

If $Q_{BESS\_ref} \ge Q_{BESS\_\max}$,

$Q_{BESS\_ref} = Q_{BESS\_\max}$;

Else if $Q_{BESS\_ref} \le Q_{BESS\_\min}$,

$Q_{BESS\_ref} = Q_{BESS\_\min}$;

End

(2) Active power control algorithm of central BESS

Step 1: Measure active power P_s and calculate the SOC of the central BESS (SOC_{BESS}).

Step 2: If ((*SOC*$_{BESS}$ ≥ 80%) and (*P*$_S$ ≤ *0*)) or ((*SOC*$_{BESS}$ ≤ 20%) and (*P*$_S$ ≥ 0))

$$P_{BESS\_ref} = K_p(V_{DC\_ref} - V_{DC}) + K_i \int (V_{DC\_ref} - V_{DC}) \tag{4.3}$$

Else, $P_{BESS\_ref} = K_p(0 - P_S) + K_i \int (0 - P_S)$ (4.4)

If $P_{BESS\_ref} \geq P_{BESS\_max}$, then $P_{BESSi\_ref} = P_{BESS\_max}$;

Else if $P_{BESS\_ref} \leq P_{BESS\_min}$, then $P_{BESS\_ref} = P_{BESS\_min}$;

End

Here, P_s is the active power flow between the MG and the utility grid;

V_{bus_i} is the voltage magnitude of local bus i (i = 2,…,6);

V_{upper_limit} is the upper voltage limit; V_{lower_limit} is the lower voltage limit;

P_{BESS_ref} is a reference value used to control the central BESS active power, and this value is limited to the range P_{BESS_min} to P_{BESS_max};

Q_{BESS_ref} is a reference value used to control the central BESS reactive power, and this value is limited to the range Q_{BESS_min} to Q_{BESS_max}; and

V_{DC} is the voltage of the DC-link inverter.

4.2.2. LRT tap position control algorithm

The LRT coordinates with the central BESS to stabilize local bus voltages. Actions by the central BESS have higher priority than those of the LRT. However, the BESS's apparent power rate is limited, so the LRT tap position must be controlled to ensure that the local bus voltage is stable and within the acceptable limit when the BESS reactive power approaches the limit. The control algorithm is as follows.

Step 1: Wait for LRT ready to control

Step 2: If (S_{BESS}>S_{limit}) or (abs(Q_{BESS})>Q_{limit})

If Q_{BESS}>*0*,

Increase tap position;

Else,

Decrease tap position

End

Here, S_{BESS} and Q_{BESS} are the apparent power and reactive power of the central BESS, respectively; Q_{BESS} is reactive power, and S_{limit} and Q_{limit} are conditional values for LRT tap control. Note that these are different from S_{BESS_max} and Q_{BESS_max}. The tap position is changed one step at a time. The time required for one step change is 3 s.

4.3. Online power loss minimization using an OPF method based on HPSO-TVAC

4.3.1. Formulation for power loss minimization

Finding the OPF is a optimization problem with a objective function and constraints. In this chapter, the objective function is total power distribution loss. The objective function is given by Eq. (4.5).

$$\min P_L = \frac{1}{2}\sum_{i=1}^{N}\sum_{\substack{j=1 \\ j\neq i}}^{N} g(i,j)[V_i^2 + V_j^2 - 2V_iV_j\cos(\delta_i - \delta_j)] \tag{4.5}$$

Here, P_L is the total distribution power loss;

δ_i is the phase angle of the bus i voltage;

$g(i,j)$ is the conductance of the distribution line between buses i and j for distinct i and j;

N is the number of buses; and

V_i is the magnitude of the bus i voltage.

The optimization problem has the following constraints.

a) The active power limits of the local BESSs are

$$P_{BESSi\_\min} \le P_{BESSi} \le P_{BESSi\_\max}, \quad i = 3,4,5 \tag{4.6}$$

where

$$P_{BESSi\_\max} = \begin{cases} 0, & \text{if } SOC_{BESSi} \le 20\% \\ P_{PCS\_BESSi}^{rate}, & \text{if } SOC_{BESSi} > 20\% \end{cases}$$

$$P_{BESSi\_\min} = \begin{cases} 0, & \text{if } SOC_{BESSi} \ge 80\% \\ -P_{PCS\_BESSi}^{rate}, & \text{if } SOC_{BESSi} < 80\%, \end{cases} \quad \text{and}$$

$P_{PCS\_BESSi}^{rate}$ and SOC_{BESSi} are, respectively, the rate of the power conditioning system (PCS) and the SOC of batteries in the local BESSi.

b) The LRT tap position constraint is

$$T_{\min} \le \bar{} \le T_{\max} . \tag{4.7}$$

c) The local bus voltage constraints are

$$V_{lower\_limit} \le \bar{} \le \bar{} \quad = 2,...,6 . \tag{4.8}$$

4.3.2. OPF method based on HPSO-TVAC

For all the considered objective functions, the vector of control variables x is represented by

$$x = [P_{BESS3}, P_{BESS4}, P_{BESS5}, T]^T \tag{4.9}$$

and dependent variables u are represented by

$$u = [V_{bus1}, ..., V_{bus6}]^T . \tag{4.10}$$

It is assumed that power flow from the grid to the MG is always at the substation limits. Therefore, the fitness function is used as the objective function and the constraints of the dependent variable act as safety constraints for the voltage at the load buses. Thus, the fitness function is

$$FT = \quad + \quad \sum_{i=2}^{6} \left(\quad - V_{busi}^{\lim} \right)^2 , \tag{4.11}$$

where K_v is a penalty factor for not satisfying the voltage limits at load buses. The limit of the dependent voltage variables in (4.11) is determined from their calculated values as follows:

$$V_{bus}^{\lim} = \begin{cases} V_{upper\_limit}, \text{if } V_{bus} > V_{upper\_limit} \\ \bar{} \quad \le \bar{} \le V_{upper\_limit} \\ V_{lower\_limit}, \text{if } V_{bus} < V_{lower\_limit} \end{cases} . \tag{4.12}$$

The implementation steps of the online OPF method for minimizing active power loss using HPSO-TVAC are as follows.

Step 1: Choose the maximum number of iterations $iter_{\max}$, the population size NP, and the initial and final values of the cognitive and social acceleration factors c_{1i}, c_{1f}, c_{2i}, and c_{2f}, and penalty factors K_v. Line impedance values are collected from MG model information. Power flow at the feeders (P_{Fj} and Q_{Fj}, j=1,…,5) and SOCs of the local BESSs are measured from the MG model.

Step 2: Initialization of the swarm: create initial particle positions and velocities as

$$X^{(0)} = X_{\min} + \text{rand}_1 \times (X_{\max} - X_{\min}) \tag{4.13}$$

$$v_d^{(0)} = v_{d,\min} + \text{rand}_2 \times (v_{d,\max} - v_{d,\min}), \tag{4.14}$$

where $rand_1$ and $rand_2$ are values selected uniformly randomly from [0, 1], and $X_{\min}$, $X_{\max}$ are the upper and lower bounds of the vector in Eq. (4.9). The upper and lower velocity bounds are based on the upper bound of each particle's position:

$$v_{d,\max} = \frac{X_{\max}}{2}, \quad v_{d,\min} = -v_{d,\max}. \tag{4.15}$$

Step 3: If the SOCs of the local BESSs do not change, then each random swarm particle is assigned the g_{best}^{k-1} position from the previous search. Because the HPSO-TVAC is a random search method, the results of a subsequent search can be markedly different from the previous result. This step helps to orient the search results for the next time, and helps to prevent overly large parameter fluctuations after each search.

Step 4: Initialization of p_{best} and g_{best}: for the initial particles, calculate the dependent variable values and power flow by using the Newton–Raphson algorithm and evaluate the personal best of the fitness function,, in Eq. (4.11). The best value from among all p_{best} values is identified as g_{best}.

Step 5: Evaluation of velocity: the velocity is updated using the following equation.

$$\begin{aligned} v_{id}^{k+1} = &\left(\qquad\qquad \right) \times \text{rand}_3 \times \left(p\_best_{id} - x_{id} \right) \\ &+ \left(\qquad\qquad \right) \times \text{rand}_4 \times \left(g\_best_{id} - x_{id} \right) \end{aligned} \tag{4.16}$$

If $v_{id} = 0$ and $rand_3 < 0.5$, then $v_{id} = rand_4 \times v_{d,max}$, else $v_{id} = -rand_5 \times v_{d,max}$. Here

rand$_1$, *rand*$_2$, *rand*$_3$, *rand*$_4$, and *rand*$_5$ are random numbers between 0 and 1.

Step 6: Update the position: the particle position vector is updated according to

$$x_{id}^{k+1} = \text{ш} + v_{id}^{+1}. \tag{4.17}$$

Step 7: Update p_{best} and g_{best}: Using the new position to solve the power flow of each particle, evaluate the fitness function for each particle. Compare the new value of *FT* to previous p_{best} values to update the personal best of each particle, then update the global best g_{best}.

Step 8: If $k < iter_{\max}$ then let $k = k + 1$ and go back to Step 5.

Otherwise, stop and send the local BESS reference power to the local BESS controller.

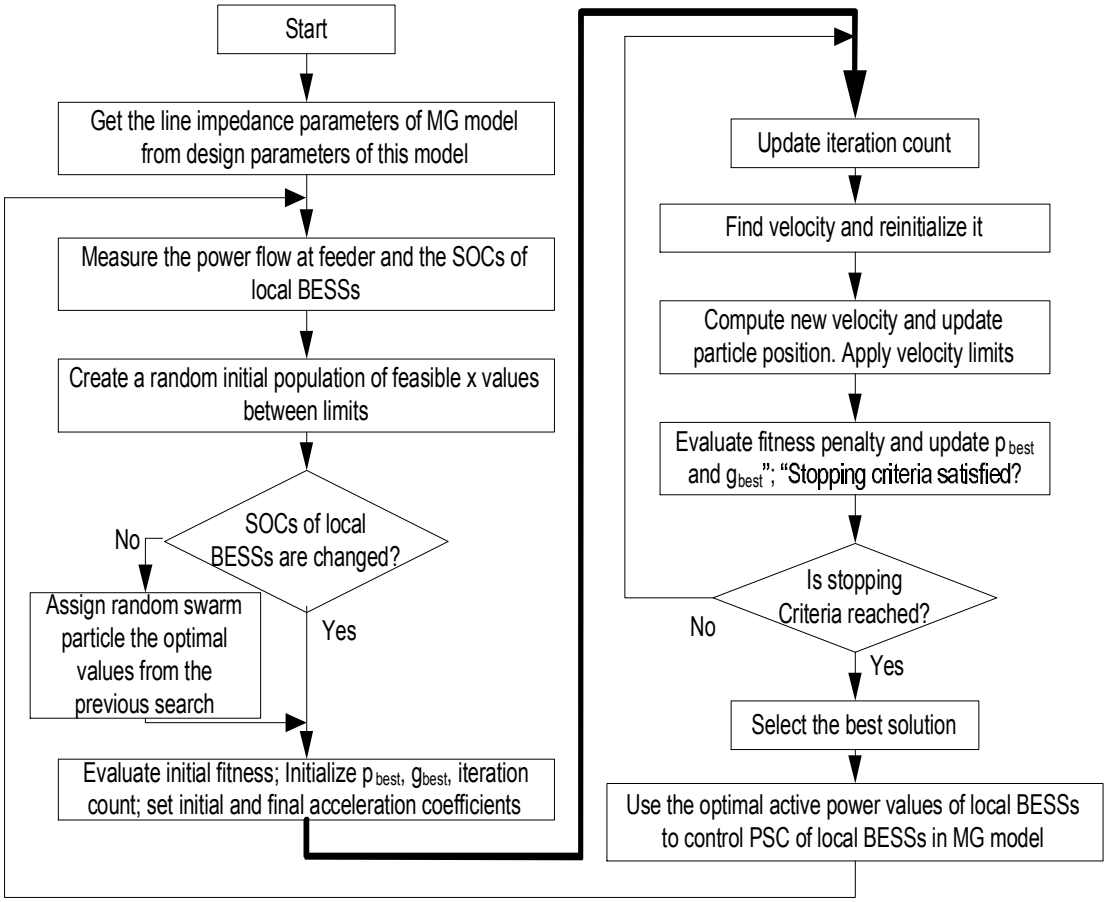

Fig. 4.3. OPF method to minimize active power loss using HPSO-TVAC.

4.4. Modeling and simulation results

The MG model is simulated by the MATLAB/Simulink software. The MG model has residential loads, PVs, LRT, and BESSs. Voltages, power flow, and SOCs of local BESSs are measured from this model and used as input parameters to solve the OPF problem by a MATLAB/M-file model called the reference model. The result of applying the OPF method is used to control the Simulink model. A conventional decentralized local BESS control is used to verify the effectiveness of the proposed control method. In the conventional method, a local BESS is controlled to store the surplus energy when local PV power generation exceeds local load consumption, and to generate active power when load consumption exceeds what the PV generates. Local BESS SOCs were kept between 20% and 80%.

4.4.1. Effectiveness of HPSO-TVAC on different benchmarks

The HPSO-TVAC method is used to minimize distribution power loss, and its performance is compared with the results from the original PSO (SPSO) [58] and PSO-TVIW [79] methods. The performance of each system was judged over 20 trials. In SPSO, the constriction factors were set at c_1=c_2=2. In PSO-TVIW the constriction factors were c_1=c_2=2.05, and w varied from 0.9 to 0.4. With HPSO-TVAC, the best ranges for the constriction factors c_1 and c_2 were (2.5, 0.5) and (0.5, 2.5), respectively. Thus, the values of the cognitive and social acceleration factors are chosen as c_{1i}=0.5, c_{2i}=2.5, c_{1f}=2.5, and c_{2f}=0.5. In this chapter, the population size of the swarm is randomly selected with the intent of verifying the algorithm, rather than analyzing the effect of population size on the result of optimization. Hence, all simulations were carried out with a population size of 50. Table I shows the MG simulation parameters. Figure 4.5 shows the five groups' power levels for PV and residential load power flow. PV data represent a sunny day and a cloudy day. These methods were programmed for MATLAB/Simulink on a 2.8-GHz processor with 8 GB of random access memory (RAM).

Figure 4.4 shows the convergence characteristics of PSO strategies at 12:00, with SOCs of local BESSs held between 20% and 80%. The HPSO-TVAC found the global best after just 28 iterations. The computational time was 0.5732 s. Therefore, the OPF

cycle is chosen as 1 s. The HPSO-TVAC method obtained stable results after 20 trials over two methods, PSO-TVIW and SPSO, as shown in Table 4.2.

4.4.2. Online power loss minimization by using an OPF method based on HPSO-TVAC

This section describes a simulation of online power distribution loss minimization using an OPF method based on HPSO-TVAC, coordinated between a centralized central BESS and an LRT to stabilize the local bus voltage. The simulation time is 48 h.

The values for the active and reactive power ranges are [–1, 1] pu. S_{limit} and Q_{limit} values are taken as 1.1 pu and 0.5 pu, respectively. The LRT has 17 tap positions. When the LRT tap position is zero, the LRT secondary voltage is the base voltage.

Figures 4.6, 4.7, and 4.8 show the simulation results in the case of a radially structured MG. Local bus voltages V_{bus2} to V_{bus6} remained between 0.982 and 1.018 pu for the full 48 h, as shown in Fig. 4.6(a). The interconnection point's power flow *Ps* and the central BESS's active power flow are shown in Fig. 4.6(b). Figure 4.6(c) shows that the SOCs of the central and local BESSs are kept between 20% and 80%.

Figure 4.6(d) shows the LRT tap position. The red line is controlled by a centralized control for the central BESS and the LRT, and the dark blue line is the path searched by the HPSO-TVAC OPF algorithm. This figure illustrates that the LRT tap position discovered using the HPSO-TVAC method cannot be used to control the MG voltage because the value varies greatly among searches.

Figure 4.8(a) shows the waveform of power distribution loss for an MG controlled by the proposed method and the waveform calculated by the HPSO-TVAC OPF reference model. The two waveforms are almost the same, showing the effectiveness of the proposed method. When $SOC_{BESSi} \leq 20\%$, the local BESS PCS will control the active power so that it equals 0, but because of the PI controller the output of the PCS will not be exactly 0. There is, therefore, a small difference between power loss in the Simulink model and in the reference model. As shown in Fig. 4.8(b), the active power flows of the three local BESSs are controlled to be the same as the reference signals from the HPSO-TVAC OPF controller 2.

Figure 4.7 shows the total energy loss curves for four simulation cases. Table 4.3 shows a comparison of total energy loss over 48 h between the proposed and conventional methods. When a radially structured MG is controlled by the proposed method, the total energy loss is reduced by 15.68% from the conventional method. This ratio is 8.75% when the MG has a loop structure.

Table 4.1. Simulation Parameters

		Simulation
Central BESS	Capacity	2 MWh
	Power rating	1.5 MVA
Each local $BESS_4$, $BESS_5$	Capacity	1.5 MWh
	Power rating	0.3 MVA
Local $BESS_3$	Capacity	2 MWh
	Power rating	0.3 MVA
3-phase source	Base voltage	6600 V
	Base power	1 MVA
	Frequency	50 Hz
Line 1 impedance		2+j2.04 Ω
Line 2 impedance		2+j2.04 Ω
Line 3 impedance		2+j2.04 Ω
Line 4 impedance		2+j2.04 Ω
Line 5 impedance		2+j2.04 Ω
Line 6 impedance		2+j2.04 Ω
LRT	Tap	17 positions[-8, +8]
	Voltage step ΔU per tap step	±0.0045 pu

Table 4.2. Comparison of different PSO strategies

PSO method	Minimum P_{Loss} (MW)	Maximum P_{Loss} (MW)	Average P_{Loss} (MW)
HPSO-TVAC	0.0011185298	0.0011185298	0.0011185298
PSO-TVIW	0.0011191238	0.0011286965	0.0011212026
SPSO	0.0011192263	0.0011424188	0.0011303914

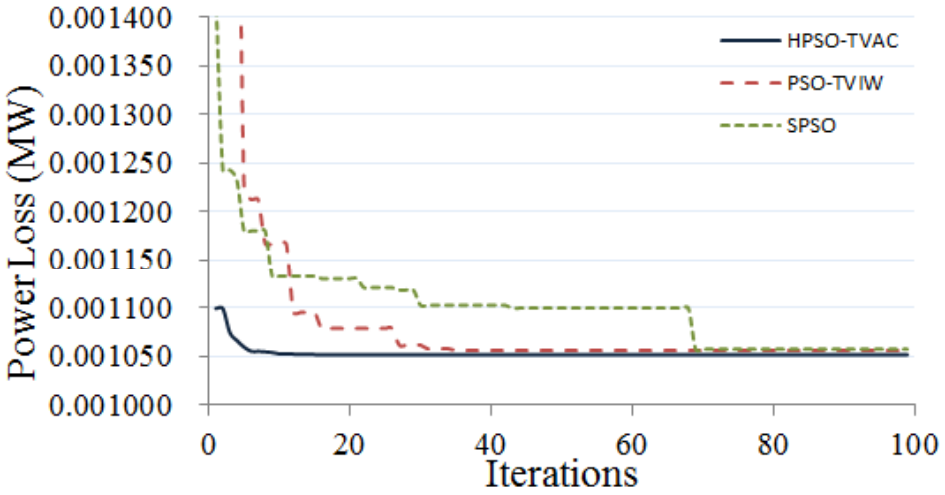

Fig. 4.4. Convergence curves of PSO strategies for MG loop structure.

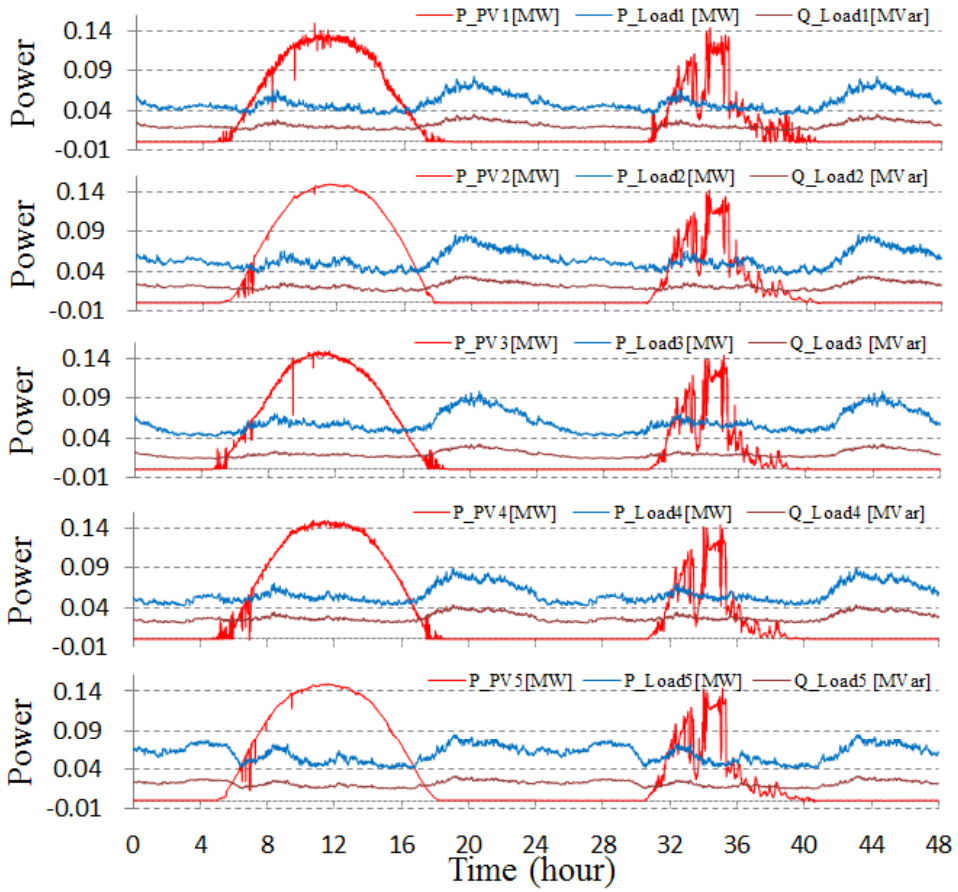

Fig. 4.5. Daily power output of PV curves and residential load curves.

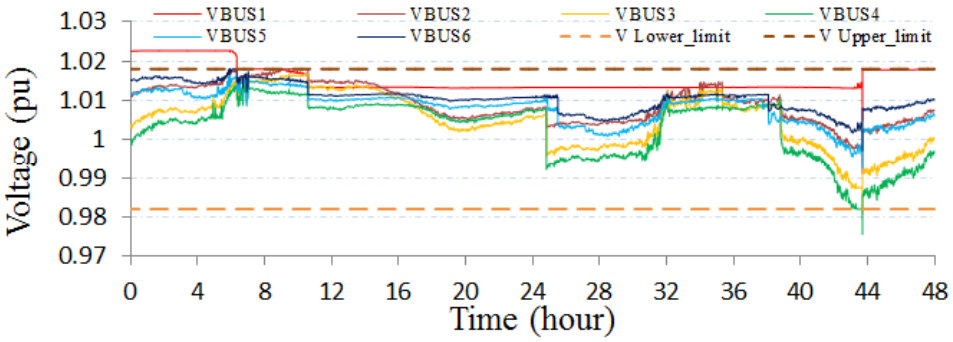

a) Local bus voltages

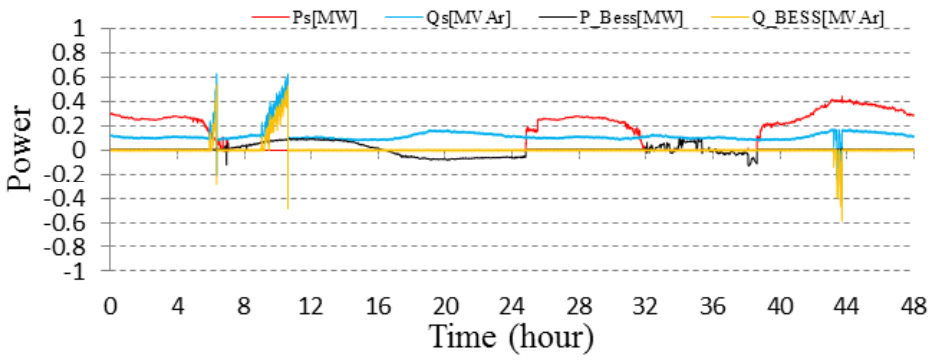

b) Power flow at interconnection point and central BESS

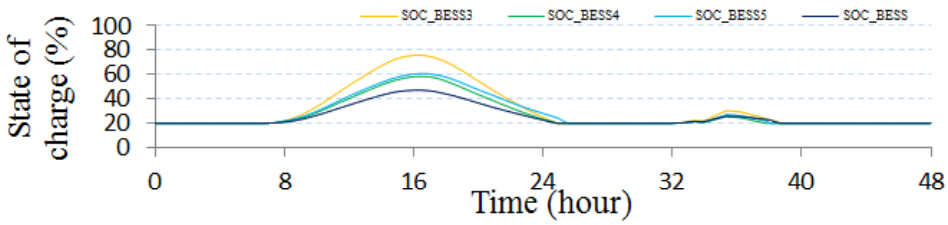

c) BESS energy storage

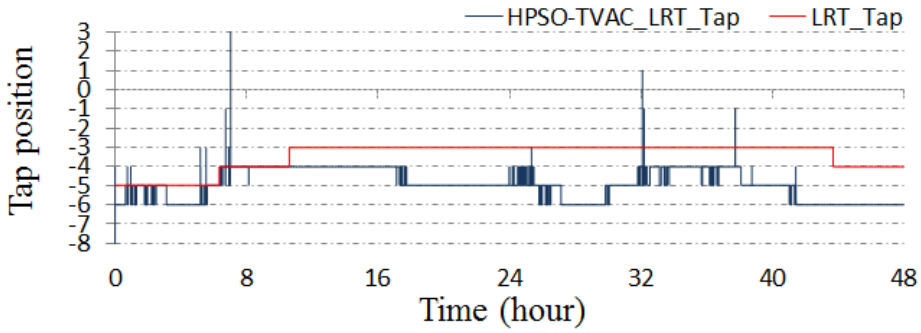

d) LRT tap position

Fig. 4.6. Radial structure with BESSs and LRT.

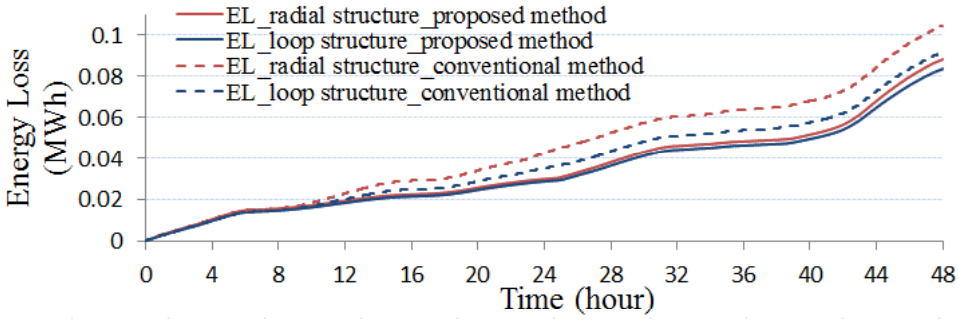

Fig. 4.7. Total energy loss waveform.

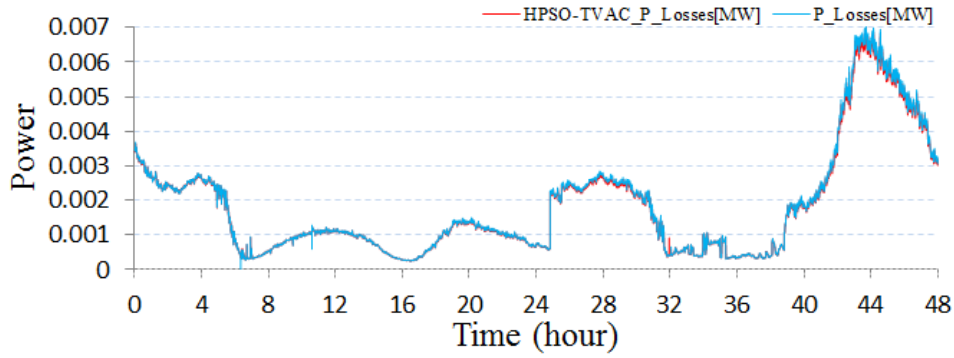

a) Power loss

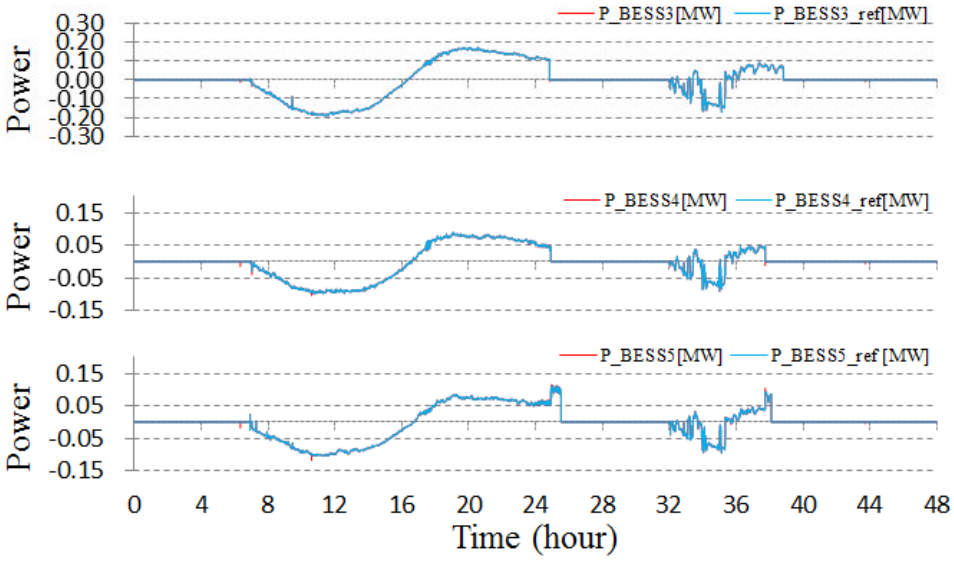

b) Local BESS active power

Fig. 4.8. Radial structure with BESSs and LRT control.

Table 4.3. Total energy distribution loss

	Proposed method [MWh]	Conventional method [MWh]
MG, loop structure	0.08355487	0.09156828
MG, radial structure	0.08820179	0.10461378

4.5. Experimental results

ANSWER is used to model the MG, which has residential loads, PVs, LRT, and BESSs. Voltages, power flow, and SOCs of local BESSs are measured from this model and used as input parameters to solve the OPF problem by using a MATLAB/M-file model called the reference model. The result of solving for OPF is used to control the ANSWER model of the MG. A conventional decentralized local BESS control is used as a reference to validate the effectiveness of the proposed control technique. In the conventional method, a local BESS is controlled to store the surplus energy when local power generation from PV sources exceeds local load consumption and to generate active power when load consumption exceeds what the PV generates. Local BESS SOCs were kept between 20% and 80%. In this experiment, η_d and η_c are each fixed at 100%.

4.5.1. Effectiveness of HPSO-TVAC on various benchmarks

The HPSO-TVAC method is used to solve for minimization of distribution power loss, and its performance is compared with the performances of the SPSO [58] and PSO PSO-TVIW [79] methods. The performance of each system was judged over 20 trials. The constriction factors and cognitive and social acceleration factors are chosen to be the same as in the simulation model. In this chapter, the population size of the swarm is randomly selected with the aim of verifying the algorithm, rather than analyzing the effect of population size on the result of optimization. Hence, all simulations and experiments were carried out with a population size of 50 and 100 iterations. Table 4.4 shows the MG parameters. Figure 4.9 shows the five groups' powers for PV and resident load power flow. PV data represent a sunny day and a cloudy day. These methods were programmed for MATLAB/Simulink on a 2.8-GHz processor with 8 GB of RAM.

Table 4.5 shows the results from PSO strategies over 20 trials at hour 12, with SOCs of local BESSs held between 20% and 80%. The HPSO-TVAC method obtained stable results after 20 trials over two methods, PSO-TVIW and SPSO. The HPSO-TVAC method found the global best after just 23 iterations. The computational time over 30 iterations was 1.3806 s. Therefore, the OPF cycle is chosen as 2 s.

4.5.2. Power loss minimization by using an OPF method based on HPSO-TVAC

This section describes the experimental results. The experiment time is 48 h.

Figure 4.10 shows that the MG load bus voltages oscillate outside the acceptable voltage range when no BESS is connected to the MG. The experimental results for a loop-structured MG controlled by the proposed control method is shown in figure 4.12. Load bus voltages V_{bus2} to V_{bus6} remained between 0.98 and 1.02 pu for the full 48 h, as shown in Fig. 4.12(a). Figure 4.12(b) shows the power flow *Ps* and central BESS. The BESS's SOCs were kept between 20% and 80%, as shown in Fig. 4.12(c).

The BESS voltage and LRT tap position are shown in Fig. 4.12(d). When the battery of the central BESS was fully discharged, the BESS switched to DSTACOM mode to control the voltage by using reactive power. However, when the reactive power reached the limit, the central BESS changed the LRT tap position to control the load bus voltage, as shown in Fig. 4.12 at hours 10.62 and 42.67.

Figure 4.11 shows the total energy loss curves in four experiment cases. Table 4.6 shows a comparison of total energy loss over 48h between the proposed and conventional methods. When a radially structured MG is controlled by the proposed method, total energy loss is reduced by 10.7% from the conventional method. This ratio is 3.8% when the MG has a loop structure.

The experiment results and simulation results prove the effectiveness of the proposed method.

Table 4.4. Experimental parameters

Central BESS	Capacity	12.5 kWh
	Power rating	10 kVA
	$[Q_{BESSmax};P_{BESSmax}]$	[7.2 kVar;7.2 kW]
	$[Q_{limit};S_{limit}]$	[5.6 kVar;7.2 kVA]
	ΔV	0.0001 pu
Each local $BESS_3$, $BESS_4$, $BESS_5$	Capacity	12.5 kWh
	Power rating	2 kVA
3-phase source	Base voltage	200 V
	Base power	10 kVA
	Frequency	50 Hz
Line 0 impedance		0.191+j0.085 Ω
Line 1 impedance		0.291+j0.158 Ω
Line 2 impedance		0.290+j0.162 Ω
Line 3 impedance		0.285+j0.161 Ω
Line 4 impedance		0.301+j0.156 Ω
Line 5 impedance		0.296+j0.169 Ω
Line 6 impedance		0.280+j0.160 Ω
LRT	Tap	9 positions [0, +8]
	Voltage step per tap	±0.02pu

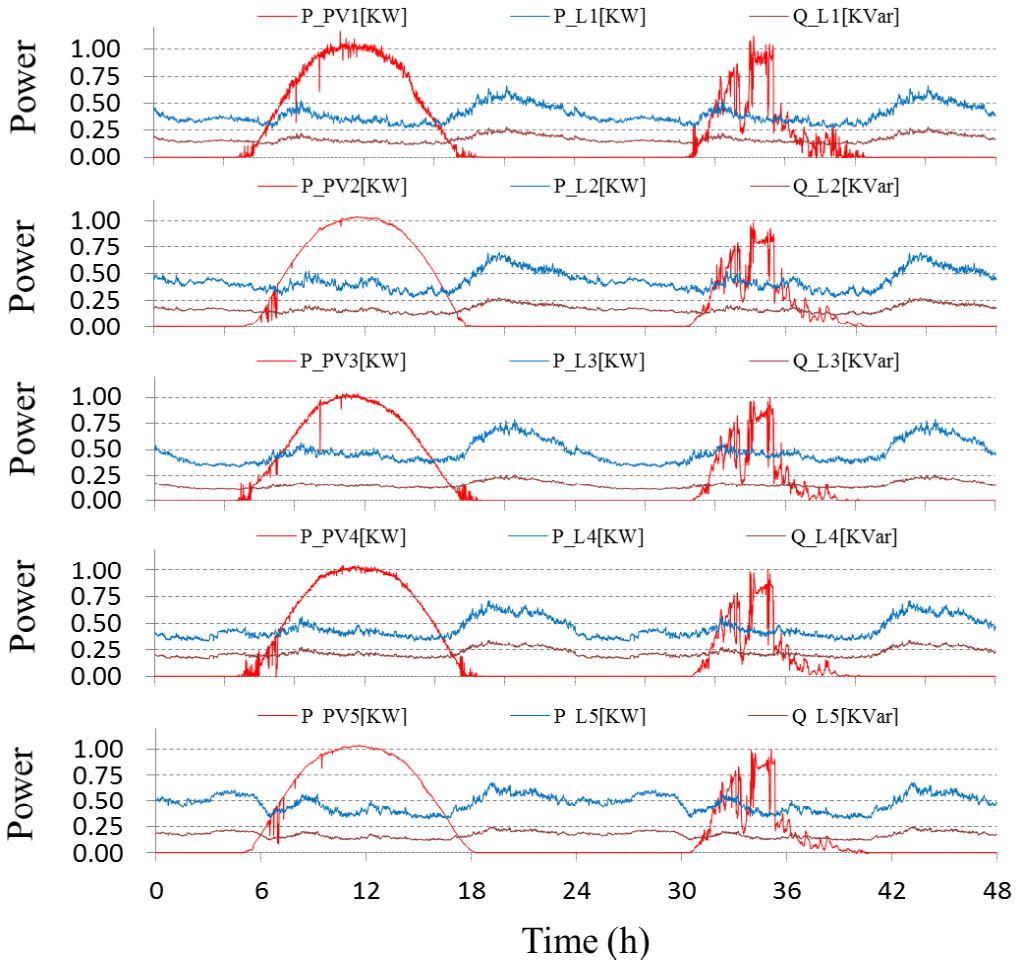

Fig. 4.9. Daily active power output of the PV and daily residential load profile over 48 h.

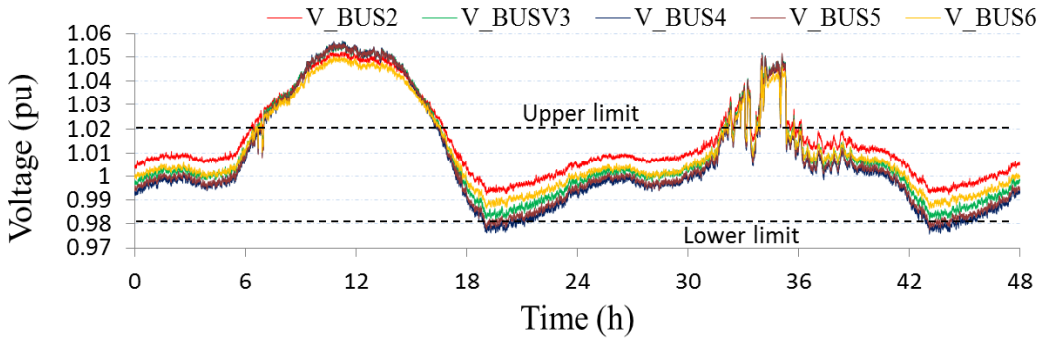

Fig. 4.10. Load bus voltage profile of an MG with a loop structure, without BESS and LRT control.

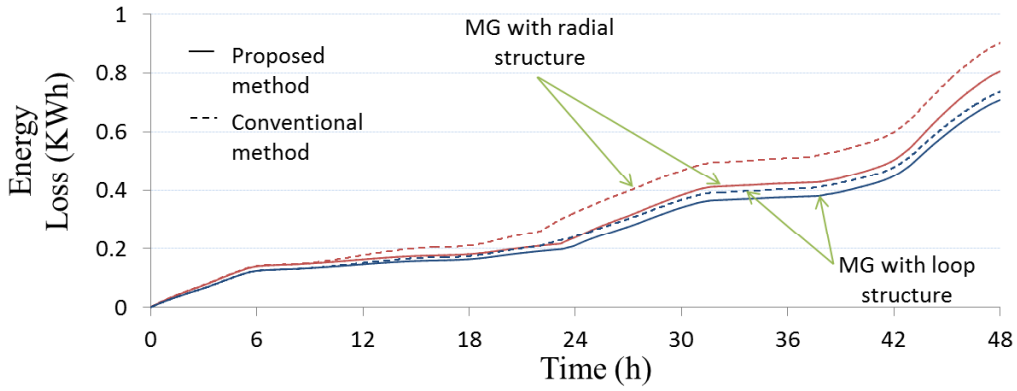

Fig. 4.11. Total energy loss curves.

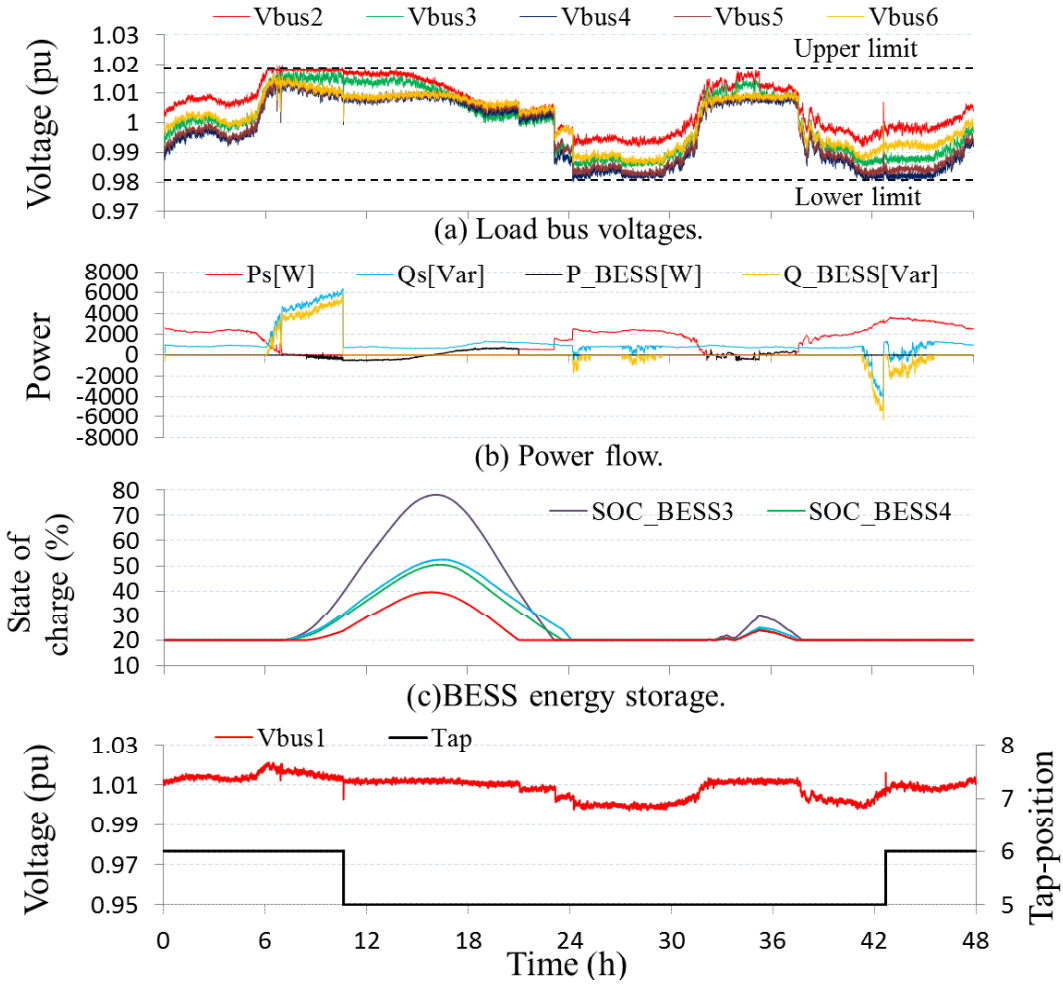

(d) Central BESS voltage and LRT tap position

Fig. 4.12. MG with a loop structure, with the proposed BESSs and LRT control.

Table 4.5. Comparison of different PSO strategies

PSO method	Minimum P_{Loss} (kW)	Maximum P_{Loss} (kW)	Average P_{Loss} (kW)
HPSO-TVAC	0.01028979	0.01028980	0.01028979
PSO-TVIW	0.01029132	0.01032425	0.01029924
SPSO	0.01029912	0.01041271	0.01033816

Table 4.6. Total energy distribution loss

	Proposed method [kWh]	Conventional method [kWh]
MG, loop structure	0.709021	0.737574
MG, radial structure	0.806612	0.903495

4.6. Conclusion

This chapter had two goals: minimizing power distribution loss and stabilizing local voltage to within an acceptable range. The complex problem of the first goal is solved by HPSO-TVAC, and a centralized BESS and LRT are used to achieve the second goal. The simulation and experimental results illustrate the effectiveness of the proposed method. Comparing the simulation results shows that an MG with a loop structure has less energy loss than one with a radial structure. However, when using the proposed method, this disparity is reduced. The control of energy storage and release for BESSs is a complex issue. The proposed method also presents an energy control method for BESSs in MGs.

CHAPTER 5: OPTIMIZING PLACEMENT AND SIZES OF BESSs TO STABILIZE VOLTAGE IN PV-SUPPLIED MG

5.1. Introduction

The proposed control algorithms described in previous chapters are used to control the central BESS and installed local BESSs in a PV-supplied MG. In this chapter, the author proposes a two-step algorithm to optimize the placement and sizes of BESSs in a grid-connected PV-supplied MG. In the first step, an algorithm based on HPSO-TVAC is used to find the best locations at which to install BESSs so that the number of BESSs is the lowest that will ensure the voltage constraints can be met. Among the candidates for the lowest number of BESSs, the minimum total absolute value of active power flows of BESSs is chosen for the optimal solution. The second step determines the sizes of BESSs on the basis of the optimal locations and prediction data for demand and output from PVs. Finally, the author proposes a control algorithm for BESSs chosen by the optimal algorithm for keeping the local bus voltages within the allowed voltage range. The local BESS controls the active power to regulate the local bus voltages. The effectiveness of the approach is validated by a detailed study of a sample radially structured PV-supplied MG simulation model. The HPSO-TVAC method obtained stable results after many trials. The effectiveness of the BESS control algorithm is verified by analyzing simulation results and experimental results.

5.2. Network effects

This chapter studies an MV 6.6-kV PV-supplied MG model with four feeders. This model contains 18 load buses, as shown in Fig. 5.1. Six PV systems are arranged on four feeders. Residential load groups connect to buses 2 to 18. Actual residential load groups and PV data were taken from data on the electricity supply to 500 houses in Ota City, Japan, as shown in Figs. 5.5 and 5.6.

The voltage range scale for the 6.6 KV network is 0.98 to 1.02 per unit (pu). Furthermore, this range is used to control the load voltage bus containing the load. Thus, in this chapter, load buses 2 to 18 will have controlled voltage. Every load bus is assumed to have equipment sufficient to monitor the bus voltage and send those values to a central controller through a communication network. Communication is assumed to

be fast enough for the central controller to receive data every second.

In this chapter, it is assumed that the minimum load data and the maximum output of PV data are known. When PVs are not connected to the system, all load bus voltages are taken as stable in the allowed voltage range under full load. When PV systems connect to an MG, they can make the load bus voltage exceed the upper limit. Therefore, the author proposes a solution to stabilize the load bus voltage to within the desired range by using BESSs. When BESSs are connected to the system, the PV power can be controlled by the BESSs to reduce fluctuation of the load bus voltages.

Figure 5.2 shows a control diagram of the BESS inverter used in this chapter. The BESS operates in VSI mode. Active power is used to control the load bus voltage of the feeder to which it connects.

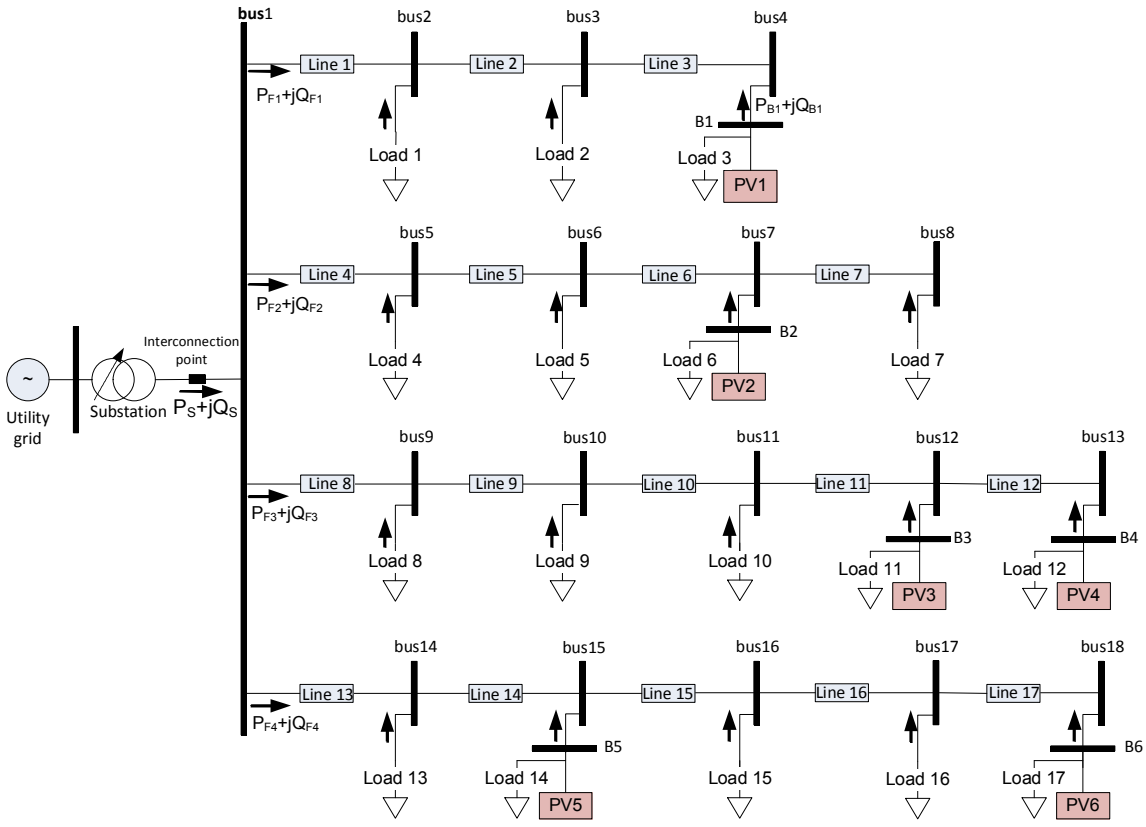

Fig. 5.1. Single-line diagram of the microgrid model.

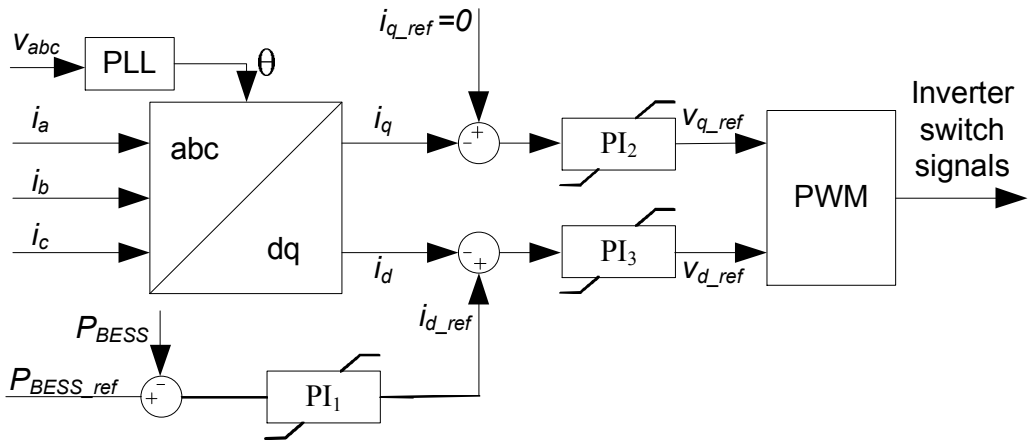

Fig. 5.2. Active power control diagram of the BESS inverter.

5.3. Optimal BESS placement and sizes, based on HPSO-TVAC

The two-step optimization algorithm is proposed for determining the optimal BESS placement and sizes as follows.

Step 1 (Screening): Use an optimal algorithm to search the candidates for optimal placement of BESSs by HPSO-TVAC.

Step 2 (Selection): Calculate the sizes of the optimal candidates by using the proposed control algorithm to determine the optimal placement and sizes of BESSs.

5.3.1. Formulation for BESS placement minimization.

OPF calculation is a optimization problem with a objective function and constraints. In this chapter, the objective function, to be minimized, is the total number of BESSs together with the total absolute active power value of the BESSs. The objective function is given by Eq (5.1).

$$\min f = \sum_{i=1}^{NoB} \text{abs}(P_{BEESi}) \tag{5.1}$$

Here, NoB is the total number of BESSs; abs(P_{BESSi}) is the absolute value of active power of BESS*i* in pu.

The constraints of this problem are as follows.

a) Active power limits of local BESS are

$$P_{BESSi\_\min} \le P_{BESSi} \le P_{BESSi\_\max}, i = 1,...,n. \tag{5.2}$$

b) The load bus voltage constraints are

$$V_{lower\_limit} \le V_{busj} \le V_{upper\_limit}, j = 2,...,m. \quad (5.3)$$

Here, $P_{BESSi\_\max}$ and $P_{BESSi\_\min}$ are, respectively, the maximum and minimum rates of the PCS; V_{upper_limit} is the upper voltage limit; V_{lower_limit} is the lower voltage limit; n is the number of BESSs, and m is the number of buses.

5.3.2. Optimal BESS placement based on HPSO-TVAC.

For all the considered objective functions, the vector of control variables x is represented by

$$x = [P_{BESS1},...,P_{BESSn}, po_{BESS1},..., po_{BESSn}]^T \quad (5.4)$$

and the dependent variables u are represented by

$$u = [V_{bus1},...,V_{busm}]^T. \quad (5.5)$$

Here, n is the number of PV systems that connected to the MG. Typically, when n PV systems are connected to the MG, we need n BESSs connected to the MG at the same bus to control the voltage. Hence, the initial number of BESSs is chosen to coincide with the number of PV systems; m is the number of buses in the MG.

It is assumed that the power flow from the grid to the MG is always at substation limits. Therefore, the fitness function is used as the objective function, and the constraints of the dependent variable are used as safety constraints for the voltage at load buses. Thus, the fitness function is

$$FT = f(x,u) + K_v \sum_{i=2}^{18} \left(V_{busj} - V_{busj}^{\lim}\right)^2, \quad (5.6)$$

where K_v is a penalty factor for not satisfying the voltage limits at load buses. The limit of the dependent voltage variables in Eq. (5.6) is determined from their calculated values, as follows.

$$V_{bus}^{\lim} = \begin{cases} V_{upper\_limit}, \text{if } V_{bus} > V_{upper\_limit} \\ V_{bus}, \text{if } V_{lower\_limit} \le V_{bus} \le V_{upper\_limit} \\ V_{lower\_limit}, \text{if } V_{bus} < V_{lower\_limit} \end{cases} \quad (5.7)$$

The implementation steps for the online OPF method to minimize active power loss using HPSO-TVAC are as follows.

Step 1: Choose a maximum number of iterations i_{termax}, the population size NP, initial and final values of cognitive and social acceleration factors c_{1i}, c_{1f}, c_{2i}, and c_{2f}, and penalty factors K_v. Collect line impedance values from the MG model information.

Step 2: Initialize the swarm. To do so, create initial particle positions and velocities as

$$X^{(0)} = X_{\min} + \text{rand}_1 \times (X_{\max} - X_{\min}), \tag{5.8}$$

$$v_d^{(0)} = v_{d,\min} + \text{rand}_2 \times (v_{d,\max} - v_{d,\min}). \tag{5.9}$$

Here, $rand_1$ and $rand_2$ are random values in [0, 1], and $X_{\min}$, $X_{\max}$ are the upper limit and lower limit, respectively, of the vector in Eq. (5.4). The upper and lower velocity bounds are based on the upper bound of each particle's position, express as Eq. (5.10).

$$v_{d,\max} = \frac{X_{\max}}{2}, \quad v_{d,\min} = -v_{d,\max} \tag{5.10}$$

Step 3: Assign a random swarm particle the g_{best}^{k-1} position from the previous search. Because the HPSO-TVAC is a random search method, the results of a subsequent search can be very different from the previous result. This step helps to orient the search results for the next time and helps to prevent overly large parameter fluctuations after each search.

Step 4: Initialize p_{best} and g_{best}. To do so for the initial particle, calculate dependent variable values and power flow by using the Newton–Raphson algorithm and then evaluate the personal best of the fitness function p_{best} in Eq. (5.6). The best value from among all p_{best} values is identified as g_{best}.

Step 5: Evaluate the velocity. The velocity is updated by using the following equation:

$$\begin{aligned} v_{id}^{k+1} = &\left(\qquad\qquad \right) \times \qquad \text{rand}_1 \times \left(p\text{best}_{id} - x_{id} \right) \\ &+ \left(\qquad\qquad \right) \times \qquad \text{rand}_2 \times \left(g\text{best}_{id} - x_{id} \right) \end{aligned} \tag{5.11}$$

If $v_{id} = 0$ and $rand_3 < 0.5$, then $v_{id} = rand_4 \times v_{d,max}$, and otherwise $v_{id} = -rand_5 \times v_{d,max}$. Here $rand_1$, $rand_2$, $rand_3$, $rand_4$, and $rand_5$ are random numbers between 0 and 1.

Step 6: Update the position. The particle position vector is updated by Eq. (5.12).

$$x_{id}^{k+1} = x_{id}^{k} + v_{id}^{k+1}. \quad (5.12)$$

Step 7: Update p_{best} and g_{best}. Use the new position to solve the power flow of each particle. In cases where more than one BESS connects to a single load bus, they will function as a single BESS. Evaluate the fitness function FT for each particle. Compare the calculated FT value to previous p_{best} values to update the personal best of each particle, and then update the global best g_{best}.

Step 8: If $k < iter_{\max}$, then let $k = k + 1$ and go back to Step 5.

Otherwise, stop and determine the optimal placement of BESSs.

The results for optimal BESS placement obtained from this screening step are candidates for optimal BESSs. The next selection step will determine which candidates are the optimal BESSs.

5.3.3. Determining the sizes of the BESSs.

Each target of the selection step algorithm uses BESS*i* to stabilize the load bus voltages on the feeder *i* to which it connects. A PI controller maintains compliance with voltage constraints by using the active power of BESSs. The sizes of the BESSs are calculated from the SOC curves of BESSs controlled by the PI controller. For the initial capacity of BESSs, it is assumed that they are large enough to keep the SOC between 20% and 80%. The control algorithm is defined as follows.

Step 1: Measure all load bus voltages $V_{bus\ l}$ to $V_{bus\ m}$ of feeder i that BESSi is connected to and determine the maximum voltage $V_{\max i}$ as $V_{\max i}=\max(V_{bus\ l}, \ldots, V_{bus\ m})$.

Step 2: If $V_{\max i} \geq V_{upper\_limit}$

$$P_{BESSi\_ref} = K_{p1}(V_{upper\_limit} - V_{maxi}) + K_{i1}\int (V_{upper\_limit} - V_{maxi})$$

Else if $V_{maxi} < (V_{upper\_limit} - \Delta V)$ *and* $(P_{Fi} > \Delta P$ *or* $P_{BESSi} > \Delta P)$

$$P_{BESSi\_ref} = K_{p3}(0 - P_{Fi}) + K_{i3}\int (0 - P_{Fi})$$

Else $P_{BESSi\_ref} = 0$

End

Here, V_{bus} is the voltage magnitude of the load bus and V_{upper_limit} is the upper voltage limit. P_{BESSi_ref} is a reference value used to control BESS*i*'s active power, and this value is limited to the range $P_{BESS\_\min}$ to $P_{BESS\_\max}$. P_{Fi} is the active power flow at feeder *i*.

5.3.4. Control algorithm of optimal BESSs.

In this part, the control algorithm for use with optimal BESSs having optimal placement and sizes of BESSs is described. The SOC is constrained to be between 20% and 80%. The first PI controller keeps the load bus voltage of feeder *i* in an appropriate voltage range when the load bus voltages exceed the upper limit by using the active power of BESS*i*. In contrast, the second PI controller controls the active power of BESS*i* to minimize the active power flow in feeder *i*. The second PI controller helps BESS*i* to discharge the stored energy, which keeps BESS*i* ready for the next charge cycle to stabilize the load bus voltages. The flow chart of the control algorithm is as follows.

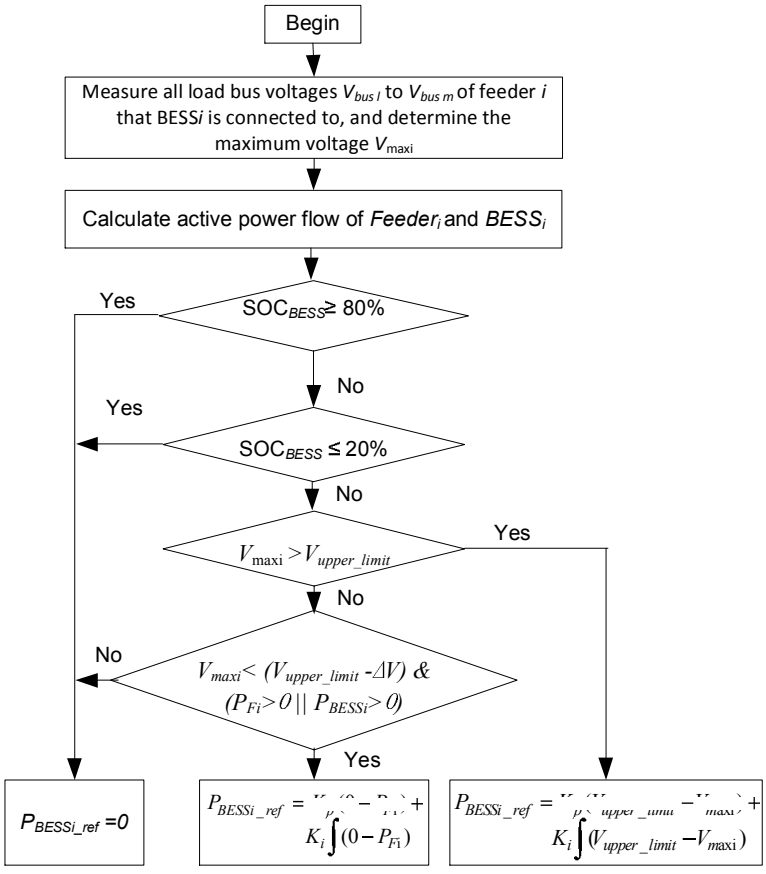

Fig. 5.3. Control algorithm for BESSs.

5.4. Modeling and simulation results

The MG model, which has residential loads, PVs, and BESSs, is simulated by the MATLAB/Simulink software tool, as shown in Fig. 5.3. Figures 5.4 and 5.5 show the maximum PV output and minimum load profiles, respectively, over 24 h. Table 5.1 shows the parameters of the MG in the model.

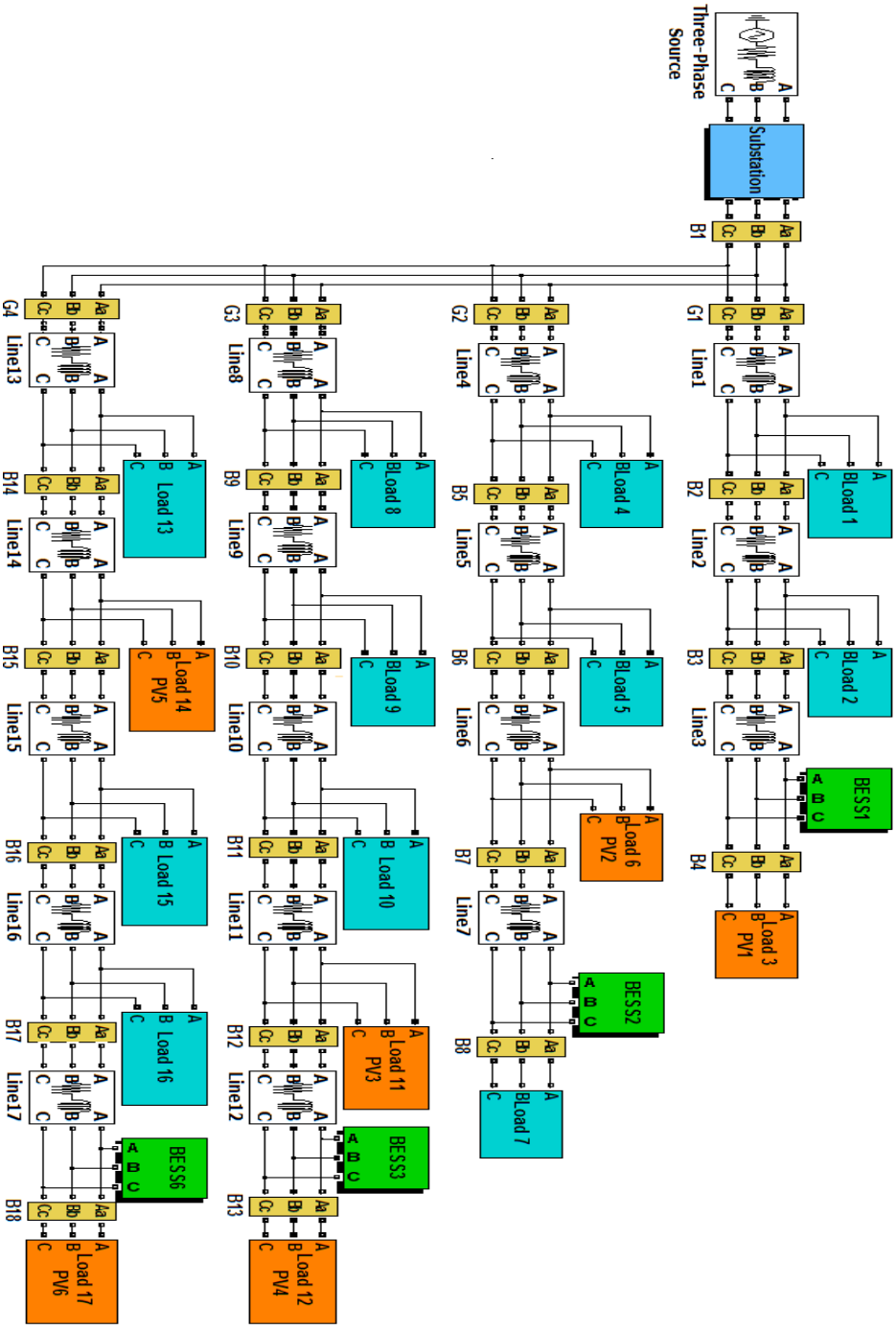

Fig. 5.4. MATLAB /Simulink implementation of the MG model.

Table 5.1. Simulation parameters

3-phase source	Base voltage	6600 V
	Base power	1 MVA
	Frequency	50 Hz
Line impedance for lines 1–7		2+j2.04 Ω
Line impedanc for lines 8–17e		1.5+j1.53 Ω

5.4.1. Effectiveness of HPSO-TVAC on different benchmarks.

The HPSO-TVAC is used to solve (minimize) the objective function, and its performance is compared with that of SPSO [58] and PSO-TVIW [79]. The performance of each system was judged over 20 trials. In SPSO, the constriction factors were c_1=c_2=2. In PSO-TVIW, the constriction factors were c_1=c_2=2.05, and w varied from 0.9 to 0.4. In HPSO-TVAC, the constriction factors c_1 and c_2 are chosen as (2.5,0.5) and (0.5,2.5), respectively. Thus, the values of the cognitive and social acceleration factors are chosen as c_{1i}=0.5, c_{2i}=2.5, c_{1f}=2.5, and c_{2f}=0.5. In this chapter, the population size of the swarm is randomly selected with the aim of verifying the algorithm, rather than analyzing the effect of population size on the result of optimization. Hence, all simulations were carried out with a population size of 150. These methods were programed for MATLAB/Simulink on a 2.8-GHz processor with 8 GB of RAM.

Figure 5.6 shows the convergence characteristics of PSO strategies at 12:00. The HPSO-TVAC found the globally best configuration faster than either SPSO and PSO-TVIW did. The HPSO-TVAC method obtained stable results after 20 trials over two methods, PSO-TVIW and SPSO, as shown in Table 5.2.

Table 5.2. Comparison of different PSO strategies

PSO method	Minimum FT	Maximum FT	Average FT
HPSO-TVAC	4.995905	4.995962	4.995915
PSO-TVIW	4.995905	6.857187	5.502273
SPSO	5.036156	6.116458	5.257662

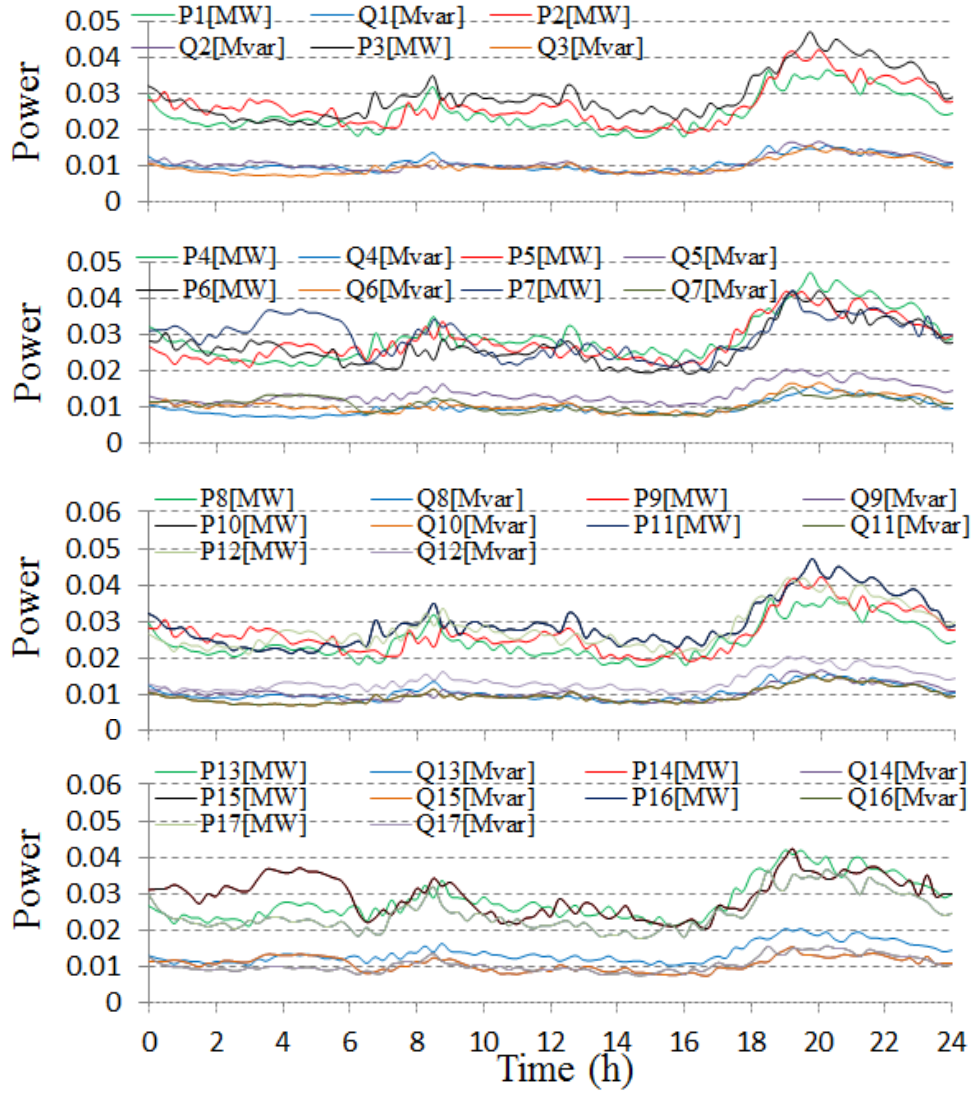

Fig. 5.5. Daily residential load profile over 24 h.

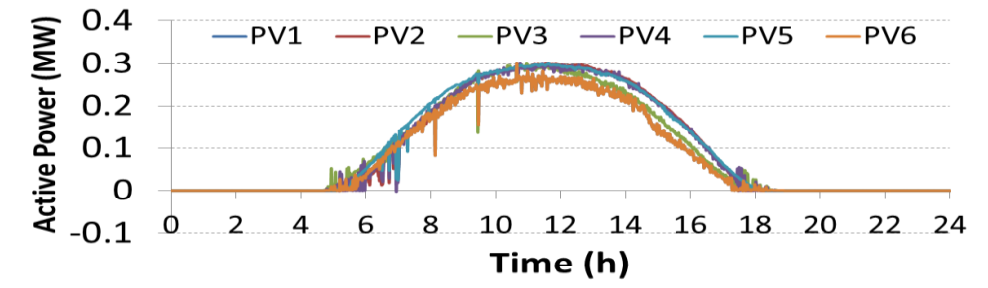

Fig. 5.6. Daily active power output of the PV sources over 24 h.

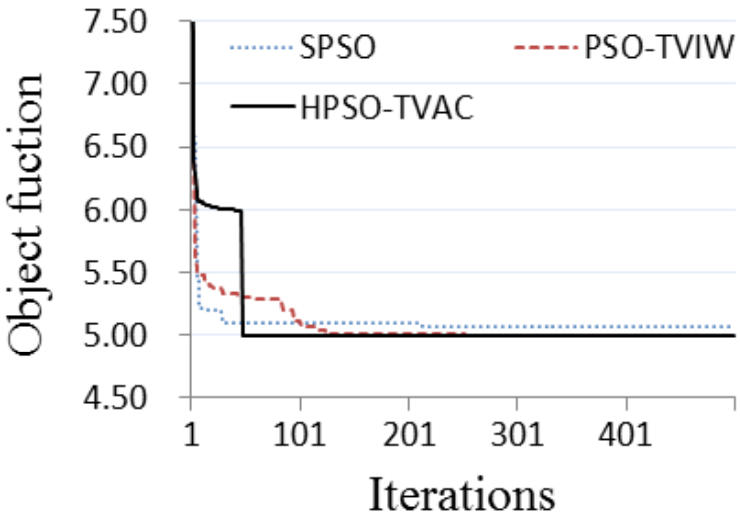

Fig. 5.7. Convergence characteristics of PSO strategies.

5.4.2. Optimal BESS placement based on HPSO-TVAC.

This section shows simulation results for optimizing the placement of BESSs by using an OPF method based on HPSO-TVAC. The simulation time is chosen as 24 h.

Figure 5.7 shows the optimal BESS locations that were identified by HPSO-TVAC. Although in the vector control x there are six BESSs, the proposed optimal method found that the MG needs only four BESSs to control the load bus voltage. These include $BESS_1$ connected to load bus 4 on $Feeder_1$, $BESS_2$ connected to load bus 8 on $Feeder_2$, $BESS_3$ connected to load bus 13 on $Feeder_3$.

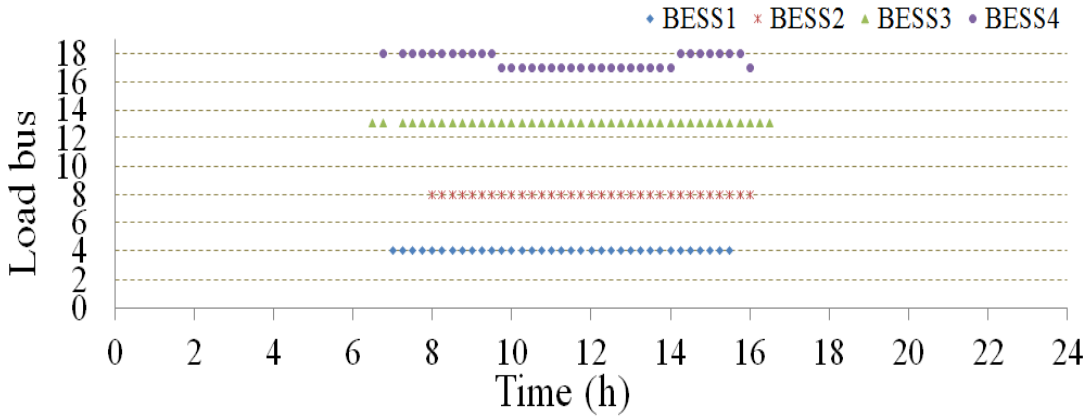

Fig. 5.8. Optimal BESS locations.

$BESS_4$ has two distinct candidate positions: load bus 17 or 18 on $Feeder_4$. In this case, the final optimal location of $BESS_4$ will be selected according to the size of $BESS_4$ as

determined in the selection step.

5.4.3. Determining the sizes of BESSs.

In the previous step, candidates for the optimal placement of BESSs were obtained. In this selection step, BESSs are used to control the voltage of load buses by means of a PI controller. Figure 5.8 shows the load bus voltages of an MG without BESSs. When the loaddemand is lower than generation from the PVs, the load bus voltages exceed the upper limit. When BESSs are connected to the optimal locations and controlled by the proposed control method, the load bus voltages are kept within the specified range, as shown in Fig. 5.9.

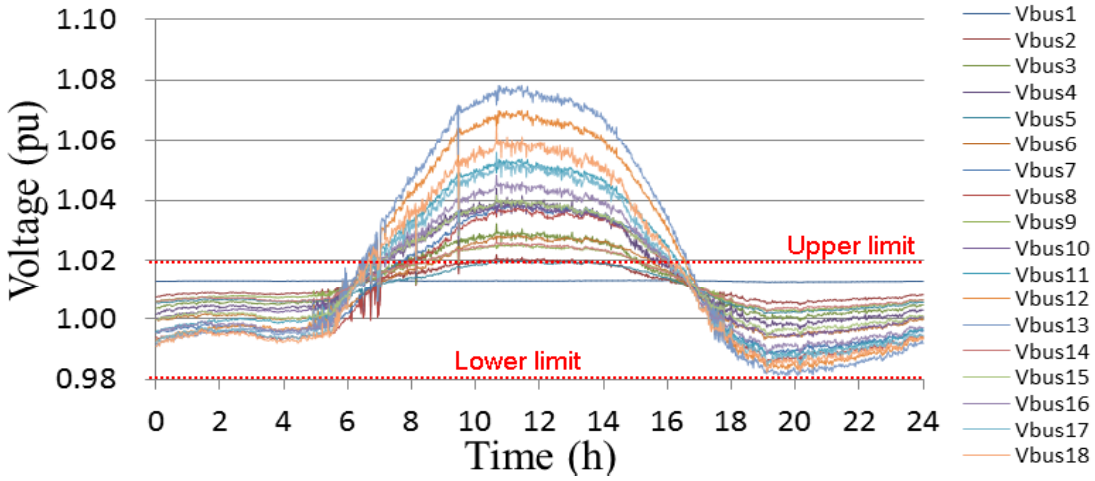

Fig. 5.9. Load bus voltages without BESSs.

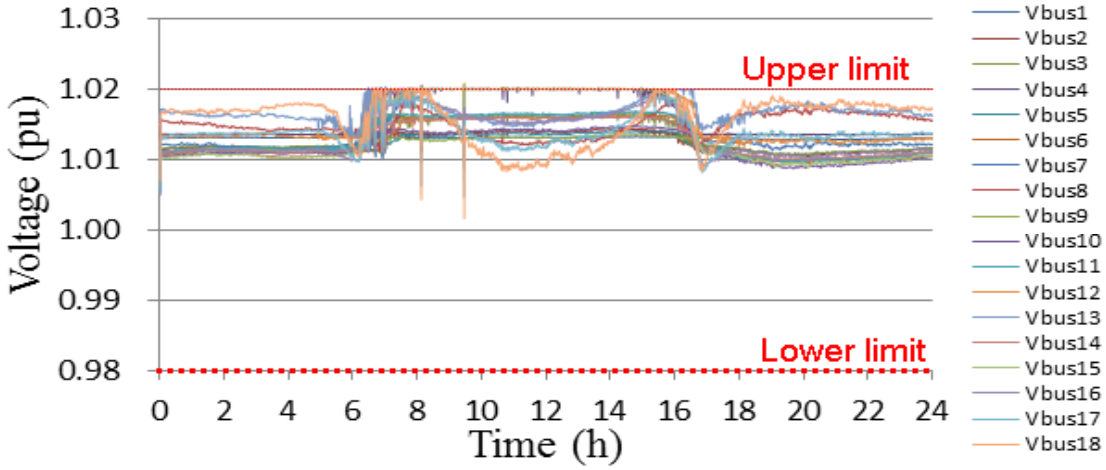

Fig. 5.10. Load bus voltages with BESSs.

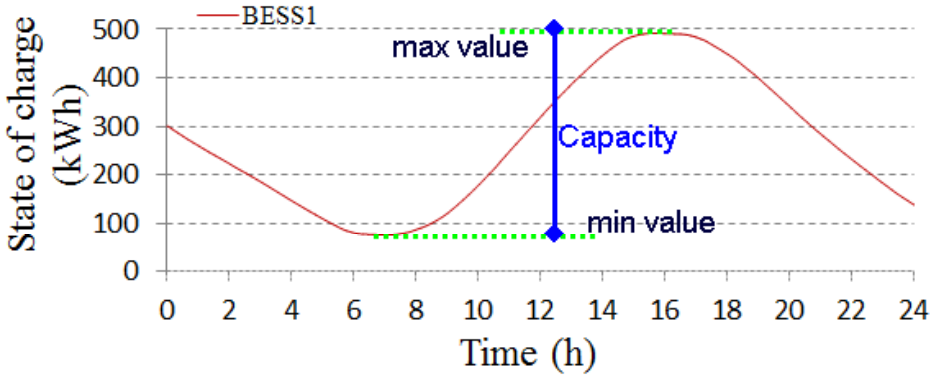

Fig. 5.11. Energy storage of $BESS_1$.

Table 5.3. Determined sizes of BESSs

	Location	Capacity
$BESS_1$	Bus 4	416.4 kWh
$BESS_2$	Bus 8	374.64 kWh
$BESS_3$	Bus 13	1315.3 kWh
$BESS_4$	Bus 17	929.6 kWh
	Bus 18	913.78 kWh

Figure 5.10 shows how to calculate the necessary BESS capacities. The capacity of each BESS was chosen by using the charge curve, which measures SOC. In Fig. 5.10, the charge curve moves from the minimum value to the maximum value, and the capacity of the BESS can be found as (maximum value – minimum value). Table 5.3 shows the obtained capacities of the BESSs. The results show that the capacity needed when $BESS_4$ is connected to bus 18 is less than when it is connected to bus 17. Thus, bus 18 is the optimal location for $BESS_4$. After using a two-step optimization algorithm, the optimal placement and sizes of the BESSs are determined.

5.4.4. MG with optimal BESSs.

In this section, the effectiveness of the control algorithm for BESSs is discussed. Because of the similarity and independence of the 4 feeders of the MG in the sample case, $Feeder_4$ from the MG is used when showing the simulation results (Fig. 5.12). Figure 5.13(a) shows the load bus voltages of $Feeder_4$, which should be controlled to remain in the specified voltage range. From hour 7 to hour 17, $BESS_4$ charges by

accepting energy from the PV source to decrease the load bus voltage, as shown in Fig. 5.9. From hour 17 to hour 24, $BESS_4$ discharge is stored energy to supply a load. As $BESS_4$ discharges, the voltage drops are decreased. If the simulation were extended, the discharged process would continue to hour 7 of the next day. This process ensures that $BESS_4$ is fully discharged and ready for the next operating cycle. Figure 5.13(c) shows the SOC of $BESS_4$. The SOC was kept between 20% and 80%. This case has been assumed as the worst for the MG with minimum demand and maximum PV output, and so because $BESS_4$ can ensure the SOC remains in the specified range to control the load bus voltage of the feeder in this case, it can do so in all cases.

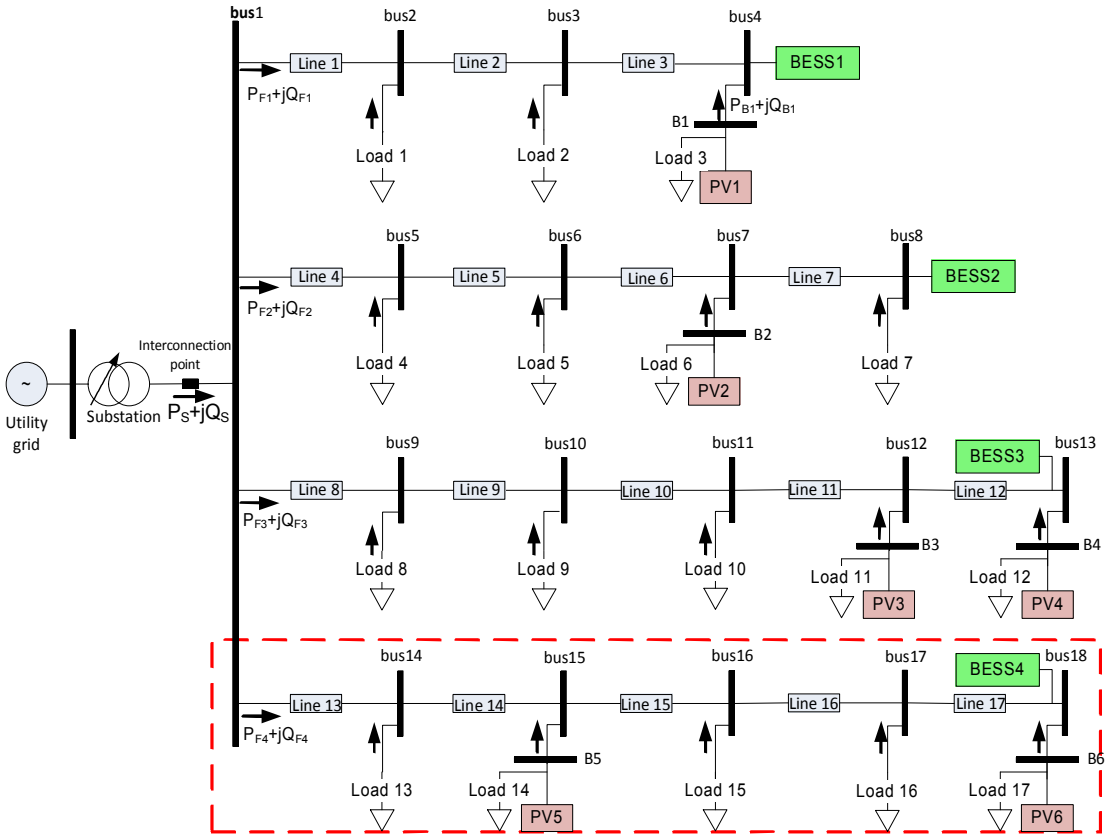

Fig. 5.12. Simulation MG model with BESSs.

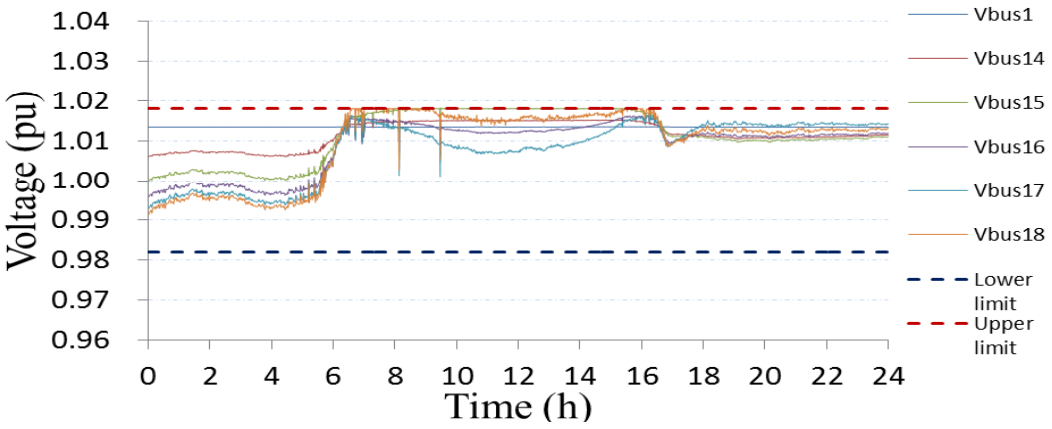

a) Load bus voltages of Feeder$_4$

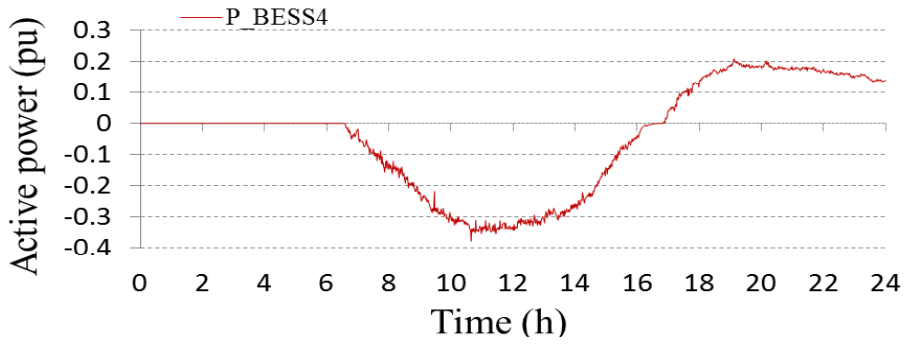

b) Active power of BESS$_4$

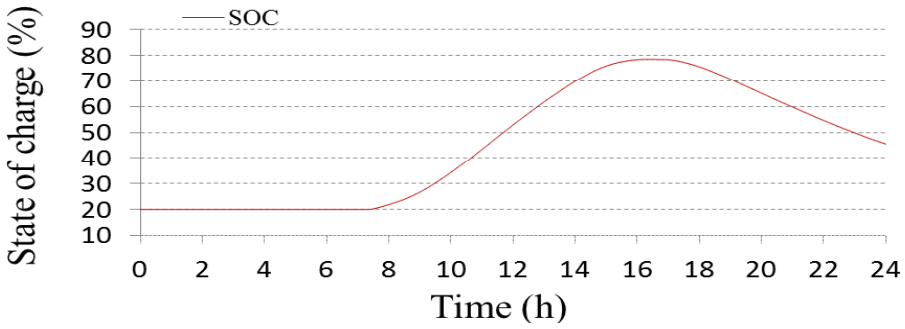

c) State of charge of BESS$_4$

Fig. 5.13. Feeder$_4$ of MG with BESS$_4$.

5.5. Experimental results

In this section, the control algorithm for BESSs located at the optimal positions and having the optimal capacities was applied in the real-time distribution network simulator. Because the number of loads buses is large, only Feeder$_3$ is examined in detail for this experiment, as shown in Fig. 5.14.

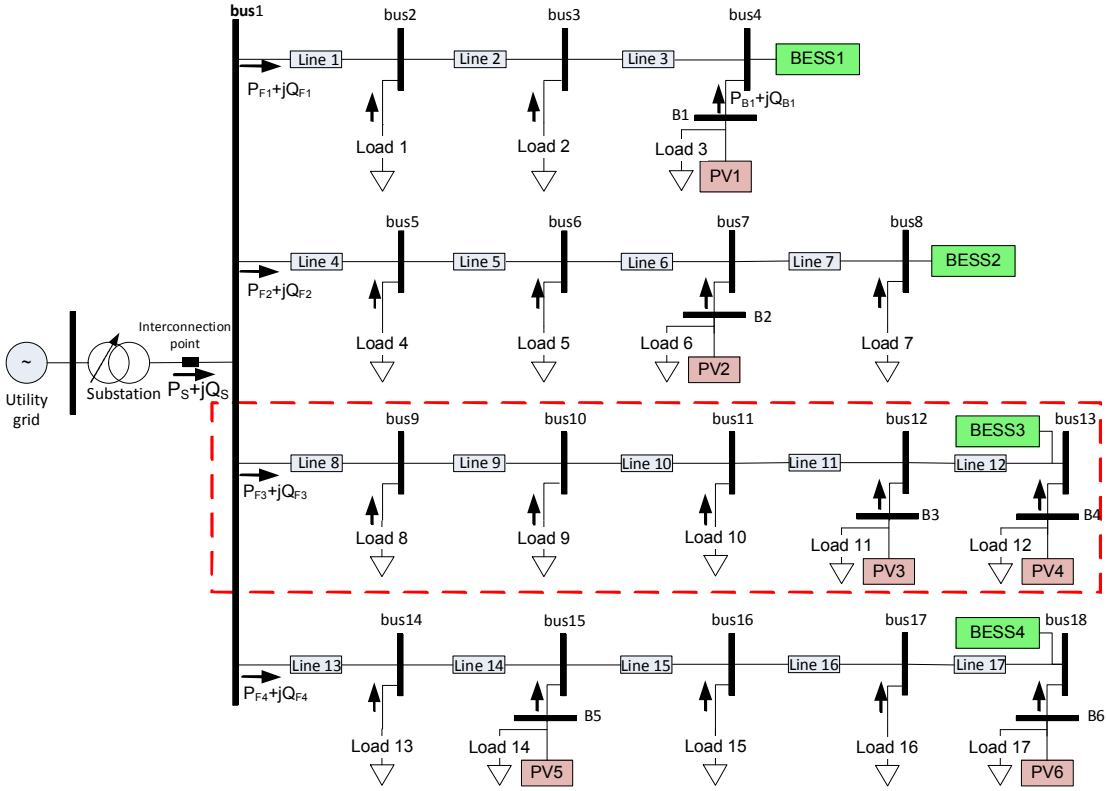

Fig. 5.14. Experimental MG model with BESSs.

In the experiment, PV generation levels are decreased to check the effectiveness of the proposed method under normal operating conditions, rather than with maximum generation from PV sources. Figure 5.15 shows the load bus voltages when $BESS_3$ is not connected to $Feeder_3$. The load bus voltage exceeds the upper limit when PV_3 and PV_4 generate active power to $Feeder_3$. As the result of the optimization algorithm, the optimal location of $BESS_3$ is on bus 13. Then, $BESS_3$ is controlled by the proposed control method to stabilize the load bus voltages. As shown in Fig. 5.16, the load bus voltages are kept in the allowable voltage range by this control. As shown in Figs. 5.17 and 5.18, from hour 9.5, $BESS_3$ charges its batteries from active power to decrease the load bus voltage. From hour 17, the feeder begins to receive active power from the MG; therefore, $BESS_3$ is discharging active power to the feeder. During this period, the

voltage drop of the load bus voltages is reduced. At hour 19, $BESS_3$ is fully discharged, and the active power from $BESS_3$ is controlled as zero to keep the SOC no lower than 20%.

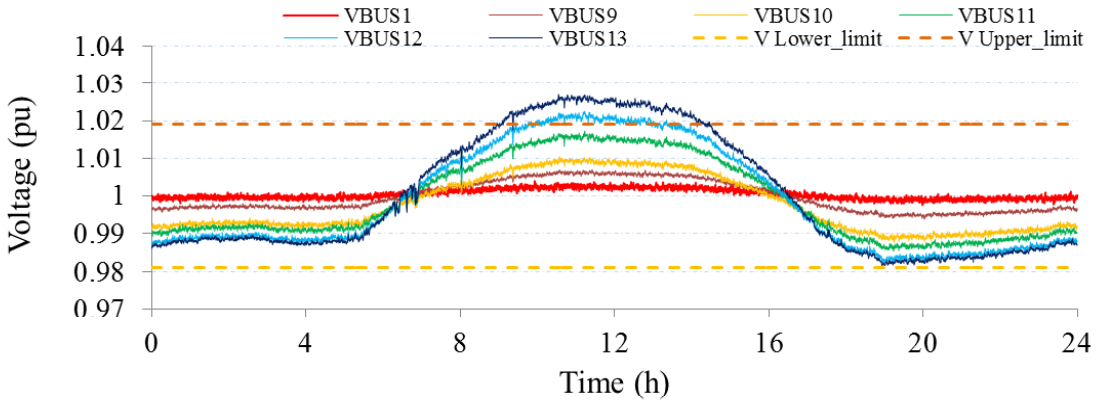

Fig. 5.15. Load bus voltage of $Feeder_3$ without $BESS_3$.

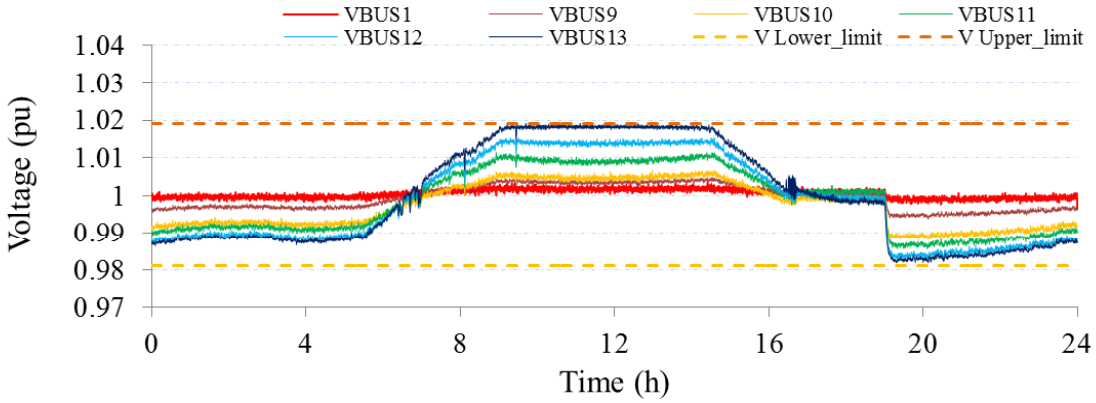

Fig. 5.16. Load bus voltage of $Feeder_3$ with $BESS_3$.

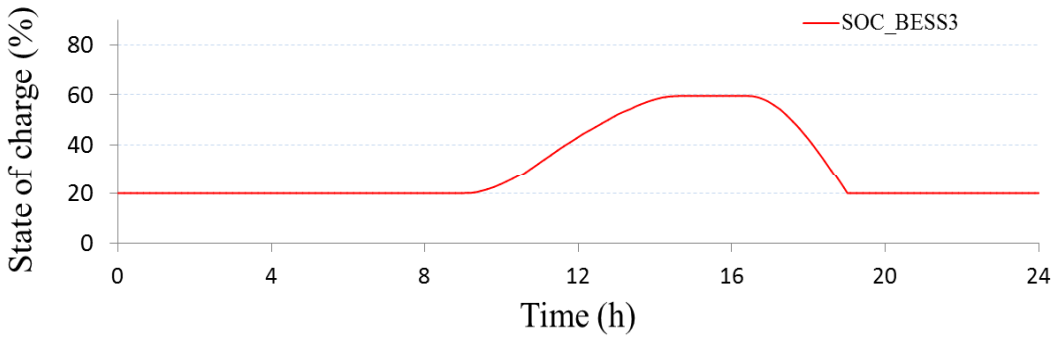

Fig. 5.17. Energy storage of $BESS_3$.

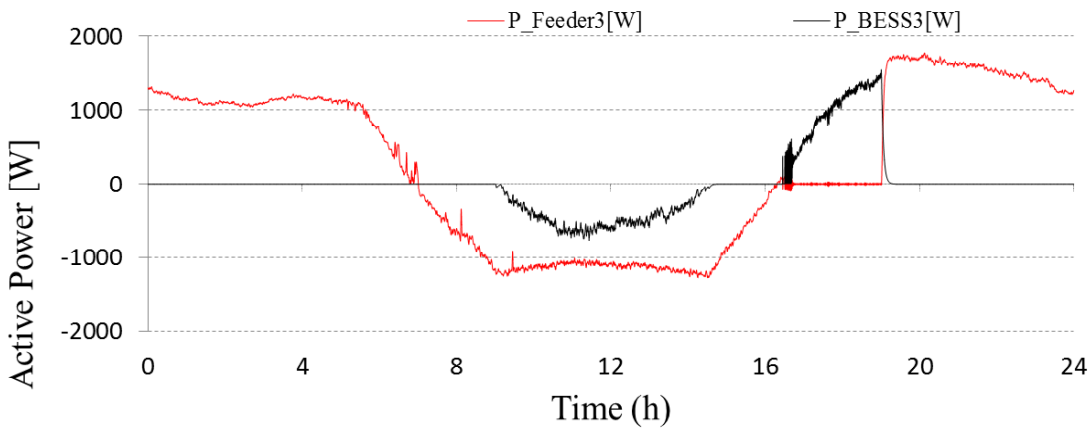

Fig. 5.18. Active power flow of $Feeder_3$ and $BESS_3$.

5.6. Conclusion

The proposed method is used to optimize the placement and sizes of BESSs. The minimal number of BESSs is determined by using HPSO-TVAC, and the sizes of these BESSs are calculated from the SOC curves. The proposed method also presents an energy control method for BESSs in MGs. The simulation and experimental results verify the effectiveness of the control algorithm for optimal BESSs.

CHAPTER 6: CONCLUSIONS, LIMITATIONS, AND FUTURE WORKS

6.1. Summary

In this thesis, four improvements have been proposed.

First, installing a central BESS in a PV-supplied MG at the interconnection point with the grid was proposed. This BESS can operate as a VSI and a DSTATCOM to control the voltage of MGs by using a reactive power controller instead of using DSTATCOMs in the MGs.

Second, a novel coordinated voltage control for the central BESS, local BESSs, and LRT was proposed. The control regulates the load bus voltages of the MGs. The effectiveness of the coordinated control was verified by simulation results and experiment results.

Third, an optimal active power flow for controlling the local BESSs so as to minimize distribution loss was proposed. In this method, coordination occurs to effect centralized control of the central BESS and LRT to stabilize the voltages of a PV-supplied MG. The proposed method also includes an energy control method for BESSs in MGs. The validity of the proposed control methods was checked by numerical simulations and by experiments on a real-time distribution network simulator.

Last, a novel two-step optimization method for determining the placement and sizes of BESSs by using HPSO-TVAC was proposed for stabilizing the voltages of a PV-supplied MG. The proposed method helps to find the best places in the MG to install BESSs and to determine the needed capacities of the BESSs. Further, a control algorithm for the optimal BESSs was proposed for stabilizing the load bus voltage to within the allowable voltage range. The method was verified by simulations and experiments.

6.2. Limitations and future works

This thesis does not handle islanded MGs. As a result, frequency control is not covered. In fact, BESSs control active power to stabilize the frequency in islanded MGs. Moreover, the capacities and placement of the BESSs play an important role in determining the control system for islanded MGs. Exploring this topic is one of the future directions for research.

In this thesis, the focus was the influence of PV power on MGs. However, the recent expansion of various RESs, such as wind power and fuel cells, makes them increasingly attractive as candidates for mitigating global warming and easing the energy problem. The author plans to study the effects of multiple types of RES on the MGs and to develop a control algorithm for BESSs in such MGs.

Forecasting of electricity demand is quite important for planning and controlling power systems. When using the algorithm to optimize the sizes and placement of BESSs, the author has assumed that data on PV output and load demand are provided by a forecasting algorithm. In the future, the author plans to focus on a forecasting algorithm to improve the method proposed in this thesis.

References

[1] G. T. Heydt: “The next generation of power distribution systems”, IEEE Trans. Smart Grid, Vol.1, No.3, pp.225-235, 2010.

[2] N. D. Hatziargyriou and A. P. S. Meliopoulos: “Distributed energy sources: Technical challenges”, in Proc. IEEE Power Eng. Soc. Winter Meeting, New York, Vol.2, pp.1017-1022, 2002.

[3] R. A. Reigh, R. Saint, R. C. Dugan, J. Burke, and L. A. Kojovic: “Summary of distributed resources impact on power delivery systems”, IEEE Trans. Power Del., Vol.23, No.3, pp.1636 -1644, 2008.

[4] R. H. Lasseter and P. Piagi: “Microgrid: A conceptual solution”, in Proc. Power Electronics Specialists Conf., Aachen, Germany, Vol.6, pp.4285-4290,2004..

[5] T. L. Vandoorn, J. D. M. De Kooning, B. Meersman, J. M. Guerrero, and L. Vandevelde: “Voltage-based control of a smart transformer in a microgrid,” Industrial Electronics, IEEE Transactions on, issue 99, 2011.

[6] T. Logenthiran, D. Srinivasan, A. M. Khambadkone, and H. N. Aung: “Multiagent system for real-time operation of a microgrid in real-time digital simulator”, Smart Grid, IEEE Transactions on, issue 99, pp.1-9, 2012.

[7] F. Katiraei, M. R. Iravani, and P. W. Lehn: “Micro-grid autonomous operation during and subsequent to islanding process”, IEEE Trans. Power Del., Vol.20, No.1, pp.248-257 , 2005.

[8] C. K. Sao and P. W. Lehn: “Control and power management of converter fed micro-grids”, IEEE Trans on Power Systems, 23[3], pp.1088-1098, 2008.

[9] C. Cho , J. Jeon , J. Kim , S. Kwon , K. Park and S. Kim “Active synchronizing control of a microgrid”, IEEE Trans. Power Electron., vol. 26, No. 12, pp.3707 -3719, 2011.

[10] A. G. Madureira, J. C. Pereira, N. J. Gil, J. A. Pecas Lopes, G. N. Korres and N. D. Hatziargyriou “Advanced control and management functionalities for multi-microgrids” Euro. Trans. Electr. Power, No. 21, pp. 1159–1177, 2011.

[11] F. Shahnia, R. Majumder, A. Ghosh, G. Ledwich, and F. Zare,"Operation and control of a hybrid microgrid containing unbalanced and nonlinear loads" Electric Power Systems Research, Vol. 80, pp. 954-965, 2010.

[12] A. L. Dimeas and N. D. Hatziargyriou: "Operation of a multiagent system for microgrid control", IEEE Trans. on Power Systems, Vol. 20, No.3, pp.1447-1455, 2005.

[13] P. Trichakis, P. C. Taylor, P. F. Lyons, and R. Hair, "Predicting the technical impacts of high levels of small-scale embedded generators on low-voltage networks", Renewable Power Generation, IET, Vol. 2, pp. 249-262, 2008.

[14] N. Jayasekara and P. Wolfs, "Analysis of power quality impact of high penetration PV in residential feeders", in Universities Power Engineering Conference [AUPEC], 2010 20th Australasian, pp. 1-8, 2010.

[15] A. Canova, L. Giaccone, F. Spertino, and M. Tartaglia, "Electrical Impact of Photovoltaic Plant in Distributed Network", Industry Applications, IEEE Transactions on, Vol. 45, pp. 341-347, 2009.

[16] J. C. Hernández, A. Medina, and F. Jurado, "Impact comparison of PV system integration into rural and urban feeders", Energy Conversion and Management, Vol. 49, pp. 1747-1765, 2008.

[17] R. Passey, T. Spooner, I. MacGill, M. Watt, and K. Syngellakis, "The potential impacts of grid-connected distributed generation and how to address them: A review of technical and non-technical factors", Energy Policy, Vol. 39, pp. 6280-6290, 2011.

[18] I. T. Papaioannou, M. C. Alexiadis, C. S. Demoulias, D. P. Labridis, and P. S. Dokopoulos, "Modeling and Field Measurements of Photovoltaic Units Connected to LV Grid. Study of Penetration Scenarios", Power Delivery, IEEE Transactions on, Vol. 26, pp. 979-987, 2011.

[19] M. Mes, G. M. A. Vanalme, J. M. A. Myrzik, M. Bongaerts, G. J. P. Verbong, and W. L. Kling, "Distributed generation in the Dutch LV network - self-supporting residential area", in Universities Power Engineering Conference, 2008. UPEC 2008. 43rd International, pp. 1-5, 2008.

[20] J. R. Rodriguez, F. Ruiz, D. Biel, and F. Guinjoan, “Simulation and analysis of distributed PV generation in a LV network using MATLAB-Simulink”, in Circuits and Systems [ISCAS], Proceedings of 2010 IEEE International Symposium on, pp. 2322-2325, 2010.

[21] R. Tonkoski and L. A. C. Lopes, “Voltage Regulation in Radial Distribution Feeders with High Penetration of Photovoltaic”, in Energy 2030 Conference, 2008. ENERGY 2008. IEEE, pp. 1-7, 2008.

[22] C. L. Masters, “Voltage rise - the big issue when connecting embedded generation to long 11 kV overhead lines”, Power Engineering Journal, Vol. 16, pp. 5-12, Feb 2002.

[23] P. P. Barker, R. W. de Mello, and Ieee, “Determining the impact of Distributed Generation on power systems: Part 1 - Radial distribution systems”. New York: IEEE, 2000.

[24] M. E. Elkhatib, R. El Shatshat, and M. M. A. Salama: “Novel coordinated voltage control for smart distribution networks with DG”, IEEE Trans. Smart Grid, Vol. 2, No.4, pp.598 -605,2011.

[25] M. R. Salem, L. A. Talat, and H. M. Soliman, “Voltage control by tap-changing transformers for a radial distribution network”, Generation, Transmission and Distribution, IEE Proceedings-, Vol. 144, pp. 517-520, 1997.

[26] R. Tonkoski and L. A. C. Lopes, “Voltage Regulation in Radial Distribution Feeders with High Penetration of Photovoltaic”, in Energy 2030 Conference, 2008. ENERGY 2008. IEEE, pp. 1-7, 2008.

[27] M. H. J. Bollen and A. Sannino “Voltage control with inverter-based distributed generation”, IEEE Trans. Power Delivery, Vol. 20, No. 1, pp.519 -520, 2005.

[28] R. Tonkoski, L. A. C. Lopes, and T. H. M. El-Fouly: “Coordinated active power curtailment of grid connected PV inverters for overvoltage prevention”, IEEE Trans. Sustain. Energy, Vol.2, No.2, pp. 139-147, 2011.

[29] J. M. Guerrero, J. Matas, V. Luis Garcia de, M. Castilla, and J. Miret, “Decentralized Control for Parallel Operation of Distributed Generation Inverters

Using Resistive Output Impedance", Industrial Electronics, IEEE Transactions on, Vol. 54, pp. 994- 1004, 2007.

[30] H. E. Farag, E. F. El-Saadany, and R. Seethapathy: "A two-way communication-based distributed control for voltage regulation in smart distribution feeders", IEEE Trans. Smart Grid, Vol.3, No.1, pp.271-281, 2012.

[31] M. Castillo-Cagigal, A. Gutiérrez, F. Monasterio-Huelin, E. Caamaño-Martín, D. Masa, and J. Jiménez-Leube, "A semidistributed electric demand-side management system with PV generation for self-consumption enhancement", Energy Conversion and Management, Vol. 52, pp. 2659-2666, 2011.

[32] K. K. Turitsyn, P. Šulc, S. Backhaus, and M. Chertkov: "Options for control of reactive power by distributed photovoltaic generators", Proc. of the IEEE, Vol.99. No.6, 2011.

[33] F. A. Viawan and D. Karlsson: "Voltage and reactive power control in systems with synchronous machine-based distributed generation", IEEE Trans. Power Del., Vol.23, No.2, pp.1079-1087, 2008.

[34] P. M. S. Carvalho, P. F. Correia, and L. A. F. M. Ferreira: "Distributed reactive power generation control for voltage rise mitigation in distribution networks", IEEE Trans. Power Syst., Vol.23, No.2, pp.766-772,2008.

[35] C. Schauder and H. Mehta: "Vector analysis and control of the advanced static VAr compensators", Proc. Inst. Elect. Eng., Gen., Transm., Distrib., Vol.140, No.4, pp.299-306, 1993.

[36] M. E. Baran , S. Teleke , L. Anderson , A. Q. Huang , S. Bhattacharya and S. Atcitty "STATCOM with energy storage for smoothing intermittent wind farm power", Proc. Power and Energy Soc. General Meeting—Conv. and Delivery of Elect. Energy in the 21st Century, pp.1 -6, 2008.

[37] S. M. Muyeen , R. Takahashi , T. Murata , J. Tamura and M. H. Ali "Application of STATCOM/BESS for wind power smoothening and hydrogen generation", Electric Power Syst. Res., Vol. 79, No. 2, pp.365 -373, 2009.

[38] J. Cappelle, J. Vanalme, S. Vispoel, T. Van Maerhem, B. Verhelst, C. Debruyne, and J. Desmet, "Introducing small storage capacity at residential PV installations

to prevent overvoltages", in Smart Grid Communications [SmartGridComm], 2011 IEEE International Conference on, 2011, pp. 534-539.

[39] K. C. Divya and J. Oøstergaard, "Battery energy storage technology for power systems-An overview", Electric Power Systems Research, Vol. 79, pp. 511-520, 2009.

[40] J. N. Baker, A. Collinson, G. W. Hunt, A. Green, A. Price, S. Bartley, S. Male, G. Cooley, A. Shibata, K. Sato, E. Kodama, Y. Kurashima, P. Lex, B. Jonshagen, R. Schottler, R. G. Coney, A. Campbell, R. McHattie, C. Tarrant, and O. Weinmann, "Special feature: Electrical energy storage at the turn of the Millennium", Inst. Elect. Eng. Power Eng. J., Vol. 13, No. 3, pp.107 -180 1999.

[41] J. P. Barton and D. G. Infield: "Energy storage and its use with intermittent renewable energy", IEEE Trans. Energy Convers., Vol.19, No.2, pp.441-448,2004.

[42] S. Chen and H. Gooi: "Scheduling of energy storage in a grid-connected PV/battery system via simplorer", Proc. TENCON IEEE Region 10 Conf., pp.1-5, 2009.

[43] J. Mitra: "Reliability-based sizing of backup storage", IEEE Trans. Power Syst., Vol.25, No.2, pp.1198-1199, 2010.

[44] J. P. Barton and D. G. Infield, "Energy storage and its use with intermittent renewable energy", IEEE Trans. Energy. Conv., Vol. 19, No. 2, June 2004.

[45] G. Mulder, F. D. Ridder, and D. Six, "Electricity storage for gridconnected household dwellings with PV panels", Solar Energy, Vol. 84, pp. 1284-1293, 2010.

[46] S. J. Chiang, K. T. Chang, and C. Y. Yen, "Residential photovoltaic energy storage system", Industrial Electronics, IEEE Transactions on, Vol. 45, pp. 385-394, 1998.

[47] K. Kurokawa, N. Kawasaki, and M. Ito, "Particularity of PV aggregations incorporating with the power grids - Development of a power router", in Photovoltaic Specialists Conference [PVSC], 2009 34th IEEE, pp. 001632-001637, 2009.

[48] S. Suryanarayanan, F. Mancilla-David, J. Mitra, and L. Yunwei, "Achieving the Smart Grid through customer-driven microgrids supported by energy storage", in

Industrial Technology [ICIT], 2010 IEEE International Conference on, pp. 884-890, 2010.

[49] N. K. C. Nair and N. Garimella, “Battery energy storage systems: Assessment for small-scale renewable energy integration”, Energy and Buildings, Vol. 42, pp. 2124-2130, 2010.

[50] P. J. Hall, E. J. Bain, "Energy-storage technologies and electricity generation", Energy Policy, Vol 36, Issue 12, pp. 4352-4355, 2008.

[51] X. Li, D. Hui, and X. Lai, “Battery energy storage station -based smoothing control of photovoltaic and wind power generation fluctuations”, IEEE Trans. on sustainable energy, Vol. 4, No. 2, pp. 464-473, April 2013.

[52] K. Yoshimoto , T. Nanahara and G. Koshimizu “New control method for regulating state-of-charge of a battery in hybrid wind power/battery energy storage system”, Proc. IEEE Power Syst. Conf. and Exposition, pp.1244 -1251 2006.

[53] S. S. G. Jayasinghe, D. M. Vilathgamuwa and U. K. Madawala, “Direct integration of battery energy storage systems in distributed power generation”, IEEE Transactions on Energy Conversion, Vol. 26, Issue: 2, pp. 677 – 685, June 2011.

[54] N. Kawakami , Y. Iijima , Y. Sakanaka , M. Fukuhara , K. Ogawa , M. Bando and T. Matsuda “Development and field experiences of stabilization system using 34 MW NAS batteries for a 51 MW wind farm”, Proc. IEEE Int. Symp. Ind. Electronics [ISIE2010], pp.2371, 2010.

[55] S. X. Chen, H. B. Gooi and M. Q. Wang "Sizing of energy storage for microgrids", IEEE Trans. Smart Grid, Vol. 3, no. 1, pp.142 -151, 2012.

[56] D. Bhatnagar and V. Loose “Evaluating utility procured electric energy storage resources: A perspective for state electric utility regulators”, SANDIA REPORT, SAND2012-9422, Unlimited Release, Printed November 2012.

[57] A. A. Akhil, G. Huff, A. B. Currier, B. C. Kaun, D. M. Rastler, S. B. Chen, A. L. Cotter, D. T. Bradshaw, and W. D. Gauntlett “DOE/EPRI 2013 Electricity storage handbook in collaboration with NRECA”, SANDIA REPORT, SAND2013-5131, Unlimited Release, Printed July 2013.

[58] J. Kennedy and R. Eberhart, “Particle swarm optimization”, in Proc.IEEE Conf. Neural Networks [ICNN’95], Perth, Australia, 1995, Vol. 4, pp. 1942–1948.

[59] J. Kennedy, “The particle swarm: Social adaptation of knowledge”, Proc. IEEE Int. Conf. Evolutionary Computation, pp.303 -308, 1997.

[60] J. Kennedy, “Behavior of particles”, Lecture Notes in Computer Science, Vol. 1447, pp.581 -589, 1998.

[61] J. Kennedy and R. Eberhart, “A discrete binary version of the particle swarm algorithm”, Proc. IEEE Int. Conf. Systems, Man, Cybernetics, Computational Cybernetics, Simulation, Vol. 5, pp.4104 -4108 , 1997.

[62] J. Kennedy, “Stereotyping: Improving particle swarm performance with cluster analysis”, Proc. IEEE Int. Conf. Evolutionary Computation, Vol. 2, pp.303 -308, 2000.

[63] P. J. Angeline, “Evolutionary optimization verses particle swarm optimization: Philosophy and the performance difference”, Lecture Notes in Computer Science, Vol. 1447, pp.600 -610 , 1998.

[64] J. Kennedy and W. M. Spears, “Matching algorithms to problems: An experimental test of the particle swarm and some genetic algorithms on the multi-modal problem generator”, Proc. IEEE World Congr. Computational Intelligence, pp.78 -83, 1998.

[65] P. J. Angeline, “Using selection to improve particle swarm optimization”, Proc. IEEE Int. Conf. Computational Intelligence, pp.84 -89, 1998.

[66] R. C. Eberhart and Y. Shi, “Particle swarm optimization: Developments, applications and resources”, Proc. IEEE Int. Conf. Evolutionary Computation, Vol. 1, pp.81 -86, 2001.

[67] R. C. Eberhart and Y. Shi, “Comparing inertia weights and constriction factors in particle swarm optimization”, Proc. IEEE Int. Congr. Evolutionary Computation, Vol. 1, pp.84 -88, 2000.

[68] Y. Shi and R. C. Eberhart, “Comparison between genetic algorithms and particle swarm optimization”, Lecture Notes in Computer science- evolutionary programming VII, Vol. 1447, pp.611 -616, 1998.

[69] Y. Shi and R. C. Eberhart, “Parameter selection in particle swarm optimization”, Lecture Notes in computer science-evolutionary programming VII, Vol. 1447, pp.591 -600, 1998.

[70] Y. Shi and R. C. Eberhart, “A modified particle swarm optimizer”, Proc. IEEE Int. Conf. Evolutionary Computation, pp.69 -73, 1998.

[71] Y. Shi and R. C. Eberhart, “Fuzzy adaptive particle swarm optimization”, Proc. IEEE Int. Congr. Evolutionary Computation, Vol. 1, pp.101 -106, 2001.

[72] R. C. Eberhart and Y. Shi, “Tracking and optimizing dynamic systems with particle swarms”, Proc. IEEE Congr. Evolutionary Computation 2001, pp.94 -97, 2001.

[73] T. Krink, J. S. Vesterstrom, and J. Riget, “Particle swarm optimization with spatial particle extension”, Proc. IEEE Congr. Evolutionary Computation 2002, Vol. 2, pp.1474 -1479, 2002.

[74] M. Lovbjerg and T. Krink, “Extending particle swarm optimizers with self-organized critically”, Proc. IEEE Int. Congr. Evolutionary Computation, Vol. 2, pp.1588 -1593, 2002.

[75] J. S. Vesterstrom, J. Riget, and T. Krink, “Division of labor in particle swarm optimization”, Proc. IEEE Int. Congr. Evolutionary Computation 2002, Vol. 2, pp.1570 -1575,2002.

[76] M. Lovbjerg, T. K. Rasmussen, and T. Krink, “Hybrid particle swarm optimizer with breeding and subpopulation”, Proc. 3rd Genetic Evolutionary Computation Conf. [GECCO-2001], pp.469 -476, 2001.

[77] P. N. Suganthan, “Particle swarm optimizer with neighborhood operator”, Proc. IEEE Int. Congr. Evolutionary Computation, Vol. 3, pp.1958 -1962, 1999.

[78] X. F. Xie, W. J. Zhang, and Z.-L. Yang, “A dissipative particle swarm optimization”, Proc. IEEE Congr. Evolutionary Computation 2002, Vol. 2, pp.1456 -1461, 2002.

[79] Y. Shi and R. C. Eberhart, “Empirical study of particle swarm optimization”, in Proc. IEEE Int. Congr Evolutionary Computation, Vol. 3, pp. 101–106, 1999.

[80] M. Clerc, “The swarm and the queen: Toward a deterministic and adaptive particle swarm optimization”, Proc. IEEE Int. Congr. Evolutionary Computation, Vol. 3, pp.1957, 1999.

[81] M. Clerc and J. Kennedy, “The particle swarm-explosion, stability, and convergence in a multi-dimensional complex space”, IEEE Trans. Evol. Comput., Vol. 6, pp.58 -73, 2002.

[82] F. van den Bergh and A. P. Engelbrecht, “Effect of swarm size on cooperative particle swarm optimizers”, Proc. Genetic Evolutionary Computation Conf. [GECCO-2001] , pp.892 -899 ,2001.

[83] T. M. Blackwell and P. bentley, “Improvised music with swarms”, Proc. IEEE Congr. Evolutionary Computation 2002, Vol. 2, pp.1462 -1467, 2002.

[84] E. C. Laskari, K. E. Parsopoulos, and M. N. Vrahatis, “Particle swarm optimization for minimax problems”, Proc. IEEE Int. Congr. Evolutionary Computation, Vol. 2, pp.1576 -1581, 2002.

[85] E. C. Laskari, K. E. Parsopoulos, and M. N. Vrahatis, “Particle swarm optimization for integer programming”, Proc. IEEE Int. Congr. Evolutionary Computation, Vol. 2, pp.1582 -1587, 2002.

[86] K. E. Parsopoulos and M. N. Vrahatis, “Particle swarm optimization method in multiobjective problems”, Proc. ACM Symp. Applied Computing 2002 [SAC 2002], pp.603 -607, 2002.

[87] J. Kennedy and R. C Eberhart, “A discrete binary version of the particle swarm algorithm”, Proc. World Multiconf. Systemics, Cybernetics, Informatics, pp.4104 -4109, 1997.

[88] E. Ozcanand and C. K. Mohan, “Particle swarm optimization: Surfing the waves”, Proc. IEEE Congr. Evolutionary Computation 1999, Vol. 3, pp.1944 -1999, 1999.

[89] V. Tandon, H. E. Mounayri, and H. Kishawy, “NC end milling optimization using evolutionary computation”, Int. J. Mach. Tools Manuf., Vol. 42, No. 5, pp.595 -605 2002

[90] G. Ciuprina, D. Ioan, and I. Munteanu, "Use of intelligent-particle swarm

optimization in electromagnetics", IEEE Trans. Magn., Vol. 38, pp.1037 -1040, 2002.

[91] N. Higashi and H. Iba, “Particle swarm optimization with Gaussian mutation”, Proceedings of the IEEE Swarm Intelligence Symposium 2003 [SIS 2003], pp.72 -79, 2003.

[92] A. Ratnaweera, H. C. Watson, and S. K. Halgamuge, “Optimization of valve timing events of internal combustion engines with particle swarm optimization”, Proc. 2003 Congr. Evolutionary Computation [CEC 2003], Vol. 4, pp.2411 -2418, 2003.

[93] A. Ratnaweera, S. K. Halgamuge and H. C. Watson “Self-organizing hierarchical particle swarm optimizer with time-varying acceleration coefficients”, IEEE Trans. Evol. Comput., Vol. 8, No. 3, pp.240 -255, 2004.

[94] A. Cagnano, E. De Tuglie, M. Liserre and R. A. Mastromauro “Online optimal reactive power control strategy of PV inverters”, IEEE Trans. Ind. Electron., Vol. 58, No. 10, pp.4549 -4558, 2011.

[95] S. Toma , T. Senjyu , Y. Miyazato , A. Yona , T. Funabashi , A. Y. Saber and K. Chul-Hwan “Optimal coordinated voltage control in distribution system”, Proc. Power and Energy Society General Meeting—Conversion and Delivery of Electrical Energy in the 21st Century, 2008 IEEE, pp.1 -7 2008.

[96] Y. Riffonneau, S. Bacha, F. Barruel, and S. Ploix, “Optimal power flow management for grid connected PV systems with batteries”, Sustainable Energy, IEEE Transactions on, Vol. 2, pp. 309-320, 2011.

[97] H. Yoshida, K. Kawata, Y. Fukuyama, and Y. Nakanishi, “A particle swarm optimization for reactive power and voltage control considering voltage stability”, Proc. Int. Conf. Intelligent System Application to Power System, pp.117 -121, 1999.

[98] Y. Fukuyama and H. A. Yoshida, “Particle swarm optimization for reactive power and voltage control in electric power systems”, Proc. IEEE Congr. Evolutionary Computation 2001 [CEC 2001], Vol. 1, pp.87 -93, 2001.

[99] C. Lo and M. Anderson, “Economic dispatch and optimal sizing of battery

energy storage systems in utility load-leveling operations", IEEE Transactions on Energy Conversion 14 [3] 824–829, 1999.

[100] K. H. Jung, H. Kim and D. Rho, "Determination of the installation site and optimal capacity of the battery energy storage system for load leveling", IEEE Transactions on Energy Conversion 11 [1] 162–167, 1996.

[101] T. Y. Lee and N. Chen, "Determination of optimal contract capacities and optimal sizes of battery energy storage systems for time-of-use rates industrial customers", IEEE Transactions on Energy Conversion 10 [3] 562–568, 1995.

[102] JEAC 9701-2006 Grid-interconnection Code, 2006.

Acknowledgement

I owe my deepest gratitude to my mentor, Professor Yasuhiro HAYASHI for guiding this work. Without the close guidance and critiques from you, this thesis could never have come so far.

I also wish to thank advisors, Prof. Shinichi IWAMOTO, Prof. Atsushi ISHIYAMA, and Prof. Shinji WAKAO, who give me helpful advice to complete this thesis.

I would like to thank Associate Professor Masakazu ITO and Associate Professor Yu FUJIMOTO for examining this thesis and for many helpful contributions.

I am indebted to all members of Hayahsi Lab who help me to conduct my research, and guide me in life issues in Japan.

Especially, I would like to express my sincere appreciation to the Asia Special Scholarship program by Waseda University for the financial support during my doctoral course. This scholarship helps me to accomplish my dream to study at this famous university. The knowledge gathered during the course helped me a lot for my work and study later.

My sincere thanks should also be sent to all my dear Vietnamese friends in Waseda University and in Japan, who encouraged me in the difficult moments, and help me balance in life to be able to study well.

Last but not least, I would like to express my sincere appreciation to my dear family. At my down times, you were always there for me. There are no better family members like you all.

The listed names do not represent the complete list of people I would like to thank. Nonetheless, I truly hope that all my friends and helpful schoolmates can feel this sincere thankfulness from the bottom of my heart. Thank you all very much!

Date, February 13th, 2015

Achievements

Journal Paper

[1] Khoa Le Dinh, Yasuhiro Hayashi, "Coordinated BESS and LRT Control for Voltage Stabilization of a PV-Supplied Microgrid", IEEJ Transactions on Power and Energy, Vol.134, No.10, 2014, pp.875-884.

International conference paper

[1] Khoa Le Dinh, Yasuhiro Hayashi, "Experiment with an OPF Controller Based on HPSO-TVAC for a PV-Supplied Microgrid with BESS", IEEE Power and Energy Society General Meeting, 27 – 31 July, 2014, Washington DC, USA, pp.1-5.

[2] Khoa Le Dinh, Yasuhiro Hayashi, "Optimal BESS Placement and Sizing Based on HPSO-TVAC to Stabilize Voltage in PV-Supplied Micro-grid" The 20th International Conference on Electrical and Engineering (ICEE), 15 – 19 June, 2014, Korea, pp.348-353.

[3] Khoa Le Dinh, Yasuhiro Hayashi, "Online optimal power flow based on HPSO-TVAC coordinates with centralized BESS and LRT control to stabilize voltage in a PV-supplied microgrid" Innovative Smart Grid Technologies Europe (ISGT EUROPE) 2013 4th IEEE/PES, 6-9 October 2013, Denmark, pp 1-5.

[4] Khoa Le Dinh, Yasuhiro Hayashi, "Coordinated BESS control for improving voltage stability of a PV-supplied microgrid", Power Engineering Conference (UPEC) 2013 48th International Universities', 2-5 September 2013, Ireland, pp.1-6.

[5] Khoa Le Dinh, Yasuhiro Hayashi, "Centralized BESS Controlled to Minimize Demand of PV Supplied Micro-grid Under Voltage Constraint", 2012 IEEE International Power and Energy Conference (PECON), 2-5 December, 2012 Malaysia, pp. 864 – 869.

Domestic conference paper

[1] Khoa Le Dinh, Yasuhiro Hayashi, "Optimal BESSs Placement to Control Voltage of a PV-Supplied Microgrid Based on HPSO-TVAC", The 25th annual Conference of Power & Energy Society IEE Japan, 10-12 September 2014, Kyoto, Japan.

[2] Khoa Le Dinh, Yasuhiro Hayashi, "Coordinated Battery Energy Storage Systems and LRT Control to Stabilize Voltage in PV-Supplied Micro-grid", The 24th annual Conference of Power & Energy Society IEE Japan, 27 - 29 August, 2013, Niigata, Japan.

[3] Khoa Le Dinh, Yasuhiro Hayashi, "A Concept of Control Voltage and Power Flow by Using BESS in Micro-grid", The 23th annual Conference of Power & Energy Society IEE Japan, 12-14 September, 2012, Hokkaido, Japan.